INTERNATIONAL SCIENTIFIC JOURNAL

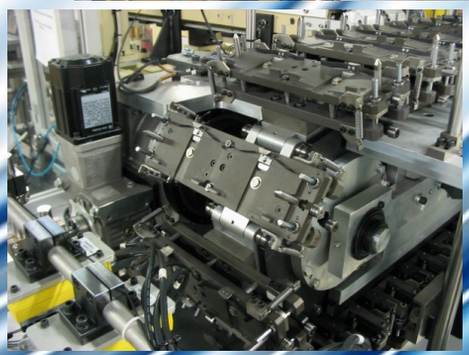


trans & MOTAUTO WORLD

YEAR I, ISSUE 3/2016, ISSN 2367-8399









SCIENTIFIC TECHNICAL UNION OF MECHANICAL INGENEERING
108 RAKOVSKI STR., SOFIA 1000, BULGARIA

INTERNATIONAL SCIENTIFIC JOURNAL

TRANS MOTAUTO WORLD

PUBLISHER:

SCIENTIFIC TECHNICAL UNION OF MECHANICAL ENGINEERING

108, Rakovski Str., 1000 Sofia, Bulgaria
tel. (+359 2) 987 72 90,
tel./fax (+359 2) 986 22 40,
office@stumejournals.com

ISSN 2367-8399
YEAR I, ISSUE 3 / 2016

EDITORIAL BOARD

CHIEF EDITOR
Prof. Petar Kolev, Bulgaria

RESPONSIBLE SECRETARY:
Prof. Nikolay Tonchev, Bulgaria

MEMBERS:

Prof. Ahmet H. Ertas, TR
Prof. Aleksandar Kostikj, MK
Prof. Andrey Ferenets, RU
Prof. Angel Dimitrov, BG
Prof. Beti Angelevska, MK
Prof. Dainis Berjoza, LV
Prof. Dan Scarpete, RO
Prof. Daniela Todorova, BG
Prof. Emilia Andreeva-Moschen, AT
Prof. Gordana Marunic, HR
Prof. Hristo Stanchev, BG
Prof. Igor Penkov, EE
Prof. Igor Smirnov, UA
Prof. Iliyan Lilov, BG
Prof. Lech Sitnik, PL
Prof. Lilo Kunchev, BG
Prof. Ljudmila Boyko, UA
Prof. Madaminjon Aripdzanov, UZ
Prof. Martin Kendra, SK
Prof. Massimo Borghi, IT
Prof. Murat Dogruel, TR
Prof. Natasa Tomic-Petrovic, RS
Prof. Nikolay Georgiev, BG
Prof. Oleg Sharkov, RU
Prof. Pepo Yordanov, BG
Prof. Polatbeg Zhunisbekov, KZ
Prof. Rosen Ivanov, BG
Prof. Teymuraz Kochadze, GE
Prof. Tomaz Morchadze, GE
Prof. Vadim Zhmud, RU
Prof. Valyo Nikolov, BG
Prof. Zoran Jovanovic, RS

C O N T E N T S

VIRTUAL TESTING ACCORDING TO ECE R66 AS A TOOL FOR ESTIMATING PASSENGER COMPARTMENT SAFETY ON A SNOW GROOMER VEHICLE
Ass. Prof. Nikola Avramov PhD., Prof. Milan Kjosevski PhD., Prof. Petar Simonovski PhD. 3

CONSTRUCTIVE SOLUTIONS TO REDUCE THE NOx AND SOx IN THE MARINE BOILER BURNERS.
Phd Eng. Ivaylo Bakalov 7

ANALYSIS OF A COMBINED CASE OF INTERNAL AND EXTERNAL RESONANCES FOR A QUADRATIC COUPLED PITCH – ROLL SHIP
Assoc. Prof. Dr. Deleanu D. 10

STABILITY OF NONLINEAR AUTONOMOUS SYSTEMS WITH TWO DEGREES OF FREEDOM. AN ANALYTICAL STUDY
Prof. DSc. Nikolov S. PhD., M.Sc. Nedkova N. 14

VEGETABLE OILS AS ALTERNATIVE FUEL FOR NEW GENERATION OF DIESEL ENGINES. A REVIEW
PhD Student Eng. Vrabie V., Prof. Dr. Eng. Scarpete D., PhD Student Eng. Zbarcea O. 18

DETERMINING THE EFFECTS OF CANOLA BIODIESEL ON ENGINE PERFORMANCE AND TORQUE RISE
Prof. Dr. Sessiz A., Assoc. Dr. Bayhan Y., Assoc.Dr. Sümer S. K., Phd. Student Erol O. 23

DEVLOPMENT AND STUDY OF A MATHEMATICAL MODEL USED IN THE AUTOMATIC CONTROL SYSTEMS OF SMALL-SIZE UAVS
M.Sc. Kambushev M. PhD., M.Sc. Biliderov S. PhD. 27

1D SIMULATION AS AN ELEMENT OF AN EFFICIENT METHODOLOGY FOR ENGINE CONCEPT DEVELOPMENT
Dr. Dimitrov D., Dr. Pirker G., Dr. Schnessl E., Prof. Dr. Wimmer A. 31

THE INFLUENCE OF VEHICLE OPERATION ON THE BRAKE FLUID BOILING POINT
Ing. Skrucany T., Ing. Semanova S., dr hab. inz. Tomasz Figlus. , Bc. Scurok O. 35

DATABASE DESIGN AT SYNTHESIS OF ELECTROMECHANICAL MODULES
Assoc. Prof. Dahterova D., M. Eng. Nikolova I. 38

VIRTUAL TESTING ACCORDING TO ECE R66 AS A TOOL FOR ESTIMATING PASSENGER COMPARTMENT SAFETY ON A SNOW GROOMER VEHICLE

Ass. Prof. Nikola Avramov PhD., Prof. Milan Kjosevski PhD., Prof. Petar Simonovski PhD.
nikola.avramov@mf.edu.mk, milan.kjosevski@mf.edu.mk, petar.simonovski@mf.edu.mk
Faculty of Mechanical Engineering – Skopje, Macedonia

Abstract: *The concept of virtual testing is generally used method for understanding the structures behavior during loading. It can be used as accurate replacement of real tests only if they are correctly modeled and verified. The regulation UNECE R66 is uniform technical prescription concerning the approval of large passenger vehicles with regard to the strength of their super structure. The rollover test is the basic approval test, but virtual tests can be the adequate testing methods of the physical test. The verified computer simulation according to the regulation can be equivalent approval method. There is a need that snow groomer vehicle sometimes accommodates larger number of people (for sport, work or rescue missions). Because of the terrain those vehicles have to pass, there is significant danger of rollover. So far, there are no regulations for testing of such a superstructure. This paper describes the effort and results in the use of virtual testing according to ECE R66 as a tool for estimating the safety of passengers inside such a vehicle. A computer simulation of a rollover test of the snow groomer vehicle was made. The virtual test was conducted according to the ECE R66 which allows this kind of testing. By following the standard guidelines for computer simulation of a rollover test the vehicle superstructure was analyzed. Series of virtual test were carried for meeting the standard requirements and the customer needs. The final snow groomer superstructure had to undertake serious reinforcement considering the passengers surviving area.*

Keywords: SNOW GROOMER, PASSENGER COMPARTMENT, VIRTUAL TESTING

1. Introduction

Snow groomer vehicles are powered by tracks, equipped with front mounted blades and snow cutter at the back. Their main application is maintaining ski slopes during winter time. They can handle very steep slopes as a result of their low centre of gravity, large width and large contact area. Snow groomer can be used to transport employees at the skiing centers, rescuing injured skiers or touristic sightseeing. Some of these activities can be replaced by cable cars. But the only mean of transport for carrying enthusiastic skiers up the hills for off-track skiing is the snow groomer. For that reason one running snow groomer was adopted for passenger transport, Figure 1. The vehicle had to be equipped with passenger cabin for transporting maximum 12 people. Because of no passenger compartment safety regulation for this kind of specialized vehicles, one existing regulation for large passenger transport was used. The worst scenario that can arise during transportation on the mountain hills is the case when the vehicle rolls over one of its sides. For that reason ECE R66 regulation rollover test of large passenger vehicles was preformed. The initial compartment design was provided and virtual simulations were conducted according to the regulation.



Fig. 1 *Snow groomer Piston Bully 200 with the model of the passenger cabin*

2. Challenges of use ECE R66 as a virtual testing procedure

The large passenger vehicles should have superstructure that will ensure maximum safety of passengers during rollover. Or in other words after a rollover the surviving area should be provided. According to the regulation no part of the vehicle which is outside of the passenger surviving area or the residual space should intrude during the test. Parts that are already in that space can remain there. The residual space is continuous in the passenger, crew and the driver compartment between the furthermost and the front plane in the vehicle. It is defined as a vertical plane moving trough the length of the vehicle limited with straight lines. The boundary lines of the vertical plane are trough the Sr points on both sides of the vehicle. The Sr points are positioned on the seat-back on each passenger seat, 500 mm above the floor under the seat and 150mm from the inside surface of the side wall, as presented on Figure 2 [1].

The rollover test is an approval test for strength of the large passenger vehicle superstructure. It is a lateral tilting test with the following basic characteristics. The complete vehicle is standing on a tilting platform with a blocked suspension. It is slowly tilted to its unstable equilibrium position with the axis of rotation that runs trough the wheel-ground contact points. The vehicle overturns into a ditch with depth of 800mm, Figure 3. For equivalent approval test one of the following stated approval tests can be carried out: rollover test on a body section, quasi-static loading test on a body section, quasi-static calculations based on the results of component tests and computer simulation via dynamic calculations [2]. The basic challenge is to fully represent the tested vehicle behavior. Virtual testing is more economical compared to the real crash tests and as well time consuming procedure for evaluating different behaviors. A lot of parameters can influence the simulation output, especially in the case of impact analysis. Impact or the impulse is a sudden increase in force compared to the static, quasi static or dynamic analysis. This sudden change of structure behavior can lead to numerical instabilities of the solver in the virtual environment.

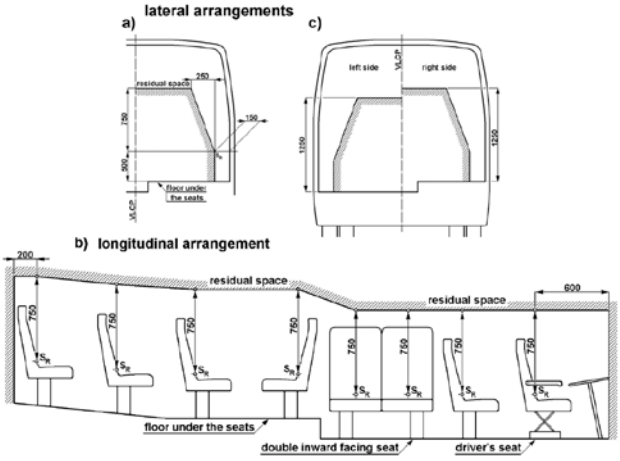


Fig. 2 *Specification of the residual space - passenger surviving area (source: E/ECE/324; E/ECE/TRANS/505; Rev.1/Add.65/Rev.1; Regulation No.66, page 14, 22 February 2006)*

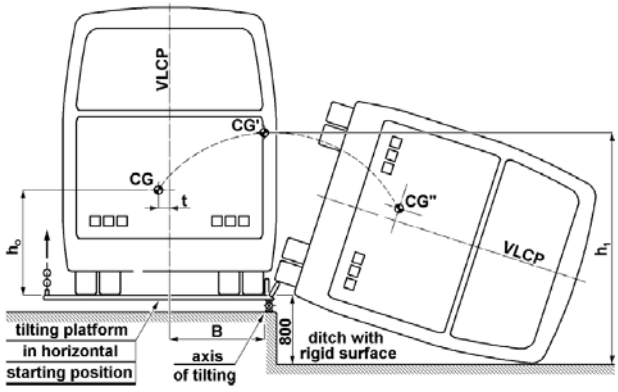


Fig. 3 *Specification of the vehicle rollover test (source: E/ECE/324; E/ECE/TRANS/505; Rev.1/Add.65/Rev.1; Regulation No.66, page 15, 22 February 2006)*

3. FEM model

The snow groomer passenger compartment is a cabin for 10-12 people together with a space for baggage. Passengers are seating backwards to the vehicle driving direction and the baggage area is on the side of the driver seating position. For bringing the model behavior more realistic and on the other side lowering the simulation time some adjustments had to be done:

- the show groomer is modeled with shell elements as hollow block. The block mass is defined as the vehicle total weight and it is achieved using element mass. Also it is rigid and no deformation on the snow groomer can occur, and it is also rigidly connected to the passenger compartment. The dimensions on the block are the outer dimension of the snow groomer, Figure 4.

- for accurate representation on the vehicle during roll over the position of the centre of gravity was defined as the position of the vehicle itself raised for the centre of gravity of the compartment together with the mass of the crew and baggage.

- all the compartment elements are modeled as shell triangular and quadratic elements with three integration points. The number of elements of the passenger compartment is 120814 and the element size is 15mm. All of the parts are connected using spot weld elements. The material properties are some of the examined parameters. The numerical simulation runs for 18 hours on a stand-alone 8 core 2.5GHz CPU with 16 GB of RAM.

- element mass was used on all of the compartment nodes. Element mass is a virtual mass that is added on the elements without changing the parts inertial properties. In this case it was used to achieve the weight of the passengers together with the baggage in the virtual simulation of the rollover test, Figure 5.

- contact surface to surface was defined between the square block representing the snow groomer and the tilting platform. One of the problems that were faced during the modeling was contact between two rigid bodies. In our case that was the rigid block and platform. This was overcome by first defining surfaces that will be in contact and then the contact type that prevents penetration between master nodes and slave elements.

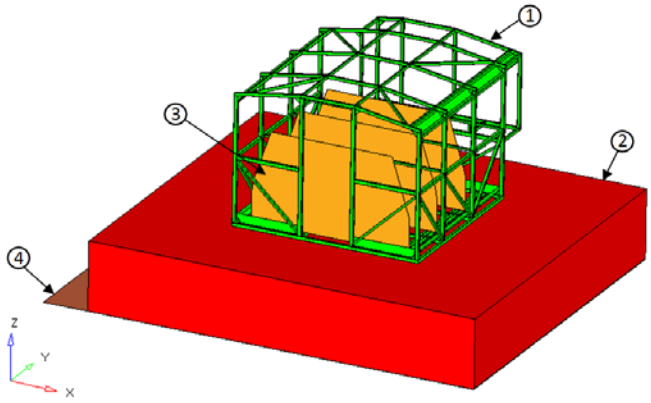


Fig. 4 *Virtual model components 1) passenger compartment 2) snow groomer vehicle 3)passenger surviving area 4) tilting platform*

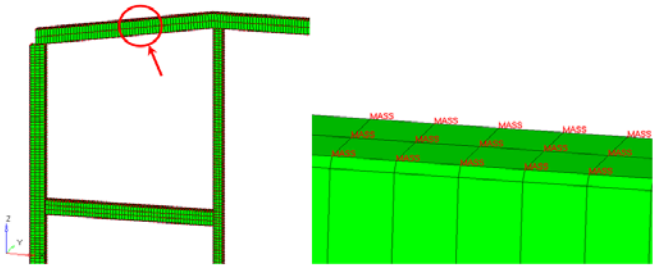


Fig. 5 *FEM element mass distribution*

4. Performing virtual testing

The virtual testing procedure according to the ECE R66 with a tilting platform was conducted on a passenger compartment together with the snow groomer. The compartment itself should be strong enough to restrain the inertial mass of the rigid block during rollover. The starting angle of rotation 75° is used as a point before which no change in the conditions occurs. The rollover happens after the rotation angle of 75°. The results are compared with the prescribed values in the standard. Or the minimum surviving area for group of passengers in the compartment are boundary limits from the sidewalls, top and bottom [1]. In the following are given some of the parameters of the virtual simulation:

- the snow groomer mass or the shell block in the model weights 7.3t. This is the vehicle mass given in the technical sheets.

- the passenger compartment, structure only without passengers, weights 517kg.

- for 12 passenger, each with average weight of 68kg plus 3kg of baggage gives 71kg. The total weight of 12 passengers together with baggage is 812kg.

- the rotation angular velocity is 0.1 radians/sec and that is equal to 5.7 degrees/sec.

- the passenger compartment or its frame is made out of square and rectangular steel tubes with thickness of 3mm. Each of them is made either S235JR or S355J2 according to the European designation system (EN10027) [3]. The minimum yield strength or

the yielding point for the first steel is Reh=235 MPa and Reh=355 MPa for the second.

Virtual testing procedures are known methods often used by the author as a tool for acknowledging structures behavior. One example where mathematical model was verified by laboratory experiment is the doctoral thesis realized by the author. The connection between two guardrail segments as part of the highway infrastructure was analyzed. According to the thesis methodology first one quasi-static experiment was conducted of the bolted connection between two segments and then the same experiment was mathematically modeled [4]. The experiment was used as verification mean after which model improvements were following. The same modeling techniques were used in these simulations as well.

5. Improvement of the body structure through analysis of test results

The virtual simulations were carried out as a co-simulation where HyperMesh was used for preparing the finite element models and analysis were done in the solver LsDyna. The initial and the boundary conditions or the model limitations were determined according to the standard ECE R66 [5][6].

The total mass and the centre of gravity position used in the mathematical model are identical to those of the vehicle to be approved. The friction coefficient used in the ground contact is considered so that produces conservative results. All possible physical contacts are modeled. The simulation runs from the equilibrium position till the maximum deformation. The energy and its components are calculated on every incremental time step. A lot of problems were faced defining the time step. It was computed based on the smallest element mass increased by the scale factor for resolving numerical instabilities. Non-physical mass is added to certain elements to increase stability in dynamic analysis. This can affect the outcome in a manner of inertial forces (F=m·a) and it has to be closely monitored to get good results. Numerous simulations were run and each of them with different sets of reinforcements. At first one rollover test was simulated on the preliminary passenger compartment provided as a CAD model without the trapezium inside, representing the passenger residual space. With the same impact conditions the cabin was completely wrecked by the block. Some of the modifications are shown and explained using the pictures below.

- changing the material properties of the cabin

The picture presents two identical compartments considering their construction, or no reinforcement on the compartment was made. The only difference is the material used in the FEM model. The first cabin was modeled with material structural steel S235JR as a widely used material for structure beams. The second cabin is modeled using also structural steel but with different properties S355J2. Despite the fact that the materials have different yielding point or the point where the material elastic properties end and the plasticity starts to happen. The main reason for using different type of steel is maintaining the same impact property in Joules but on different temperature ranges. The first steel has impact energy of 27 Joules but tested on room temperature (or 20°C) and the second has the same impact properties but tested on -20 degrees. This is important considering the fact that the snow groomer vehicle will be used on low environment temperatures and has to maintain impact strength on this temperature. On the left side of the picture can be seen the maximum stress in unit MPa that is reached in the most stressed elements. On the first figure the upper corner which is the initial impacting point is highly deformed and the compartment leans on the rigid trapezium simulating the surviving area. If the deformation reaches the trapezium means that it is entering inside the residual space which considering the standard is not allowed. The difference in the structure response is evident, Figure 6.

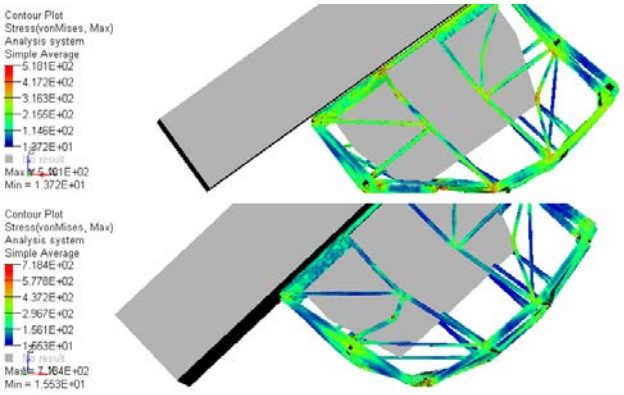


Fig. 6 *Virtual simulation of a rollover test of passenger cabin made from a) steel S235JR and b) steel S355J2*

Based on engineering practice and knowledge the cabin itself shouldn't be designed as stiff as possible. High inertial forces arising from the weight of the snow groomer and the sudden impact will provide enormous accelerations in the compartment. That main challenge is to construct the structure in a way to damp that huge amount of energy so that less will be transferred to the cabin.

- reinforcement using corner elements and double beams

One of the main reasons for buckling the compartment was the first contact between the upper corner of the cabin and the ground. Based on that conclusion the corners were reinforced with lager supports (as shown on Figure 7 a). Also the vertical UNP120 beams were closed having rectangular cross section. The reason is the higher bending moment of inertia of a closed area compared to the open profile of the beam. The second modification is reinforcing cabin structure by increasing the moment of inertia on the cabin roll bars. The residual space that will insure the passenger safety during vehicle rollover can be provided by constructing "cage" around that area. For that reason the beams were reinforced by second attached beam, at the begging and the end of the compartment (shown on Figure 7 b).

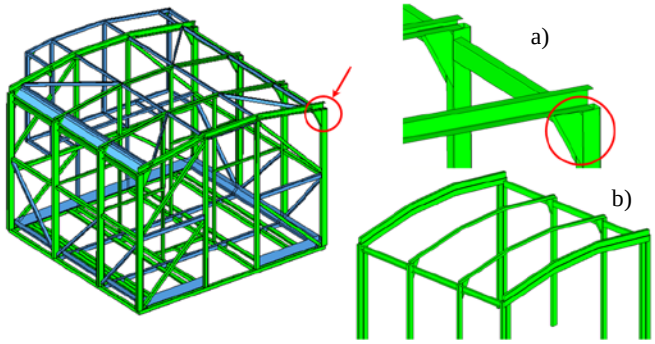


Fig. 7 *Modifications in the passenger compartment using a) corner reinforcement and closed profile vertical beams b) double beams*

The stress contour diagrams of the virtual simulations with the explained modifications are presented. The first situation with the corner reinforcing element dislocates the deformation but it is still reaching the passenger residual area. Compared with the stress state on the cabin made from steel S235JR can be noticed that the deformation expands in the direction of the passenger door seen as two vertical beams in the middle of the cabin front. The second modification is with double beams around the cabin. In this case the cabin remains its rectangular shape which because of the impact is just skewed, Figure 8. Still as mentioned before the impacting energy is not damped by the cabin deformation and as a result the compartment trapezium sustains on the ground.

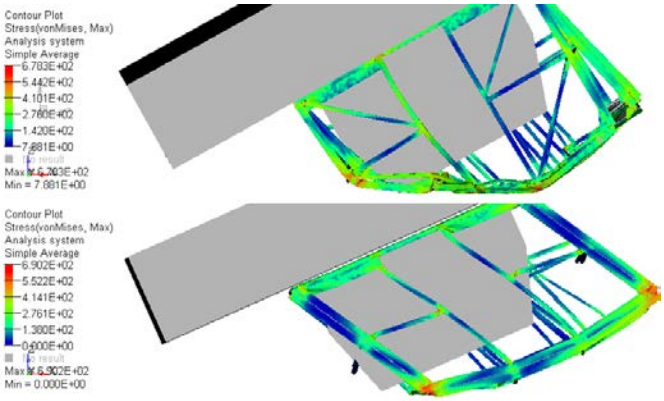


Fig. 8 *Virtual simulation of a rollover test of passenger cabin with a) corner reinforcement and closed profile vertical beams b) double beams*

- reinforcement using front and back windows frames

The most important role for keeping the passenger compartment intact in rollover test has the cabin roll bars. The front and back side of the cabin are reinforced by using other windows frames beside the existing ones. By using virtual simulations was concluded that the cabin response was much better in this case compared to the reinforcement by using just diagonal beams connecting opposite corners of the windows. Other reason not to use diagonal beams is that the window view would be as well ruined. Different offsets of the additional windows frames were tried by different simulations so that the output considering the standard will be satisfied and the maximum of the window glazing surface will be left. On the Figure 9 are shown virtual simulations with wide and narrow windows frames. Simulations were run and the satisfactory results considering the compartment strength were obtained. For strengthening not just the front and the back of the cabin other modification were done in the vehicle longitudinal direction.

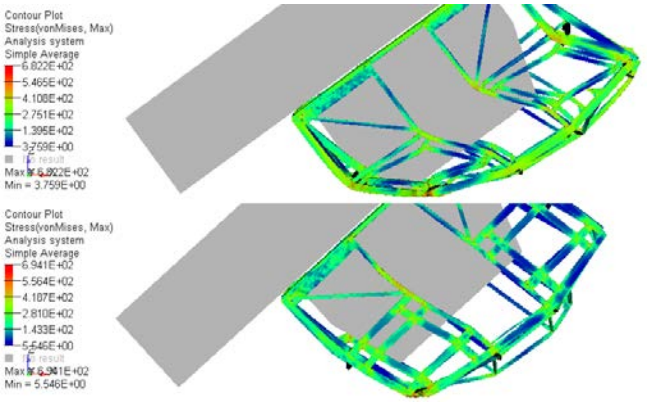


Fig. 9 *Virtual simulation of a rollover test of passenger cabin with a) wide windows frames b) narrow windows frames*

From the numerous simulations that were run below is presented the final reinforced cabin. First the stiffer compartment response during rollover was accomplished by using the material S355J2. Making the entire cabin from this material will be more expensive and more rigid solution. This as explained will lead to huge inertial force in the passenger compartment. The cabin in that case will not reside on the place of impact but because of the lack of deformation it will roll over downhill. The basic idea is to accept as mush as possible impact energy and that can only be done by structure deformation till the permitted values. The meaning of the roll bar structure was explained and achieved by larger top and vertical beams, another windows frame at the front / back side of the cabin. Also poles were positioned beside each seating place and they could be used as hand holders as well. These poles had the task of supporting the upper beams and undertaking some of the impacting energy trough the length of the passenger compartment. With red color are marked the elements made from steel S355J2, Figure 10 b.

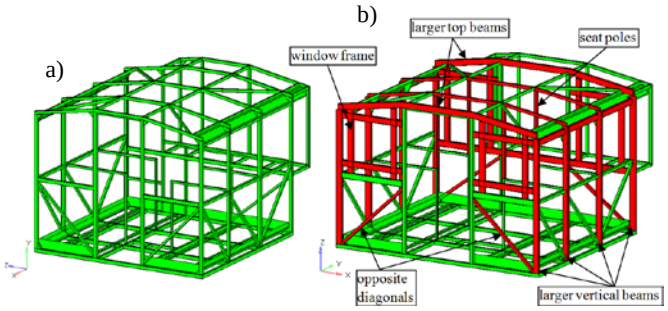


Fig. 10 *a) Preliminary passenger compartment b) Final reinforced passenger compartment*

6. Conclusions

The research effort towards analyzing snow groomer passenger structure using a computer simulations and its compliance with the regulation ECE R66 provided acceptable solution frame and large experience in the area of virtual testing as well. The developed virtual test model is capable of describing the real physical behavior of the rollover test. Proving the validity of the mathematical model and verifying the assumptions made in the model are based on the engineering practice with numerical models in similar tasks. It is expected full experimental validation process to follow that will confirm usability of the virtual testing procedure. The simulation program produces a stable solution, in which the result is independent of incremental time step. Non-physical energy components produced by the process of mathematical modeling for example the "hourglass" energy is less than the 5% of the total energy at any time. The simulation runs before the first unstable situation until maximum deformation is reached. Granting the conformity was possible only without reducing the residual space after the rollover test. This was accomplished by series of structural modifications. The basic challenge to strengthen the passenger compartment without enlarging the cabin inertial accelerations was accomplished.

7. References

[1] European Regulation, E/ECE/324; E/ECE/TRANS/505; Rev.1/Add.65/Rev.1, "Uniform technical prescriptions concerning the approval of large passenger vehicles with regard to the strength of their superstructure", 22 February 2006.

[2] Kadir Elitok, Dr. Mehmet A. Guler, Bertan Bayram, Dr.Ing Ulrich Stelzmann, "An investigation on the roll-over crashworthiness of an intercity coach, influence of seat structure and passenger weight", 9th International LS-DYNA Users Conference, p.17-34.

[3] European Standard, CEN, EN10027-1:2005, "Designation systems for steels – Part1: Steel names", 27 June, 2005.

[4] Nikola Avramov, "The influence of the construction parameters on the risk of separating the guardrail segments under vehicle run off", Doctoral thesis, Faculty of Mechanical Engineering, Department of Mechanical Constructions, Mechanization and Vehicles, Skopje, 24 April 2015.

[5] Bronislaw D. Gepner, "Rollover procedures for crashworthiness assessment of Para-transit bus structures", Doctoral thesis, Florida State University, Department of Civil and Environmental engineering, 2014.

[6] U.S. Department of Transportation, FMVSS 220, "School Bus Rollover Protection", National Highway Traffic Safety Administration, Laboratory test procedure, 16th of July, 1991.

CONSTRUCTIVE SOLUTIONS TO REDUCE THE NOx AND SOx IN THE MARINE BOILER BURNERS.

Phd Eng. Ivaylo Bakalov[1]

Faculty of "Engineering" – “N.Y. Vaptsarov” Naval Academy, Bulgaria[1]

Abstract:. *The modern world is facing two challenges - firstly, the energy crisis related to fuel the other - environmental degradation, especially in the form of air pollution and its consequences - climate change. The regulations demand specifically a significant reduction of sulphur oxide combinations (SOx), carbon dioxide (CO_2) and nitrogen oxide combinations (NOx).*

Keywords:*burner, combustion of fuel in boilers, reduction of sulphur oxide combinations (SOx), nitrogen oxide combinations (NOx), hook-up control box, heat transfer.*

1. Introduction

The modern world is facing two challenges - firstly, the energy crisis related to fuel the other - environmental pollution, especially in the form of air pollution and its consequences - climate change [1-3].

Fuel represents 3/4 of the transport costs for ships carrying oil (tankers). An international ship trading company uses more than 370 million tons of fuel each year [5], in terms of sustained upward trend in the prices of heavy fuel used in the operation of main marine diesel engines.

High oil prices leads to a spiraling increase in the prices of many goods and services production chain associated with an increase in the prices of maritime transport.

A boiler burner is a device in which fuel and air are mixed in order to provide efficient combustion and to generate heat power. A continuous combustion process of gas and liquid fuels is ensured by means of burners. Modern fuel oil burners are complex devices consisting of many components. These burners comprise different types of control and adjustment systems. Fuel oil burners are manufactured as separate modules that can be fitted to different types of burners [4].

2. Problem discussion

There are several technically and economically acceptable techniques for reducing emissions. In economic terms, these techniques are much more efficient than previous methods of reducing emissions. Methods to reduce emissions of sulfur dioxide are switching from fuels with high sulfur content to those with low sulfur content and the introduction of technology to purify.

3. Objective and research methodologies

A lot of parameters affect the quality of the combustion process and the resulting emissions. These include burner adjustment, geometry of the furnace, fuel pressure, maximum values of the temperature and the pressure in the combustion chamber (furnace space), values of the air temperature and pressure [1]. The fuel atomization can be optimized further in the operational process through analysis of the burner flame by means of the testing station.

Flame combustion is accomplished by means of burners. It is widely spread. This is the oldest method for fuel burning. It is used in boilers, furnaces, technological equipment and engines. With this type of combustion the flame is a stable flame in a regular shape. The shape of the flame depends on;

- type (form and design) of the burner;
- the degree of mixing of fuel and oxidant;
- the stream of the burning mixture.

The front of the flame is the boundary between the core and the ignition area. The core is an area where the main ignition parameters are formed. The shape and the size are determined by the intensity of the mixing of the fuel and the oxidant.

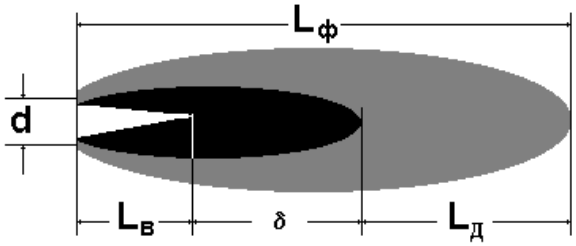


Fig.1 A scheme of flame combustion

L_B - ignition area
D – combustion front, has thickness less than L_B and L_ϕ
L_L – forcing area; has an elliptical shape
L_ϕ – length of flame as a whole; has an elliptical shape

The flame is externally seen as one dark cone with a light elliptical area. The efficiency of combustion is determined by the total length of the flame [4].

The German manufacturer, SAACKE recently unveiled their low NOx boiler ship FMB-VF, specially designed to reduce NOx emission [6] – see Fig.2.

The boiler have the following characteristics:

– Vertical two-pass fired boiler;
– Design allows very high operational reliability;
– Designed to incorporate proven low NO_X Combustion Systems;
– Flue gas recirculation enables compliance with current and known future emission regulations;
– Optional water injection possible.

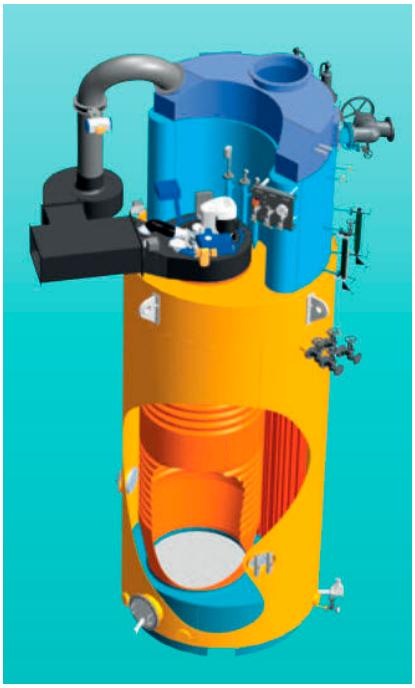


Fig. 2 Fired Marine Boiler SAACKE FMB-VF

The FMB-VF-LONOX is a vertical two-pass fired boiler. Heat transfer is performed through the corrugated or plain flame tube furnace and a number of plain smoke tubes. The design of the flame tube entrance for burner mounting allows a minimum of burner refractory which significantly enhances operational reliability.

The FMB-VF-LONOX boiler is designed to incorporate proven Low NOX Combustion Systems. In order to meet lowest emission levels the boiler package is equipped with flue gas recirculation. Flue gas recirculation, in conjunction with Marine Gas Oil (MGO) fuels, enables compliance with current and known future emission regulations and will allow boiler operation in ports worldwide. For Heavy Fuel Oil (HFO) firing the combustion system can be equipped with water injection to improve solid particle emission levels.

The burner has a rotary type, it can work with more types of fuel, and gas. Rotating cup burners have been developed as a result of the efforts to eliminate the usage of steam (air) when atomizing HFO and to ensure efficient performance for all modes of operation. With the rotating cup burners the fuel is atomized centrifugally. Various designs of this type of burners exist [4].

Rotating cup burners are the most sophisticated type of burners at present. Atomization is accomplished by means of a conical cup rotating at a speed of 4500÷8000 rev/min. They have the following characteristics:

- reliable, not sensitive to the degree of purity of fuel due to the lack of narrow channels;
- there are no high-pressure and high temperature pipelines that involve risks and dangers;
- depth adjustment d=18÷20;
- fully automated;
- complex design; hard to repair;
- efficiency depends on the change in the orifice section of the fuel channel;
- the primary atomizing air stream can be supplied by the main fan but more often it comes from a fan mounted on a common axis with the rotary cup and moving along with it – fig 3.

SAACKE Marine System has designed a system for delivering fuel and improvements in settings it is possible to adapt to all types of marine boilers. Design etc. "hook-up control box" is made in such a way that each type of boiler control panels can be revamped to safely and reliably burning light fuel without modification of existing PLC programs.

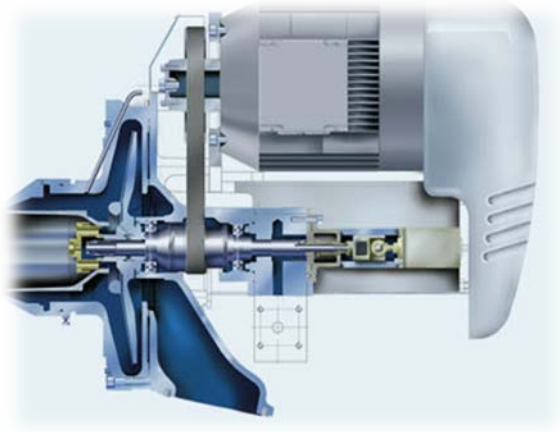




Fig.3 Rotating cup burner

All necessary additional control, signal and safety loops that are necessary for reliable and safelight fuel oil combustion are contained inside the hook-up control box. The interaction between the hook-up control box and the original boiler/burner control panel is solely made by hard-wired signal transfer from/to already existing (or duplicated) input/output terminals of the original boiler/burner controls.

In this way, any modification of the existing approved burner sequence controls and/or PLC programs is avoided, so that the already given approval of the original system is not invalidated by the modification.

Additonal safety shut-downs required in light fuel oil combustion mode are implemented into the existing hard-wired safety circuit by adding the corresponding number of relays, triggered by signals from the hook-up control box. The function of those can be easily confirmed during the function test in presence of classification surveyor after completion of the modification works [6].

Summary of features of the SAACKE Marine Systems solution:

- Complete separation of LSFO (MGO) and HSFO systems and 100% protection of the LSFO storage and service tanks from contamination with HSFO.

- Very short change-over time to LSFO (MGO) without the need to drain the FO circulation piping.

- Very short change-over time back to HSFO. The independent pipeline layout allows for permanent circulation and heating of the HSFO ring line. HSFO pumps to be kept in operation for circulating during LSFO (MGO) mode operation.

- Completely independent and redundant controls for the LSFO (MGO) operation mode. Any failure in the light fuel oil operation mode has no influence on the standard fuel oil operation mode controlled exclusively by the original boiler panel.

- Minimized downtime during system conversion. Due to the completely independent LSFO (MGO) supply system installation, the boiler can be used normally during 90% of the

conversion job duration being supplied by the existing fuel oil system.

- Minimized risk of operator mistakes. Due to the comprehensive but simple automation in the hook-up controls, Operator's tasks to change-over from one operation mode to the other is limited to the activation of one single selector switch.

The SAACKE Marine System upgrade kit for Ultra Low Sulphur Diesel Oil (ULSDO) – MGO combustion consists basically of the following mechanical components, some of which are optional items fig.4:

GO 001 ULSDO (MGO) double pump station. Specially designed for operation on low viscosity fuel

GO 004 ULSDO (MGO) suction thermometer

GO 006 Stand-by / low pressure alarm switch

GO 007 Pressure switch/gauge root valve

GO 015 Burner inlet automatic change-over valve with electro-pneumatic drive

GO 016 Burner outlet automatic change-over valve with electro-pneumatic drive

GO 020 ULSDO (MGO) non-return valve

GO 023 ULSDO (MGO) safety valve

GO 025 ULSDO (MGO) temperature transmitter

GO 028 ULSDO (MGO) radiation cooler

GO 030 Control air filter regulator

GO 033 Control air pressure monitor

GO 050 ULSDO (MGO) adjustable overflow pressure limiting/control valve

GO 058 Shut-off / By-pass valve for GO 050

GO 060 ULSDO (MGO) suction line shut-off valve

GO 062 ULSDO (MGO) pump station isolating valve

The SAACKE MARINE SYSTEMS upgrade kit for ULSDO (MGO) combustion also includes the following electrical components:

CGO 010 Hook-up control box for ULSDO (MGO) combustion mode control including MGO

pump motor starters

CGO 118 Remote indication display with alarm output for MGO temperature

CGO 131 Local manual stop/repair switch for ULSDO (MGO) pumps

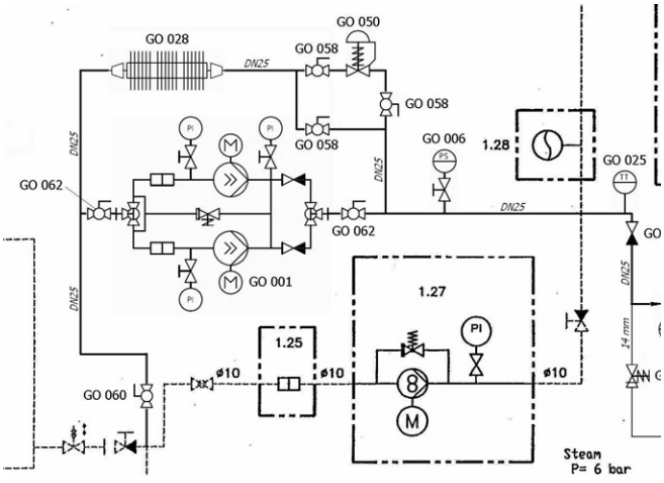


Fig.4 The SAACKE Marine System upgrade kit for ULSDO (MGO)

Upgrade SAACKE Marine System LSFO to provide a separate supply system for low-sulfur content fuel with low viscosity from storage to combustion devices. Initially, the system draws fuel from the reserve tank for light fuel using a pump. Usually the delivery of low-sulfur content fuel with low viscosity is done by screw pump specifically designed and designated for such types of fuels. The fuel passes through the valve GO 060, then through GO 062 and enters the suction side of the pump, wherein there is a filter. From there, the fuel passes through the pump. At the outlet from the pump passes through the tap GO 062. There are 2 loops. The fuel reaches the non-return valve GO 020, which dropped from white to black. This valve is designed to prevent the entry of another type of fuel. The device temperature GO 025 shows the current temperature of the fuel in the pipeline. PSL GO 006/7 is a device for pressure, which maintains the pressure in the system within certain limits. If the pressure falls below a certain value, PSL signal to the computer. The pressure regulator GO 050 is a valve that regulates the pressure of the system (running from 2.1 to 2.5 bar). It is a valve with a spring, which means that if the pressure drop - the valve is opened, and if the pressure rises - the valve is slightly closed. Thus, to maintain constant pressure in the system. This valve connects the suction GO 050 with the discharge side of the pump. The valve GO 058 is a bypass in case you need to repair GO 050 (pressure regulator). The cooler fuel GO 020 serves to maintain the fuel temperature within certain limits.

Boiler run on automatic mode. First goes the fan to purge the furnace. With the departure of fan and pump starts. While the boiler makes blowing, fuel burner valves are closed. Then we have to fuel changeover valve GO 015. Solenoid valves GO 015 definitions if the system running on fuel oil or gas oil. The system is filled with fuel and valve GO 050 maintains a constant pressure, because there is still no fuel. Fuel stop at GO 015 - the valves on the boiler. Once the pressure reached 2.5 bar the three-way valves are opened. When the valve of the boiler is opened, is obtained differential pressure with the pressure regulator GO 050 opens to compensate for the pressure loss.

While the pressure in the system reaches 2.5 bar, the fuel is rotated in the small circle. It maintains a constant temperature of the fuel. The cooler GO 028 is fuel-air type, it passes inside a fuel from outside and is blown from the air. GO 023 is a safety valve. Adjust the pressure slightly higher than what is set pressure regulator GO 050. In the event that becomes a system crash or GO 050 blocks, system pressure will increase and the valve GO 023 will open. Then Gas system will connect to the Fuel Oil System. This will unload system. GO valve 023 will remain open until the system pressure drops below a set point-in which is set.

4. Conclusion

Requirements regarding the purity of exhaust gases from the burners of the ship's boilers will continue to rise. The tendency to introduce increasingly strict limits on greenhouse gas emissions is a result of measures taken to reduce their destructive effect on the environment. The modern statutory requirements for environmental protection include strict restrictions in relation with sulphur admixtures in different types of fuels such as F.O., light fuel oil, heavy fuel oil, and diesel oil. These sulphur limits are already in force for the sea areas defined as SECA (Sulfur Emission Control Area) and they comprise the North Sea, the Baltic Sea, North America and Canada as well as all European Union ports.

5. Literature

1. Van Gerpen J, Shanks B, Pruszko R, Clements D, Knothe G, Biodiesel production technology. National Renewable Energy Laboratory, NRRL/SR-510-3624424 2 Introduction to Biodiesel Production, 2004.

2. Van Gerpen J, Shanks B, Pruszko R, Clements D, Knothe G,Biodiesel analytical methods. National Renewable Energy Laboratory, NRRL/SR-510-36240, 2004.

3. Romano SD, González Suárez E, Laborde MA, Biodiesel. In: Combustibles Alternativos, 2nd edn. Ediciones Cooperativas, Buenos Aires, 2006.

4. Bakalov I, "A TESTING STATION FOR STUDYING THE COMBUSTION OF FUEL WITH MECHANICAL CENTRIFUGAL AND ROTATING CUP BURNERS" Machines Technologies Materials – Issue 8 / 2015 ISSN 1313-0226 / p. 11 – 13

5. http://freightinvestorservices.com/

6. http://www.saacke.com/products

ANALYSIS OF A COMBINED CASE OF INTERNAL AND EXTERNAL RESONANCES FOR A QUADRATIC COUPLED PITCH – ROLL SHIP

Assoc. Prof. Dr. Deleanu D.
Faculty of Naval Electro mechanics - Maritime University of Constanta, Romania
dumitrudeleanu@yahool.com

Abstract: *In the paper, a two-degrees-of-freedom ship model with quadratic coupled pitch and roll modes under sinusoidal harmonic excitation is considered. A straightforward expansion allows for obtaining both the resonant values of external excitation frequency and one internal resonance. The Multiple Scales method yields the first-order expansions for the special resonant case where the excitation frequency is close to the roll frequency. The time series and the frequency – amplitude curves provided by numerical integration are contrasted with those given by the perturbation technique for different combination of system's parameters. If the parameters are selected within the pre-ordered range, the results of both methods are in excellent or, at least, in pretty good agreement.*

Keywords: SHIP ROLLING AND PITCHING, MULTIPLE SCALES, INTERNAL AND EXTERNAL RESONANCES

1. Introduction

Ship motion in waves is a strongly non-linear and multivariable dynamic process whose complete description requires mathematical models with six degrees of freedom. Among them, rolling has the biggest influence on ship's stability. For this reason, one degree of freedom models considering the uncoupled roll motion have been widely proposed by the scientific community [1-4] . The models are useful, for example, to obtain insight into the parametric roll resonance phenomenon, but they have too little complexity for describing the entire behavior of the ship. Since the coupling between the roll and other modes of motion was found to be extremely important in the correlation of the theoretical and experimental results, mathematical models following an increasing sophistication and capable of predicting well enough the ship dynamics for some given operational conditions have been suggested. Thus, the analysis of ship dynamics and stability by means of two-degrees-of-freedom models has received considerable attention. For example, Haddara and Xu have investigated the free response of a heaving and pitching ship from its stationary response to random waves [5]. Eissa et al. have modeled the interaction of heave and roll by a mass-spring-pendulum system where the effect of waves was included by a periodic forcing term [6]. Pan and co-workers have studied non-stationary responses of a ship model with nonlinearity coupled pitch and roll under modulated excitation [7]. Using the previously mentioned model, Kamel have applied the Multiple Scales method and obtained the bifurcation response equation near the combination resonance case in the presence of internal resonance [8].

Continuing the work of Kamel for giving a picture of the various possible cases, in the paper we retain the condition that the pitch frequency is twice the roll frequency but we seek for the ship response when the excitation (encounter) frequency is close to the roll frequency. The nonlinear coupled differential equations of motion for a ship restrained to pitch and roll modes are as follows

$$\begin{aligned} &\ddot{x}_1+2\varepsilon\mu_1\dot{x}_1+\omega_1^2 x_1+\varepsilon\alpha_1 x_1 x_2=F_1\cos\Omega t\\ &\ddot{x}_2+2\varepsilon\mu_2\dot{x}_2+\omega_2^2 x_2+\varepsilon\alpha_2 x_1^2=F_2\cos\Omega t \end{aligned} \tag{1}$$

where x_1 and x_2 are the roll and pitch modal amplitudes, μ_1 and μ_2 the modal damping coefficients, ω_1 and ω_2 the natural angular frequencies, Ω the excitation (wave) frequency, F_1 and F_2 the excitation force amplitudes, α_1 and α_2 the coefficients of nonlinear terms, and ε a small parameter [7]. Finally, the dots stand for the differentiation with respect to time *t*.

2. A Straightforward Expansion for the Coupled Pitch – Roll Equations

In this section we seek for an approximate solution to (1) in the form

$$x_1(t)=x_{10}(t)+\varepsilon x_{11}(t)+\ldots,\ x_2(t)=x_{20}(t)+\varepsilon x_{21}(t)+\ldots \tag{2}$$

Substituting (2) into (1) and equating the each of the coefficients of $\varepsilon^n, n=0,1$, in both parts yields

$$\varepsilon^0:\ \ddot{x}_{10}+\omega_1^2 x_{10}=F_1\cos\Omega t,\quad \ddot{x}_{20}+\omega_2^2 x_{20}=F_2\cos\Omega t \tag{3}$$

$$\begin{aligned} &\varepsilon^1:\ \ddot{x}_{11}+2\mu_1\dot{x}_{10}+\omega_1^2 x_{11}+\alpha_1 x_{10}x_{20}=0,\\ &\ddot{x}_{21}+2\mu_2\dot{x}_{20}+\omega_2^2 x_{21}+\alpha_2 x_{10}^2=0 \end{aligned} \tag{4}$$

The general solution of (3) can be obtained as the sum of a homogeneous solution and a particular solution. It can be expressed as

$$\begin{aligned} x_{10}&=a_1\cos(\omega_1 t+\varphi_1)+\Lambda_1\cos\Omega t\\ x_{20}&=a_2\cos(\omega_2 t+\varphi_2)+\Lambda_2\cos\Omega t \end{aligned} \tag{5}$$

where $\Lambda_1=\dfrac{F_1}{\omega_1^2-\Omega^2}$ and $\Lambda_2=\dfrac{F_2}{\omega_2^2-\Omega^2}$.

Then, (4) becomes

$$\begin{aligned} &\ddot{x}_{11}+\omega_1^2 x_{11}=2\mu_1\omega_1 a_1\sin(\omega_1 t+\varphi_1)+2\mu_1\Lambda_1\Omega\sin\Omega t-\\ &-\alpha_1 a_1 a_2\cos(\omega_1 t+\varphi_1)\cos(\omega_2 t+\varphi_2)-\alpha_1 a_1\Lambda_2\cos(\omega_1 t+\varphi_1)\cdot\\ &\cdot\cos\Omega t-\alpha_1 a_2\Lambda_1\cos(\omega_2 t+\varphi_2)\cos\Omega t-\alpha_1\Lambda_1\Lambda_2\cos^2\Omega t \end{aligned} \tag{6}$$

$$\begin{aligned} &\ddot{x}_{21}+\omega_2^2 x_{21}=2\mu_2\omega_2 a_2\sin(\omega_2 t+\varphi_2)+2\mu_2\Lambda_2\Omega\sin\Omega t-\\ &-\frac{\alpha_2}{2}\left(a_1^2+\Lambda_1^2\right)-\frac{\alpha_2 a_1^2}{2}\cos(2\omega_1 t+2\varphi_1)-\frac{\alpha_2\Lambda_1^2}{2}\cos 2\Omega t-\\ &-\alpha_2 a_1\Lambda_1\cos((\omega_1+\Omega)t+\varphi_1)-\alpha_2 a_1\Lambda_1\cos((\omega_1-\Omega)t+\varphi_1) \end{aligned}$$

Using trigonometric identities and neglecting the homogeneous solution [9, 10], from (6) it follows that

$$\begin{aligned} x_{11}=&-\mu_1 a_1 t\cos(\omega_1 t+\varphi_1)+\frac{\alpha_1 a_1 a_2}{2\omega_2(\omega_2+2\omega_1)}\cos((\omega_1+\omega_2)t+\varphi_1+\varphi_2)\\ &+\frac{2\mu_1\Lambda_1\Omega}{\omega_1^2-\Omega^2}\sin\Omega t+\frac{\alpha_1 a_1 a_2}{2\omega_2(\omega_2-2\omega_1)}\cos((\omega_1-\omega_2)t+\varphi_1-\varphi_2)+\\ &+\frac{\alpha_1 a_1\Lambda_2}{2\Omega(\Omega+2\omega_1)}\cos((\omega_1+\Omega)t+\varphi_1)+\frac{\alpha_1\Lambda_1\Lambda_2}{2(\omega_1+2\Omega)(2\Omega-\omega_1)}\cos 2\Omega t+\\ &+\frac{\alpha_1 a_1\Lambda_2}{2\Omega(\Omega-2\omega_1)}\cos((\omega_1-\Omega)t+\varphi_1)+\frac{\alpha_1 a_2\Lambda_1}{2(\omega_1+\omega_2+\Omega)(\omega_2-\omega_1+\Omega)}\cdot\\ &\cdot\cos((\omega_2+\Omega)t+\varphi_2)+\frac{\alpha_1 a_2\Lambda_1}{2(\omega_1-\omega_2+\Omega)(\Omega-\omega_1-\omega_2)}\cdot \end{aligned}$$

$$\cdot\cos\left(\left(\omega_2-\Omega\right)t+\varphi_2\right)-\frac{\alpha_1 a_1 a_2}{2\omega_1^2} \tag{7}$$

$$x_{21}=-\mu_2 a_2 t\cos\left(\omega_2 t+\varphi_2\right)+\frac{2\mu_2\Lambda_2\Omega}{\omega_2^2-\Omega^2}\sin\Omega t-\frac{\alpha_2\left(a_1^2+\Lambda_1^2\right)}{2\omega_2^2}+$$

$$+\frac{\alpha_2\Lambda_1^2}{2\left(4\Omega^2-\omega_2^2\right)}\cos 2\Omega t+\frac{\alpha_2 a_1\Lambda_1}{\left(\left(\omega_1+\Omega\right)^2-\omega_2^2\right)}\cos\left(\left(\omega_1+\Omega\right)t+\varphi_1\right)+$$

$$+\frac{\alpha_2 a_1^2}{2\left(4\omega_1^2-\omega_2^2\right)}\cos\left(2\omega_1 t+2\varphi_1\right)+\frac{\alpha_2 a_1\Lambda_1}{\left(\left(\Omega-\omega_1\right)^2-\omega_2^2\right)}\cos\left(\left(\omega_1-\Omega\right)t+\varphi_1\right)$$

The approximate solution contains both secular $-\mu_n a_n t\sin\left(\omega_n t+\varphi_n\right),\ n=1,2$ and small-divisor terms. The latter occur when $\Omega\approx 0,\ \Omega\approx\omega_n,\ \Omega\approx\frac{\omega_n}{2},\ n=1,2$, or $\Omega\approx\omega_1-\omega_2,\ \Omega\approx\omega_2-\omega_1,\ \Omega\approx\omega_1+\omega_2,\ \Omega\approx 2\omega_1$ and $\omega_2\approx 2\omega_1$. These special frequencies are called *resonant frequencies* and in their neighborhood the relationships (7) fail to give an accurate approximation for the solutions of (1). In the next section we apply the Multiple Scales method to determine uniform expansions for system (1) that do not contain secular or small-divisor terms in the special case of internal resonance $\omega_2\approx 2\omega_1$ coupled with the primary resonance $\Omega\approx\omega_1$.

3. First – order uniform expansions for coupled pitch – roll

In the combined case of primary resonance, $\Omega\approx\omega_1$, and internal resonance, $\omega_2\approx 2\omega_1$, the small – divisor terms appear both in the first term, x_{10}, of the straightforward expansion (2) and in the terms x_{11} and x_{21}. Through Λ_1, x_{10} becomes very large as $\Omega\to\omega_1$ and the nonlinear and damping terms cease to be of $O(\varepsilon)$. As pointed out by Nayfeh [9], the ordering of the terms in (1) is rendered invalid. Assuming that the excitation amplitude F_1 is relatively small, we let $F_1=\varepsilon f_1$ and seek for uniformly valid expansions of x_1 and x_2, this time by using Multiple Scales method.

We consider two time scales, namely the fast time $T_0=t$ and the slow time $T_1=\varepsilon t$, and expand the dependent variables x_1, x_2 and their derivatives in power series in the small parameter ε

$$\begin{aligned}&x_1=x_{10}\left(T_0,T_1\right)+\varepsilon x_{11}\left(T_0,T_1\right)+...\\&x_2=x_{20}\left(T_0,T_1\right)+\varepsilon x_{21}\left(T_0,T_1\right)+...\\&\frac{d}{dt}=D_0+\varepsilon D_1+...,\ \frac{d^2}{dt^2}=D_0^2+2\varepsilon D_0 D_1+...\end{aligned} \tag{8}$$

where $D_i=\frac{\partial}{\partial T_i}$, $D_i^2=\frac{\partial^2}{\partial T_i^2}$, and $D_i D_j=\frac{\partial^2}{\partial T_i\partial T_j}, i,j\in\{1,2\}$.

Substituting (8) into (1) and equating coefficients of like powers of ε yields the following set of linear partial differential equations which can be solved successively

$$\varepsilon^0\begin{cases}D_0^2 x_{10}+\omega_1^2 x_{10}=0\\ D_0^2 x_{20}+\omega_2^2 x_{20}=F_2\cos\Omega T_0\end{cases} \tag{9}$$

$$\varepsilon^1\begin{cases}D_0^2 x_{11}+\omega_1^2 x_{11}=-2D_0D_1x_{10}-2\mu_1 D_0 x_{10}-\alpha_1 x_{10}x_{20}+\\ \qquad\qquad +f_1\cos\Omega T_0\\ D_0^2 x_{21}+\omega_2^2 x_{21}=-2D_0D_1x_{20}-2\mu_2 D_0 x_{20}-\alpha_2 x_{10}^2\end{cases} \tag{10}$$

The first order solutions of (9) have the form

$$\begin{aligned}&x_{10}=A_{10}\left(T_1\right)\exp\left(i\omega_1 T_0\right)+cc\\&x_{20}=A_{20}\left(T_1\right)\exp\left(i\omega_2 T_0\right)+\frac{\Lambda_2}{2}\exp\left(i\Omega T_0\right)+cc\end{aligned} \tag{11}$$

where *cc* stand for the complex conjugates of the preceding terms. To express the nearness of Ω to ω_1 and of ω_2 to $2\omega_1$ we introduce the detuning parameters σ_1 and σ_2 as follows

$$\Omega=\omega_1+\varepsilon\sigma_1,\omega_2=2\omega_1+\varepsilon\sigma_2 \tag{12}$$

Inserting (11) and (12) into (10), one obtains

$$\begin{aligned}\left(D_0^2+\omega_1^2\right)x_{11}=&\left[-2i\omega_1\left(D_1A_{10}+\mu_1A_{10}\right)+\frac{1}{2}f_1\exp\left(i\sigma_1T_1\right)-\right.\\&\left.-\alpha_1\overline{A}_{10}A_{20}\exp\left(i\sigma_2T_1\right)\right]\exp\left(i\omega_1T_0\right)+NST_1\\\left(D_0^2+\omega_2^2\right)x_{21}=&\left[-2i\omega_2\left(D_1A_{20}+\mu_2A_{20}\right)-\alpha_2A_{10}^2\exp\left(-i\sigma_2T_1\right)\right]\\&\cdot\exp\left(i\omega_2T_0\right)+NST_2\end{aligned} \tag{13}$$

where $NST_{1,2}$ stand for the terms which do not produce secular terms. The later, in (13), will vanish if and only if the coefficients of $\exp\left(i\omega_n T_0\right),\ n=1,2$, are equal to zero

$$\begin{aligned}&-2i\omega_1\left(D_1A_{10}+\mu_1A_{10}\right)-\alpha_1\overline{A}_{10}A_{20}\exp\left(i\sigma_2T_1\right)+\frac{f_1}{2}\exp\left(i\sigma_1T_1\right)=0\\&-2i\omega_2\left(D_1A_{20}+\mu_2A_{20}\right)-\alpha_2A_{10}^2\exp\left(-i\sigma_2T_1\right)=0\end{aligned} \tag{14}$$

We consider now the polar forms of the functions $A_{n0},n=1,2$

$$A_{n0}\left(T_1\right)=\frac{1}{2}a_n\left(T_1\right)\exp\left(i\eta_n\left(T_1\right)\right),\ n=1,2 \tag{15}$$

Inserting (15) into (14) and separating real and imaginary parts gives the following first order differential system of equations

$$\begin{aligned}&a_1'=-\mu_1a_1-\frac{\alpha_1a_1a_2}{4\omega_1}\sin\varphi_2+\frac{f_1}{2\omega_1}\sin\varphi_1\\&a_1\eta_1'=\frac{\alpha_1a_1a_2}{4\omega_1}\cos\varphi_2-\frac{f_1}{2\omega_1}\cos\varphi_1\\&a_2'=-\mu_2a_2+\frac{\alpha_2a_1^2}{4\omega_2}\sin\varphi_2\\&a_2\eta_2'=\frac{\alpha_2a_1^2}{4\omega_2}\cos\varphi_2\end{aligned} \tag{16}$$

where $\varphi_1=\sigma_1T_1-\eta_1,\ \varphi_2=\sigma_2T_1+\eta_2-2\eta_1$, and primes denote the differentiation with respect to slow time T_1.

Observing that $\varphi_1'=\sigma_1-\eta_1',\ \varphi_2'=\sigma_2+\eta_2'-2\eta_1'$, the second and the fourth equations (16) may be rewritten as

$$\begin{aligned}&a_1\varphi_1'=a_1\sigma_1+\frac{f_1}{2\omega_1}\cos\varphi_1-\frac{\alpha_1a_1a_2}{4\omega_1}\cos\varphi_2\\&a_2\varphi_2'=a_2\sigma_2+\frac{a_2f_1}{a_1\omega_1}\cos\varphi_1+\left(\frac{\alpha_2a_1^2}{4\omega_2}-\frac{\alpha_1a_2^2}{2\omega_1}\right)\cos\varphi_2\end{aligned} \tag{17}$$

Thus, the first – order approximate solution for the system (1) is as follows

$$\begin{aligned}&x_1=a_1\cos\left(\omega_1T_0+\eta_1\right)=a_1\cos\left(\Omega t-\varphi_1\right)\\&x_2=a_2\cos\left(\omega_2T_0+\eta_2\right)+\Lambda_2\cos\Omega T_0=\\&\quad=a_2\cos\left(2\Omega t+\varphi_2-2\varphi_1\right)+\Lambda_2\cos\Omega t\end{aligned} \tag{18}$$

where the amplitudes $a_n,n=1,2$, and phases $\varphi_n,n=1,2$, are given by (16) and (17) after returning to the normal time *t*.

As we will see in the next section, the functions $a_n,\varphi_n,n=1,2$ tend to constant values as time *t* is large enough. If we insert these

values into (18), we obtain the so - called *steady – state solutions*, which are periodic with frequencies Ω and 2Ω.

To obtain the steady-state solutions we have two choices. First, we can integrate for a large enough period of time. Second, we can use the fact that $a_n, \varphi_n, n=1,2$, are constants, set $\dot{a}_n = \dot{\varphi}_n = 0, n=1,2$, in (17) and solve for $\sin\varphi_n$ and $\cos\varphi_n$. But $\sin^2\varphi_n + \cos^2\varphi_n = 1$, so we get a system of equations in the amplitudes $a_n, n=1,2$, called *frequency – response equations*

$$\mu_2^2 + (2\sigma_1 - \sigma_2)^2 = \frac{\alpha_2^2 a_1^4}{16\omega_2^2 a_2^2} \tag{19}$$

$$\left(\mu_1 + \mu_2 \frac{\alpha_1}{\alpha_2}\frac{\omega_2}{\omega_1}\frac{a_2^2}{a_1^2}\right)^2 + \left(\sigma_1 + (\sigma_2 - 2\sigma_1)\frac{\alpha_1}{\alpha_2}\frac{\omega_2}{\omega_1}\frac{a_2^2}{a_1^2}\right)^2 = \left(\frac{f_1}{2\omega_1 a_1}\right)^2$$

Substituting a_2^2/a_1^2 from the first equation (19) and inserting into the second, yields a cubic equation in a_1^2

$$\frac{\alpha_1^2\alpha_2^2}{256\omega_1^2\omega_2^2\left(\mu_2^2 + (\sigma_2 - 2\sigma_1)^2\right)} a_1^6 + \frac{\alpha_1\alpha_2\left(\mu_1\mu_2 + \sigma_1(\sigma_2 - 2\sigma_1)\right)}{8\omega_1\omega_2\left(\mu_2^2 + (\sigma_2 - 2\sigma_1)^2\right)} a_1^4 +$$

$$+ \left(\mu_1^2 + \sigma_1^2\right) a_1^2 - \frac{f_1^2}{4\omega_1^2} = 0 \tag{20}$$

Generally, it has only one acceptable solution a_1 which increases almost linearly with f_1, but for some parameters the number of solutions is three.

4. Numerical results

In this section, our aim is to numerically validate the approximate solutions obtained in the previous part. Thus, Fig. 1 presents a classical variation of amplitudes $a_n, n=1,2$, with time, as calculated by integrating equations (16). Some oscillations are present initially but, as time increases, the curves approach horizontal lines corresponding to steady-state motions. The amplitudes becomes increasingly larger as the wave frequency tends to roll frequency.

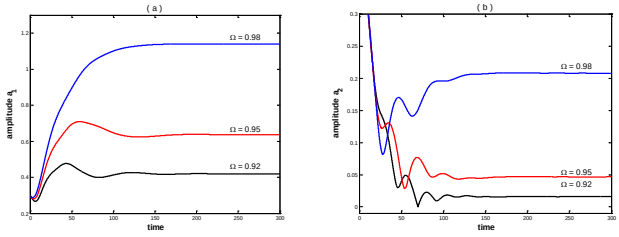
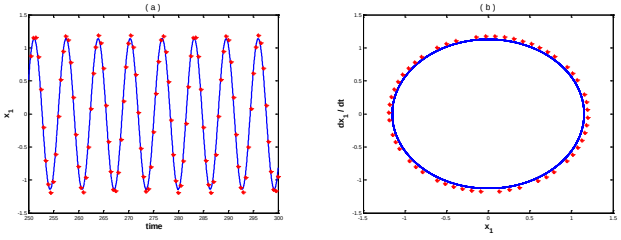


Fig. 1. *Dependence of amplitudes a_1 and a_2 on time t for $\mu_1 = 0.25$, $\mu_2 = 0.5$, $\alpha_1 = 1, \alpha_2 = 2, \omega_1 = 1, \omega_2 = 2.1, F_1 = 0.07, F_2 = 0.05$, $\varepsilon = 0.1$, and different excitation frequencies Ω.*

With amplitudes $a_n, n=1,2$ and phases $\varphi_n, n=1,2$, provided by (16), one can use (18) to represent the first-order approximations for the solutions of (1). Figs. 2 and 3 show both the transient and long-term behaviors and phase planes for rolling and pitching, respectively.



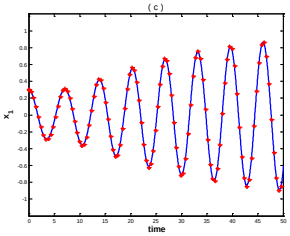


Fig. 2. *Time history and phase plane for roll mode with $\Omega = 0.98$. The other parameters are the same as in Figure 1. Red asterisks stand for the numerical solution while blue curves represent approximate solution (18).*

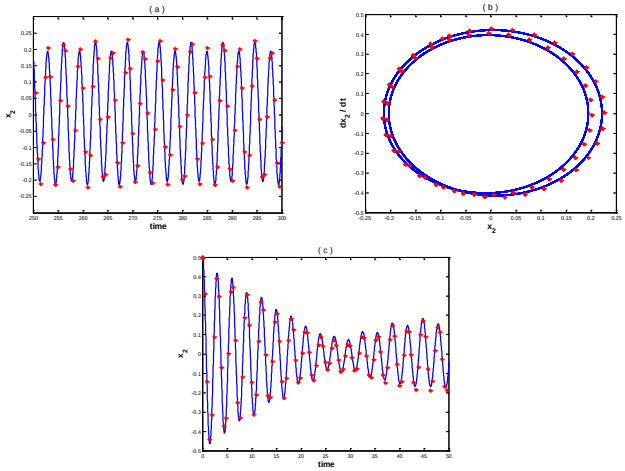


Fig. 3. *Time history and phase plane for pitch mode with $\Omega = 0.98$. The other parameters are the same as in Figure 1. Red asterisks stand for the numerical solution while blue curves represent approximate solution (18).*

It is obvious that the analytical solution (18) given by Multiple Scales method is in a pretty good agreement with the numerical one. Then, we have contrasted the amplitudes of $x_n, n=1,2$, given by (19) and (20) with those obtained by numerical integration of (1). For the rest of the paper, the range for the external frequency Ω was thought to be [0.9, 1.1]. In Figure 4, all parameters are selected within the preordered range and different ratios of natural frequencies are considered. As expected, the graphs provided by both methods are practically indistinguishable, so only numerical frequency-response curves are displayed.

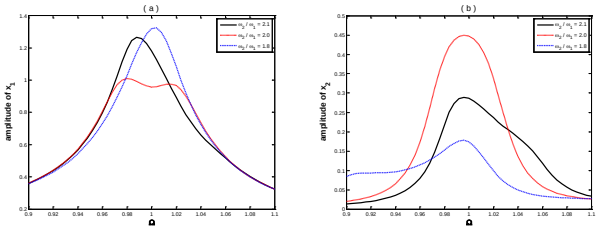


Fig. 4. *Amplitudes of roll and pitch modes versus excitation frequency for different ratios ω_2/ω_1. The other parameters are the same as in Figure 1.*

In the last part of the section, the effects of changing the system's parameters are investigated for the case $\omega_2/\omega_1 = 2$ only. Thus, Fig. 5 shows that for large damping the frequency – response curve has only one maximum, while for small damping the two maxima and one minimum suggested in Fig. 4 are better highlighted. Multiple Scales method results are labeled by red asterisks while the results provided by numerical integration are associated to dark continuous curves.

Fig. 6 reports a similar trend with decreasing / increasing of the external excitation amplitude F_1. F_2's modification has no practically effect on amplitude a_1, for a fixed F_1.

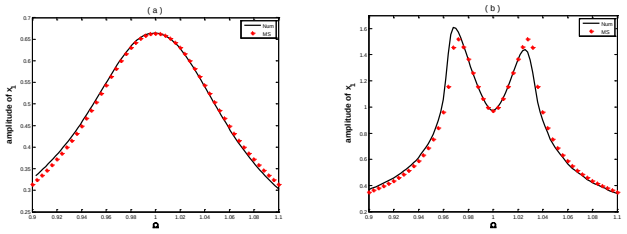


Fig. 5. *Amplitude of roll mode versus excitation frequency for* $\omega_2/\omega_1=2$.
a) $\mu_1=0.5, \mu_2=1$; *b)* $\mu_1=0.125, \mu_2=0.25$.
The other parameters are the same as in Figure 1.

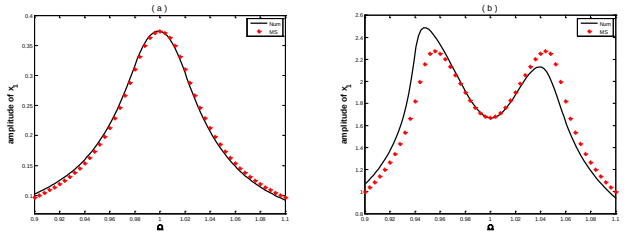


Fig. 6. *Amplitude of roll mode versus excitation frequency for* $\omega_2/\omega_1=2$.
a) $F_1=0.02$; *b)* $F_1=0.2$.
The other parameters are the same as in Figure 1.

Finally, Fig. 7 describes a mixed situation in which the nonlinearities were increased while the damping was decreased. For small forcing F_1 the only obvious change with respect to Figs. 5b and 6b consists in a clearer separation of extrema. For an increased value of F_1 there exist Ω values for that equation (20) has three positive solutions while numerical investigation shows a strange and totally different behavior in the neighborhood of the primary resonance $\Omega \approx \omega_1$ and two jumps from low to high amplitudes near $\Omega \approx 0.9$ and conversely for $\Omega \approx 1.07$.

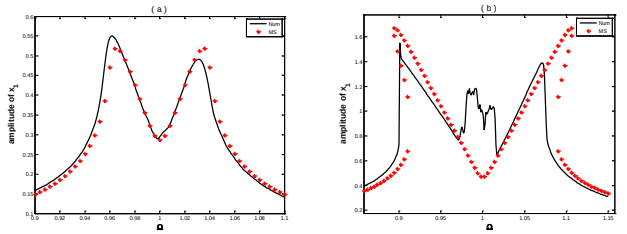


Fig. 7. *Amplitude of roll mode versus excitation frequency for* $\omega_2/\omega_1=2$, $\mu_1=\mu_2=0.2, \alpha_1=\alpha_2=5$, *and a)* $F_1=0.3$; *b)* $F_1=1$.
The other parameters are the same as in Figure 1.

5. Conclusions

In the paper, the nonlinear responses of a two-degrees-of-freedom model for pitch and roll ship motions have been studied both analytically and numerically for the particular case in which the pitch frequency is almost twice the roll frequency. The differential equations of motion are weakly nonlinear, thus we have searched, by means of a straightforward expansion of the solution, the resonant values of the external excitation frequency. Between the obtained resonant frequencies we have selected a primary one, namely that where the encounter frequency is close to the roll frequency. The Multiple Scales method permitted us to derive the governing equations for the transition towards the steady-state solutions, the first-order approximations for these solutions and the frequency-amplitudes relationships. The reliability of the analytical results derived in the paper was checked by comparing them with the numerical solutions provided by an ODEs integrator. Using time series plots and frequency-amplitude curves, we have proved that the two solutions match well if the system's parameters were selected without order violations.

References

[1] Thompson, J.M.T., Rayney, R.C.T., Soliman, M.S., *Mechanics of a ship under direct and parametric wave excitation*, Phil. Trans. R. Soc. Lond. A, 338, p. 471 – 490, 1992.

[2] Kan, M. Taguchi, H., *Capsizing of a ship in quartering seas*, J. Soc. Naval Architects Japan, 171, p. 229 – 244, 1992.

[3] Deleanu, D., *On approximating the periodic solutions of capsize equation*, Int. J. for Science, technics and innovations for the industry, Year IX, Issue 9, p. 9 – 12, 2015.

[4] Deleanu, D., *Parametric analysis of the ship capsize problem*, Int. J. for Science, technics and innovations for the industry, Year IX, Issue 7, p. 6 – 8, 2015.

[5] Haddara, M.R., Xu, J., *On the identification of the ship coupled heave – pitch motions using neural networks*, Ocean Engineering, 26, p. 381 – 400, 1999.

[6] Eissa, M., El-Sera, S., El-Sheikh, M., Sayeda, M., *Stability and primary simultaneous resonance of harmonically excited non-linear spring pendulum system*, Appl. Math. And Computation, 145, p. 421 – 444, 2003.

[7] Pan, R., Davies, H.G., *Non-stationary response of a non-linear coupled pitch-roll ship model under modulated excitation*, J. of Sound and Vibration, 192, p. 669 – 699, 1996.

[8] Kamel, M.M., *Bifurcation analysis of a nonlinear coupled pitch – roll ship*, Mathematics and Computers in Simulation, 73, p. 300 – 308, 2007.

[9] Dumitrache, C.L., Calimanescu, I., Comandar, C., *Naval standard and safety valve design using CAD solutions*, Int. Conference "Advanced Concepts in Mechanical Engineering" ACME 2014, Iasi, Romania, 12-15.10. 2014.

[10] Nayfeh, A.H., *Introduction to perturbation techniques*, John Wiley and Sons, New York, 1992.

STABILITY OF NONLINEAR AUTONOMOUS SYSTEMS WITH TWO DEGREES OF FREEDOM. AN ANALYTICAL STUDY

Prof. DSc. Nikolov S. PhD.[1,2], M.Sc. Nedkova N.[1]
University of Transport, G. Milev Str., No 158, 1574 Sofia, Bulgaria [1]
Institute of Mechanics-BAS, Acad. G. Bonchev Str, Bl. 4, 1113 Sofia, Bulgaria [2]

S.Nikolov@imbm.bas.bg

Abstract: *The Thomson-Tait-Chetayev theorem states that "if a system with an unstable potential energy is stabilized with gyroscopic forces, then this stability is lost after the addition of an arbitrarily small dissipation". The importance of this property in growing number of physical examples and engineering applications in the practice is not well good unified and understood, i.e. the destabilizing effect of dissipation needs to be compensated in various gyroscopic devices by applying accelerating forces.*

In the present paper an analytical study of the stability behaviour of a specific class of nonlinear autonomous dynamic systems (i.e. RHS of the equations is a square polynomial) with two degrees of freedom is developed. Considering the general case, we find that the system is multi-stationary and has several possible equilibria. The system is investigated with analytical tools coming from Lyapunov-Andronov theory, and our analytical calculations predict that soft (reversible) loss of stability takes place.

Keywords: STABILITY ANALYSIS, GYROSCOPIC SYSTEMS, ANALYTICAL STUDY

1. Introduction

A system is called autonomous if it explicitly not depends on time. The division of the dynamical systems into autonomous and non-autonomous is in a certain sense conventional. If we consider the values $x_1, x_2, ..., x_n$ as coordinates of point x in the n-dimensional space, then we can represent geometrically the state of the dynamical system by means of this point x. Then, x is called a phase point, and the space – *phase space* of the dynamical system.

All dynamical systems can be separated into two main groups: conservative and dissipative. In case that the system is described by autonomous ordinary differential equations then it can be shown (according to the divergence theorem) that the variation of its phase volume dV during a time dt is

$$(1) \qquad dV = dt\int\left(\frac{d\dot{x}_1}{dx_1}+\frac{d\dot{x}_2}{dx_2}+...+\frac{d\dot{x}_n}{dx_n}\right)dx_1dx_2...dx_n = dt\int div\dot{x}dx,$$

where $\dot{x}$ is a vector with components $\dot{x}_1, \dot{x}_2, ..., \dot{x}_n$. Hence, the sufficient condition for the conservation of the phase volume has the form

$$(2) \qquad div\,\dot{x} = 0.$$

Similarly, the sufficient condition for the decrease of the phase volume is

$$(3) \qquad div\,\dot{x} < 0.$$

In nature all systems are dissipative [1], yet if dissipation is very small (for a limited time) then such systems behave as conservative. Dissipative systems can also be sub-classified into passive and active ones.

The study of the stability of the movement of mechanical systems under the action of various forces has a long history. Until now, significant results were obtained for autonomous systems; in [2, 3] the theorems of Thomson (Kelvin) -Tait-Chetayev are used. Practically, the stability of non-autonomous systems influenced by gyroscopic and dissipative forces is not studied well [4].

Linear conservative gyroscopic systems have the form:

$$(4) \qquad M\ddot{x}+G\dot{x}+Kx=0, \quad \text{or} \quad \left(\ddot{x}+\frac{G}{M}\dot{x}+\frac{K}{M}x=0\right),$$

where the vector x represents the generalized coordinates, M is the mass matrix, G describes the gyroscopic forces and K potential forces. Also, M, G and K are real $n\times n$ matrices with $M^T = M > 0$ (positive definite), $G^T = -G$ (a skew-symmetric matrix) and $K^T = K$ (symmetric matrix). The linear equation (4) is typical for small oscillations of a dynamical system in the region of an equilibrium point ($x = 0$). The results on the problem of the stability of equilibrium can be found in [5].

It is well-known that gyroscopic forces can stabilize the unstable conservative systems, while they cannot destabilize a stable conservative system. In [2, 6], is shown that an unstable conservative system

$$(5) \qquad M\ddot{x}+Kx=0, \quad K\geq 0,$$

can be stabilized by gyroscopic forces if and only if the number of unstable degrees of freedom is even. Hence, when $K < 0$, then the dimension n must be even. Later, for this case in [7], Lakhadanov obtained that suitable stabilizing matrices are $G = g_0G_0$, where $\det G_0 \neq 0$ and g_0 is a sufficiently large number.

There has been a large amount of recent interest in the investigation of gyroscope dynamics. The gyroscope has attributes of great utility to navigational and aeronautical engineering, biology, optics, etc. [8-10, 12]. Different types of gyroscopes (with linear or nonlinear damping, fluid, etc.) are investigated for predicting dynamic responses such as regular and chaotic motions [10, 11].

In mechanics and control theory the problem of force influences over the dynamics of stationary (autonomous) and unstationary systems is important. We will employ potential forces F_p, dissipative forces F_d and gyroscopic forces F_g. The first two forces take care of convergence to the target point and the gyroscopic force handles the obstacle avoidance [13]. Mathematically, the three forces F_p, F_d and F_g can be written in the following form:

$$(6) \qquad F_p = -\nabla U(q), \quad F_d = -D(q,\dot{q})\dot{q}, \quad F_g = S(q,\dot{q})\dot{q},$$

where U is a (potential) function, the matrix D is symmetric and positive-definite, the matrix S is skew-symmetric, q is the position and $\dot{q}$ is a velocity vector.

Gyroscopic forces have two useful perspectives in the dynamics of mechanical systems: (i) they create coupling between different degrees of freedom, just like mechanical couplings; (ii) they rotate the velocity vector just like magnetic field acting on a charged particle. The first interpretation regards the matrix S in (6) as an interconnection matrix and the second interpretation considers S as an infinitesimal rotation. Note that gyroscopic forces are very useful in the stabilization of dynamical systems, because they are unpotential forces with zero power.

According to the Thomson (Lord Kelvin)-Tait-Chetayev and Merkin theories in many physical and engineering applications the destabilizing effect of dissipation needs to be compensated in various gyroscopic devices by applying accelerating forces. In this connection, it is well-known that the equations of perturbed motion of a system have the form

$$\frac{d}{dt}\frac{\partial T}{\partial \dot{q}_l}-\frac{\partial T}{\partial q_l}=-\frac{\partial \Pi}{\partial q_l}+D_l+\Gamma_l+R_l \qquad (l=1,2,...,n), \tag{7}$$

where T is the kinetic energy of the system; Π is the potential energy; q_l and $\dot{q}_l$ are the generalized coordinates and velocities; D_l, Γ_l and R_l are the dissipative, gyroscopic and nonconservative positional forces.

In this paper, the problems associated with analytical investigating stability of equilibriums in a general nonlinear system with two degrees of freedom (i.e. $l=2$) are considered. It is assumed that the forces in the right-hand side of (7) are nonlinear (their expansion in powers of q and $\dot{q}$ is from second order), i.e.

$$\begin{aligned} J^{(2)} &= a_1q_1q_2+a_2q_1\dot{q}_1+a_{23}q_1\dot{q}_2+a_4q_1^2+a_5q_2\dot{q}_1+a_6q_2\dot{q}_2+\\ &+a_7q_2^2+a_8\dot{q}_1\dot{q}_2+a_9\dot{q}_1^2+a_{10}\dot{q}_2^2, \end{aligned} \tag{8}$$

where a_1 to a_{10} are positive or negative parameters.

Hence, for $l=2$, the system (7) has the form

$$\begin{aligned} &\ddot{q}_1-d_1\dot{q}_2+\left(\pm\rho_1^2\right)q_1=c_1^{(1)}q_1q_2+c_2^{(1)}q_1\dot{q}_1+c_3^{(1)}q_1\dot{q}_2+c_4^{(1)}q_1^2+\\ &+c_5^{(1)}q_2\dot{q}_1+c_6^{(1)}q_2\dot{q}_2+c_7^{(1)}q_2^2+c_8^{(1)}\dot{q}_1\dot{q}_2+c_9^{(1)}\dot{q}_1^2+c_{10}^{(1)}\dot{q}_2^2,\\ &\ddot{q}_2+d_2\dot{q}_1+\left(\pm\rho_2^2\right)q_2=c_1^{(2)}q_1q_2+c_2^{(2)}q_1\dot{q}_1+c_3^{(2)}q_1\dot{q}_2+c_4^{(2)}q_1^2+\\ &+c_5^{(2)}q_2\dot{q}_1+c_6^{(2)}q_2\dot{q}_2+c_7^{(2)}q_2^2+c_9^{(2)}\dot{q}_1^2+c_{10}^{(2)}\dot{q}_2^2, \end{aligned} \tag{9}$$

where $c_i^{(1)}$, $c_i^{(2)}$ $(i=1,...,10)$ and ρ_1, ρ_2 are constants, and q_1, q_2 are normal coordinates.

Let us denote

$$y_1=q_1,\ y_2=\dot{q}_1,\ y_3=q_2,\ y_4=\dot{q}_2. \tag{10}$$

After substitution of (10) into (9) the two second-order ordinary differential equations (9) are reduced to four first-order differential equations in the form

$$\begin{aligned} &\dot{y}_1=y_2,\\ &\dot{y}_2=-\left(\pm\rho_1^2\right)y_1+d_1y_4+c_1^{(1)}y_1y_3+c_2^{(1)}y_1y_2+c_3^{(1)}y_1y_4+\\ &+c_4^{(1)}y_1^2+c_5^{(1)}y_2y_3+c_6^{(1)}y_3y_4+c_7^{(1)}y_3^2+c_8^{(1)}y_2y_4+\\ &+c_9^{(1)}y_2^2+c_{10}^{(1)}y_4^2,\\ &\dot{y}_3=y_4,\\ &\dot{y}_4=-d_2y_2-\left(\pm\rho_2^2\right)y_3+c_1^{(2)}y_1y_3+c_2^{(2)}y_1y_2+c_3^{(2)}y_1y_4+\\ &+c_4^{(2)}y_1^2+c_5^{(2)}y_2y_3+c_6^{(2)}y_3y_4+c_7^{(2)}y_3^2+c_8^{(2)}y_2y_4+\\ &+c_9^{(2)}y_2^2+c_{10}^{(2)}y_4^2. \end{aligned} \tag{11}$$

The aim of the work is to outline the main stability aspects of the system (11). Thus, a qualitative analysis of the system equations is performed in Section 2.

2. Qualitative analysis

In this section, we consider the system (11), which presents an autonomous nonlinear dynamical model. All constants of this model are real and can be negative or positive.

It is easy to see that the system (11) is multi-stationary and has several possible equilibria. The fixed points of the system, $\overline{E}=\left(\overline{y}_1,\overline{y}_2,\overline{y}_3,\overline{y}_4\right)$, represented by Eq. (11) can be analytically estimated and are defined by the following set of algebraic equations, including the constants of the model

$$\overline{y}_1=\overline{y}_2=\overline{y}_3=\overline{y}_4=0, \quad \text{if } \overline{y}_1=0, \tag{12}$$

$$\overline{y}_2=\overline{y}_4=0,\ \overline{y}_1\neq 0,\ \overline{y}_3\neq 0, \quad \text{if } \overline{y}_1\neq 0. \tag{13}$$

Investigation of the first fixed point (12)

In order to investigate the character of the first fixed point (Eq. (12)) we make the following substitutions into (11)

$$\begin{aligned} &y_1=\overline{y}_1+x_1=x_1,\ y_2=\overline{y}_2+x_2=x_2,\\ &y_3=\overline{y}_3+x_3=x_3,\ y_4=\overline{y}_4+x_4=x_4. \end{aligned} \tag{14}$$

Then, after accomplishing some transformations the system (11) has the same form but with variables x_1, x_2, x_3 and x_4. It is seen that the system (11) (for x_1, x_2, x_3 and x_4) enjoys the symmetry, i.e.

$$\left(x_1,x_2,x_3,x_4\right)\to\left(x_1,-x_2,x_3,-x_4\right). \tag{15}$$

The x_1 and x_3 axes are invariant. All trajectories, which start on the x_1-axis (respectively x_3-axis) remain on it as $t\to\infty$. In this case, the divergence of the flow (11) is

$$\begin{aligned} D_4&=\frac{\partial x_1}{\partial \dot{x}_1}+\frac{\partial x_2}{\partial \dot{x}_2}+\frac{\partial x_3}{\partial \dot{x}_3}+\frac{\partial x_4}{\partial \dot{x}_4}=\\ &=\left(c_2^{(1)}+c_3^{(2)}\right)x_1+\left(c_8^{(2)}+2c_9^{(1)}\right)x_2+\left(c_5^{(1)}+c_6^{(2)}\right)x_3+\\ &+\left(c_8^{(1)}+2c_{10}^{(2)}\right)x_4. \end{aligned} \tag{16}$$

The system (11) is dissipative and has an attractor when $D_4<0$.

Following [14], the Routh-Hurwitz conditions for stability of (12) can be written the form

$$p=r=0, \tag{17}$$

$$q=\left(\pm\rho_1^2\right)+\left(\pm\rho_2^2\right)+d_1d_2>0, \tag{18}$$

$$s=\left(\pm\rho_1^2\right)\left(\pm\rho_2^2\right)>0, \tag{19}$$

$$R=pqr-sp^2-r^2=0. \tag{20}$$

Here the notations p,q,r,s and R are taken from [14]. The characteristic equation of the system (11) can be written as

$$\chi^4+q\chi^2+s=0. \tag{21}$$

It is seen that in this case the system is structurally unstable because always $R=0$, i.e. the system is always on the boundary of stability. Note here that when $J^{(2)}=0$, then the system (11) is linear conservative.

The basis of stability theory for systems with structurally unstable equilibrium states was developed by Lyapunov [2, 15]. His studies were devoted to various aspects of stability in critical cases, as well as of bifurcation phenomena accompanying the loss of stability at equilibrium states. Here, we mention only the two most common and simple cases, where the characteristic equation of a four-dimensional system

(i) has one zero root; or

(ii) has a pair of complex-conjugated roots on the imaginary axis.

The first case is determined by the condition

$$s=0,\ R>0. \tag{22}$$

Recall that $s=(-1)^4\det A$, where A is the matrix of the linearized system at the equilibrium state. In view of this condition, the

equilibrium states associated with the first critical are also called degenerate [15, 16]. Since the implicit function theorem may no longer be applied here, the persistence of such equilibrium state in a neighbouring system is not necessarily guaranteed. Thus, a transition through the stability boundary in the first critical case may result in the disappearance of the equilibrium state. From (17) to (20) it is seen that this case is valid when ρ_1 and/or ρ_2 are zero. But according to (9), we see that ρ_1 and ρ_2 are always different from zero. Hence, we conclude that this critical case is not valid for equilibrium state (12).

The second critical case correspond to

$$R = 0\,,\ s > 0. \tag{23}$$

Here, in contrast to the first critical case, the equilibrium state is preserved in all nearby systems and can only lose its stability. For fixed point (12) this case is valid when $p_1 = \pm\rho_1^2$ and $p_2 = \pm\rho_2^2$ are positive/negative constants.

Investigation of the second fixed point (13)

In this case we have non-simple fixed points. According to [17], a fixed point of a non-linear system is said to be non-simple if the corresponding linearized system is non-simple. Recall that such linear systems contain a straight line, or possibly a whole plane, of fixed points.

The nature of the local phase portrait is now determined by nonlinear terms. Therefore, in contrast to the simple fixed points, there are infinitely many different types of local phase portraits.

There is no detailed classification of non-simple fixed points. However, the definitions of stability (which apply to both simple and non-simple fixed points) provide a classification of qualitative behavior.

In order to investigate the character of the fixed points from kind (13), we make the following substitutions in the system (11)

$$y_i = x_i + \overline{y}_i \qquad (i = 1,...,4)\,. \tag{24}$$

Hence, after some transformations system (11) in local coordinates has the form

$$\begin{aligned}
&\dot{x}_1 = x_2\,,\\
&\dot{x}_2 = m_1x_1 + m_2x_2 + m_3x_3 + m_4x_4 + c_4^{(1)}x_1^2 +\\
&\quad + c_9^{(1)}x_2^2 + c_7^{(1)}x_3^2 + c_{10}^{(1)}x_4^2 + c_2^{(1)}x_1x_2 + c_1^{(1)}x_1x_3 +\\
&\quad + c_3^{(1)}x_1x_4 + c_5^{(1)}x_2x_3 + c_8^{(1)}x_2x_4 + c_6^{(1)}x_3x_4\,,\\
&\dot{x}_3 = x_4\,,\\
&\dot{x}_4 = m_5x_1 + m_6x_2 + m_7x_3 + m_8x_4 + c_4^{(2)}x_1^2 + c_9^{(2)}x_2^2 +\\
&\quad + c_7^{(2)}x_3^2 + c_{10}^{(2)}x_4^2 + c_2^{(2)}x_1x_2 + c_1^{(2)}x_1x_3 + c_3^{(2)}x_1x_4 +\\
&\quad + c_5^{(2)}x_2x_3 + c_8^{(2)}x_2x_4 + c_6^{(2)}x_3x_4\,,
\end{aligned} \tag{25}$$

where

$$\begin{aligned}
&m_1 = -\left(\pm\rho_1^2\right) + c_1^{(1)}\overline{y}_3 + 2c_4^{(1)}\overline{y}_1,\ m_2 = c_2^{(1)}\overline{y}_1 + c_5^{(1)}\overline{y}_3\,,\\
&m_3 = c_1^{(1)}\overline{y}_1 + 2c_7^{(1)}\overline{y}_3,\ m_4 = d_1 + c_3^{(1)}\overline{y}_1 + c_6^{(1)}\overline{y}_3,\\
&m_5 = c_1^{(2)}\overline{y}_3 + 2c_4^{(2)}\overline{y}_1,\ m_6 = -d_2 + c_2^{(2)}\overline{y}_1 + c_5^{(2)}\overline{y}_3\,,\\
&m_7 = -\left(\pm\rho_2^2\right) + c_1^{(2)}\overline{y}_1 + 2c_7^{(2)}\overline{y}_3\,,\ m_8 = c_3^{(2)}\overline{y}_1 + c_6^{(2)}\overline{y}_3\,.
\end{aligned} \tag{26}$$

Now, the divergence of the flow (25) is

$$\begin{aligned}
D_4 = \sum_{i=1}^{n}\frac{\partial\dot{x}_i}{\partial x_i} &= m_2 + m_8 + \left(c_2^{(1)} + c_3^{(2)}\right)x_1 +\\
&+ \left(2c_9^{(1)} + c_8^{(2)}\right)x_2 + \left(c_5^{(1)} + c_6^{(2)}\right)x_3 + \left(c_8^{(1)} + 2c_{10}^{(2)}\right)x_4 < 0,
\end{aligned} \tag{27}$$

and the system (25) has an attractor.

According to [14], the Routh-Hurwitz conditions for stability of (13) can be written in the form

$$\begin{aligned}
&p = -\left(m_2 + m_8\right) > 0\,,\\
&q = m_2m_8 - m_1 - m_7 - m_4m_6\,,\\
&r = m_1m_8 + m_2m_7 - m_3m_6 - m_4m_5 > 0\,,\\
&s = m_1m_7 - m_3m_5 > 0,\\
&R = pqr - sp^2 - r^2 > 0.
\end{aligned} \tag{28}$$

When the last two conditions in (28) are not valid, the steady state(s) (13) becomes unstable. The characteristic equation of the system (25) can be written as

$$\chi^4 + p\chi^3 + q\chi^2 + r\chi + s = 0\,. \tag{29}$$

The stability of a steady state (13) depends on the real part of the roots of the characteristic equation (29). If all roots are negative then the equilibrium state is stable. If at least one root is positive, then the steady state is unstable.

According to [14-16], the conditions $R = 0$ and $s = 0$ are the boundaries of stability. In the boundary of stability $s = 0$, i.e. $m_1m_7 = m_3m_5$, the characteristic equation (29) has one root equal to zero, and the type of the other roots is determined by the expression

$$\Omega = 27r^2 - 18pqr + 4q^3 + 4p^3r - p^2q^2\,. \tag{30}$$

Thus, we have two cases:

1. If $\Omega < 0,\ p > 0,\ q > 0,\ r > 0,\ R > 0$ and $s = 0$, then the equation (29) has one root equal to zero and three negative real roots;

2. If $\Omega > 0,\ p > 0,\ q > 0,\ r > 0,\ R > 0$ and $s = 0$, then the equation (29) besides one zero root also has one negative root and two complex conjugate roots with negative real parts.

As we mentioned earlier, a transition through the stability boundary $s = 0$ may result in disappearance of the equilibrium state. The system is structurally unstable (un-robust) and through bifurcation it will lose its stability non-reversely. Generally, the stability of mechanical systems, from physical point of view, be connected to gyroscopic forces. However, in this case the gyroscopic devices do not compensate the destabilizing effect of dissipation.

Further, we focus our considerations on the problem of the transition over the stability boundary $s = 0$, i.e. $m_1m_7 = m_3m_5$. Here, we note that for different combinations with values of $\rho_1, \rho_2, c_4^{(1)}$, $c_4^{(2)}, c_7^{(1)}$ and $c_7^{(2)}$, the fourth Routh-Hurwitz condition for stability in (28) can be negative. This question has an immediate significance for the subject of nonlinear dynamics. For stationary regimes, the corresponding problem was solved in [14]. There the boundaries of stability are classified as safe or dangerous – safe boundaries (soft loss of stability) are such that crossing leads to only small quantitative changes of the system's state; dangerous boundaries (hard loss of stability) are such that arbitrarily small perturbations of system beyond them cause significant and irreversible changes in the system's behavior. Generally in accordance with Lyapunov-Andronov theory, the so-called first Lyapunov value $l_1(\lambda_0)$ determines the character (safe or dangerous) of the boundary of stability $s = 0$, when bifurcation parameter λ_0 is slowly changed. Thus, in order to define the type of stability loss of steady state (13) it is necessary to calculate $l_1(\lambda_0)$ on the boundary of stability $s = 0$. In the case of fourth first order differential equations, this value can be determined analytically by the formula in [14]:

(31)

$$l_1(\lambda_0)=\alpha\Big\{a_{11}^{(1)}\sigma_1^2+a_{22}^{(1)}\sigma_2^2+a_{33}^{(1)}\sigma_3^2+\frac{1}{\delta^2}a_{44}^{(1)}\left(1-\alpha\sigma_1-\beta\sigma_2-\gamma\sigma_3\right)^2+$$
$$+\frac{2}{\delta}\left(a_{14}^{(1)}\sigma_1+a_{24}^{(1)}\sigma_2+a_{34}^{(1)}\sigma_3\right)\left(1-\alpha\sigma_1-\beta\sigma_2-\gamma\sigma_3\right)+$$
$$+2\left(a_{12}^{(1)}\sigma_1\sigma_2+a_{13}^{(1)}\sigma_1\sigma_3+a_{23}^{(1)}\sigma_2\sigma_3\right)\Big\}_1+\beta\{...\}_2+\gamma\{...\}_3+\delta\{...\}_4,$$

where λ_0 is defined as a value of $\rho_1,\rho_2,c_4^{(1)}$, $c_4^{(2)},c_7^{(1)}$ and $c_7^{(2)}$. Here $a_{11}^{(1)}=c_4^{(1)}$, $a_{22}^{(1)}=c_9^{(1)}$, $a_{33}^{(1)}=c_7^{(1)}$, $a_{44}^{(1)}=c_{10}^{(1)}$, $a_{12}^{(1)}=c_2^{(1)}$,... The coefficients $\alpha,\beta,\gamma,\delta,\sigma_1,\sigma_2$ and σ_3 are defined by corresponding formulas presented in [14].

After accomplishing some transformations and algebraic operations for the first Lyapunov value $l_1(\lambda_0)$ (for system (25)), we obtain the main result in this article, i.e. $l_1(\lambda_0)=0$. Note that in (31) now $\alpha=\beta=\gamma=\delta=0$. In other words, the boundary of stability $s=0$ is safe and soft loss of stability take place.

3. Conclusion

In this paper we present an analytical study of the dynamical features of a 4D model describing the gyroscopic dynamics of a general nonlinear system using the Lyapunov-Andronov bifurcation theory. The approach proposed here has a basic advantage, which consists of the following: we can answer the question why the addition (or removal) of some members of the polynomial function $J^{(2)}$ modifies (or does not modify) a system behavior, which would pass (or would not pass) from stable to unstable or from regular to a chaotic one. During the last decade, the robustness (structural stability) has been considered as a key property of mechanical systems [4, 10, 12]. Under this assumption, small changes in the internal or external conditions of a mechanical system are neutralized by the gyroscopic forces which are able to return to the vicinity of the preliminary attractor, while intense changes on the values of parameters characterizing the dissipation can provoke the transition to a new state, potentially a different attractor with its own interval of robustness.

The analytical results lead to the following comments: 1) the general nonlinear system with two degrees of freedom (11) is multi-stationary and has several possible equilibrias; 2) for first fixed point (12) (with coordinates $(0,0,0,0)$), the system is structurally unstable because $R=0$, i.e. the system is always on the boundary of stability; 3) for second fixed point(s) (13), the boundary of stability $s=0$ is safe and soft loss of stability take place. Note that this boundary of stability not depends from gyroscopic forces, as this requirement follows directly from Routh-Hurwitz conditions (28).

To conclude, mathematical modeling and analysis can enable to understand the stabilization mechanism underlying an observed mechanical process, and at the same time, provide a testable hypothesis for future studies. Here, we qualitatively investigate the main properties of the stabilization of a general nonlinear system with two degrees of freedom. Thus, our dynamical predictions can be tested in future numerical simulations.

References

[1] Landa, P. Nonlinear Oscillations and Waves in Dynamical Systems, Dordrecht, Kluwer Academic Publishers, 1996.

[2] Chetayev, N. The Stability of Motion. New York, Pergamon Press, 1961.

[3] Merkin, D. Gyroscopic Systems. Moscow, Nauka, 1924 (in Russian).

[4] Morozov, V., V. Kalenova. Stability of non-autonomous mechanical systems with qyroscopic and dissipative forces. XII Russian Control Conference, Moscow 16-19 June 2014, 2014, 1888-1894.

[5] Bulatovic, R. The stability of linear potential gyroscopic systems in cases when the potential energy has a maximum. Prikl. Mat. Mekh. 61(3), 1997, 385-389.

[6] Thomson, W., P. Tait. Treatise on Natural Philosophy. vol. I, part I, Cambridge University Press, 1879.

[7] Lakhadanov, V. On stabilization of potential systems. PMM, 39(1), 1975, 45-50.

[8] Idowu B., U. Vincent, A. Njah. Control and synchronization of chaos in nonlinear gyros via backstepping design. Int. J. Nonliner Sci., 5(1), 2008, 11-19.

[9] Binhi, V., A. Savin. Molecular gyroscopes and biological effects of weak extremely low-frequency magnetic fields. Physical Review E, 65, 2002, 051912 (10 pages).

[10] Nikolov, S., N. Nedkova. Gyrostat model regular and chaotic behaviour. J. of Theoretical and Applied Mechanics, 45(4), 2015, 15-30.

[11] Nikolov, S. Regular and chaotic behaviour of fluid gyroscope. Comptes rendus de l'Academie bulgare des Sciences, 57(1), 2004, 19-26.

[12] Kalvouridis, T. Stationary solutions of a small gyrostat in the Newtonian field of two bodies with equal masses. Nonlinear Dynamics, 61, 2010, 373-381.

[13] Chang, D., J. Marsden. Gyroscopic forces and collision avoidance with convex obstacles. In: New Trends in Nonlinear Dynamics and Control and Their Application. Berlin, Springer,295, 2003, 145-159.

[14] Bautin, N. Behavior of Dynamical Systems near Boundary of Stability. Moscow, Nauka, 1984 (in Russian).

[15] Shilnikov, L., A. Shilnikov, D. Turaev, L. Chua. Methods of Qualitative Theory in Nonlinear Dynamics. Part II, Singapore, World Scientific, 2001.

[16] Nikolov, S., St. Stoytchev, B. Bozhov. Mathematical model of blood flow pulsations in the circle of Willis, Comptes rendus de l'Academie bulgare des Sciences, 59(8,) 2006, 811-820.

[17] Arrowsmith, D., C. Place. Dynamical Systems: differential equations, maps and chaotic behaviour, London, Chapman & Hall, 1992.

VEGETABLE OILS AS ALTERNATIVE FUEL FOR NEW GENERATION OF DIESEL ENGINES. A REVIEW

PhD Student Eng. Vrabie V., Prof. Dr. Eng. Scarpete D., PhD Student Eng. Zbarcea O
"Dunărea de Jos" University of Galati, Romania

vlad.vrabie@ugal.ro

Abstract: *One of the primary incentives for expanding the production and use of biofuels worldwide is the potential environmental benefit that can be obtained from replacing petroleum fuels with fuels derived from renewable biomass resources. The use of straight vegetable oil in diesel engines is one of the available alternatives, but its use in existing vehicles usually requires modification of engine or fuel system components. The increased viscosity, low volatility, and poor cold flow properties of vegetable oils lead to severe engine deposits, injector coking, and piston ring sticking. The paper presents a literature review on vegetable oils as alternative fuel for diesel engines.*

Keywords: STRAIGHT VEGETABLE OIL, DIESEL ENGINES, VISCOSITY, ALTERNATIVE FUEL

1. Introduction

The utilization of biofuels in diesel engines is not a recent practice [1]. The original diesel engine that Rudolph Diesel designed ran with vegetable oil. He used peanut oil to fuel one of his engines at the Paris Exposition in 1900. In 1911, Dr. Rudolf Diesel was quoted as saying: "The diesel engine can be fed with vegetable oils and would help considerably in the development of agriculture of the countries which will use it" [2].

First generation biofuels for diesel engines are produced from vegetable oils. After more or less deep purification, they can be used directly as fuel in diesel engine and are still currently used in some limited applications [1]. Renewable and alternative energy sources are becoming more demanding and necessary due to increases in crude oil prices and exhaust gas emissions due to fossil fuels throughout the world [3].

Vegetable oils have their own advantages: first of all, they are available everywhere in the world. Secondly, they are renewable as the vegetables which produce oil seeds can be planted year after year. Thirdly, they are "greener" to the environment, as they seldom contain sulphur element in them. This makes vegetable fuel studies become current among the various popular investigations. So does the evaluation of the performance of diesel engines when fuelled with vegetable oils. A number of investigations have been made, and the test results have proved that vegetable oils are feasible substitutes for diesel fuel [4].

The main problem of using vegetable oils in diesel engines is the high viscosities of such fuels [5-9]. Chemical and thermal methods are the two techniques to reduce viscosities of vegetable oils. The thermal method uses preheating of fuels, which increases the temperature and reduces viscosity [10]. Chemical methods can be divided into dilution, pyrolysis, transesterification and micro-emulsion [8,9]. Fuel blending has the advantages of improving the use of vegetable oil fuel with minimal fuel processing and without engine modifications [4].

Vegetable oils possess almost the same heat values as that of diesel fuel. But a major disadvantage of vegetable oils is their inherent high viscosity. Modern diesel engines have fuel-injection systems that are sensitive to viscosity changes. High viscosity may lead to poor atomization of the fuel, to incomplete combustion, to coking of the fuel injectors, to ring carbonization, and to the accumulation of fuel in the lubricating fuels [11,12].

2. Composition of vegetable oils

Fats and oils (lipids) consist of 95-98% triglycerides. Minor constituents present in oils include free fatty acids, mono- and di-glycerides, phospholipids, tocopherols, sterols, natural colouring agents as well as more or less volatile odorous compounds. Triglycerides are composed of a glycerol molecule esterified with three similar or different fatty acid molecules. Some twenty fatty acids are found in nature and their numerous possible combinations with the three alcohol functions of the glycerol produce a wide variety of triglycerides and therefore of oils [1].

Generally, biomass-derived feedstocks for the production of liquid biofuels can be classified into the following three categories according to the source, i.e. triglyceride-based biomass, starch- and sugar-derived biomass, and cellulosic biomass. A variety of liquid biofuels can be produced from triglycerides based biomass such as vegetable oils, animal fats, waste cooking oils and microalgae oils as shown in Figure 1 [13].

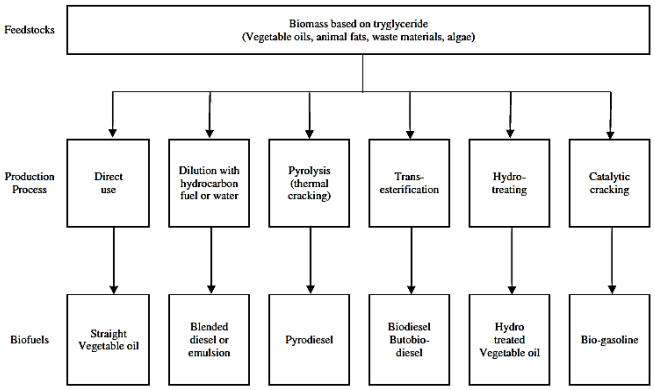


Fig. 1 *Overview of feedstocks and production process for liquid biofuels from triglycerides-based biomass [13].*

3. Direct use of vegetable oils in diesel engines

3.1. Some characteristics of vegetable oils

Vegetable oils first developed as fuel for direct use, after more or less deep purification [1].

The oil most frequently produced in Europe, rapeseed and sunflower, are composed of fatty acids with carbon chains (18 carbon atoms) including three chains globally longer than those of the hydrocarbons found in diesel. These oils have high molecular weights, about 0.88 kg/mole, density above 910 kg/m^3, and low volatility. On heating, they generally crack at temperatures in the region of 300°C [1]. The main characteristics of vegetable oils appear in table 1 [14].

The usage of vegetable oils as diesel fuel depends on world market prices for mineral products and is therefore of special interest at present only for countries with a large excess of vegetable oil production [15]

It is essential to measure three characteristic parameters to ensure that the fuel used is indeed pure vegetable oil and to confirm the vegetable origin: density, viscosity and iodine value [16]

The density specification is suitable for excluding material other than vegetable oil, or for detecting mixtures of vegetable oil with other liquids (petroleum products, glycerol, etc.). The density of vegetable oils is slightly variable between 900 and 960 kg/m^3 [16].

Table 1: *Main characteristics of vegetable oils [14].*

Vegetable oil	Viscosity at 40°C (mm^2/s)	Carbon residue (% w)	Cetane number	GCV (kJ/kg)	Ash content (% w)	Sulphur content (% w)	Iodine value (I/g oil)	Saponification value (mg KOH/g oil)	CFPP (°C)
Cotton	33.7	0.25	33.7	39.4	0.02	0.01	113.2	207.71	
Poppy	42.4	0.25	36.7	39.6	0.02	0.01	116.83	196.82	
Rapessed	37.3	0.31	37.5	39.7	0.006	0.01	108.05	197.07	+20[a]
Sunflower	34.4	0.28	36.7	39.6	0.01	0.01	132.32	191.7	+15[a]
Sesame	36	0.25	40.4	39.4	0.002	0.01	91.76	210.34	
Flax	28	0.24	27.6	39.3	0.01	0.01	156.74	188.71	
Palm	63.6 (30°C)		42				35-65		
Jatropha	49.9 (38°C)		40-45						
Castor	29.7	0.21	42.3	37.4	0.01	0.01	88.72	202.71	
Soya	33.1	0.24	38.1	39.6	0.006	0.01	69.82	220.78	+11[b]
Peanut	40	0.22	34.6	39.5	0.02	0.01	119.55	199.8	
Hazelnut	24	0.21	52.9	39.8	0.01	0.02	98.62	197.63	
Walnut	36.8	0.24	33.6	39.6	0.02	0.02	135.24	190.82	
Almond	34.2	0.22	34.5	39.8	0.01	0.01	102.35	197.56	
Olive	29.4	0.23	49.3	39.7	0.008	0.02	100.16	196.83	
Wheat	32.6	0.23	35.2	39.3	0.02	0.02	120.96	205.68	
Corn	35.1	0.22	37.5	39.6	0.01	0.01	119.41	194.14	
Diesel	2-4.5		47						0 to -20

[a]*Source: Valenergol*
[b]*Source: USDA*

The straight vegetable oils (SVO) viscosity is much higher than that of diesel fuel: it increases with the carbon chain lengths [7,17]. SVO high viscosity causes (i) a decrease in injection rate due to head losses in fuel injection pumps, filters and injectors, (ii) poor fuel atomisation and vaporisation by the injectors, which leads to incomplete combustion inside the combustion chamber [18,19,20]. This results in lower thermodynamic efficiency and an increase in soot emissions and particle matters.

Viscosity is a rapid indicator of fuel quality before use, especially if the nature of the feedstock is not well known, or if the oil could have been deteriorated or polymerized during storage [21].

As shown in Figure 2, for a typical heavy fuel viscosity of 180 cSt at 50°C, it is necessary to heat the HFO (heavy fuel oil) to between 114°C and 125°C to reach the appropriate viscosity, while SVOs require only 67°C to 78°C to achieve the same viscosity [16].

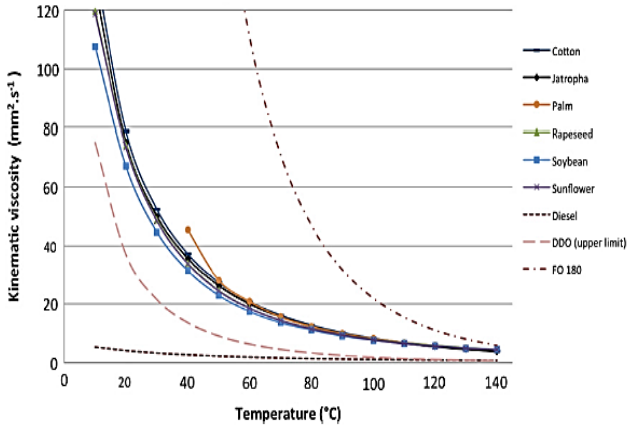


Fig. 2 *Temperature dependence of the kinematic viscosity of vegetable oil and different heavy fuel oils; DDO – distillate diesel oil; FO 180 – heavy fuel oil 180 [16].*

The iodine value is a measurement of the total unsaturation of vegetable oils, as well as an indicator of their susceptibility to oxidation [21]. Vegetable oils can be divided into four major categories depending on their iodine value: saturated oils (iodine value between 5 and 50), mono-unsaturated oils (50 and 100), di-unsaturated oils, also called semi-siccative (100 and 150) and tri-unsaturated oils called siccative (over 150) [16].

As shown in Figure 3, this parameter is specific to each oilseed, making it possible to check the nature of the biomass used. Although SVO viscosity increases with total unsaturation, the iodine value is not a parameter that can be used to draw conclusions

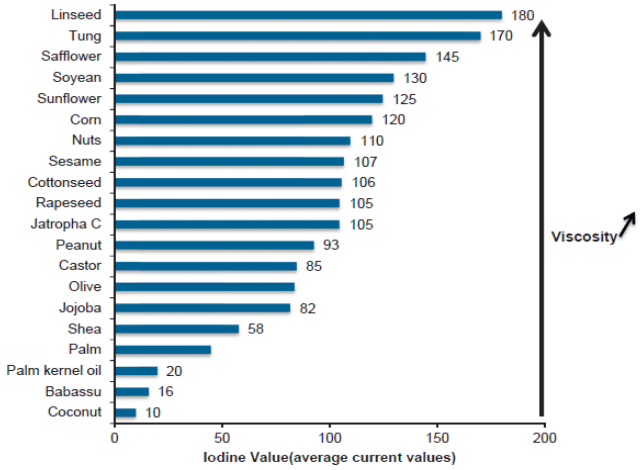


Fig. 3 *Mean iodine values of different vegetable oils viscosity increases with the degree of unsaturation)[16].*

about the quality of SVO or the potential presence of impurities [16].

As Figure 4 indicates, the viscosity of pure SVO is much higher than that of diesel fuel at normal operating temperatures. This can cause premature wear of fuel pumps and injectors and can also dramatically alter the structure of the fuel spray coming out of the injectors to increase droplet size, decrease spray angle, and increase spray penetration [22].

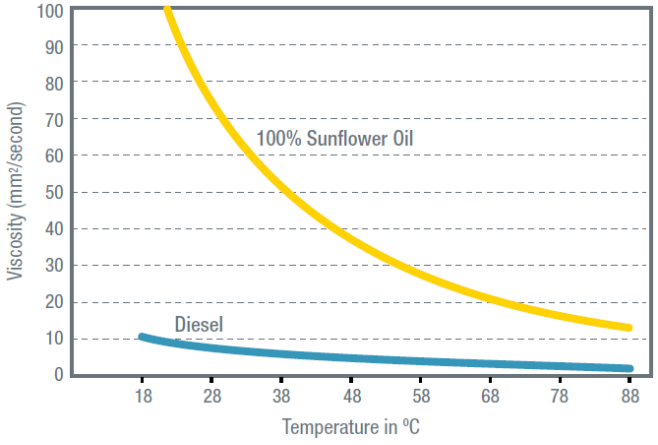


Fig. 4 *Impact of temperature on the viscosity of sunflower oil and diesel fuel [22].*

The cetane number reflects the ability of a fuel to self-ignite when compressed under standardized conditions [23].

Ash content indicates the content of minerals and oxides of an abrasive nature for the engine [16]. According to Espadafor and coworkers [24] ash constituents, such as vanadium, nickel, sodium, aluminum and silicon are harmful for the engine, and their presence merely increases engine wear and corrosion.

The cold properties of the oils, especially their Cold Filter-Plugging Point (CFPP) represent a further handicap. At low temperature, the resulting higher viscosity makes them virtually impossible to use and development of a special cold-starting technology is essential. Solutions include starting the vehicle with Diesel, or methods to warm up the fuel [1].

3.2. Impact on combustion

Vegetable oils cause serious damage to combustion systems, due to the formation of deposits, and downgrade the performance and emission quality, especially in direct injection engines. During the fuel vaporization and combustion process, due to the high molecular weights and low volatility of the oils, the molecules cracks, resulting in the formation of deposits. The high viscosity of the oils radically modifies the phenomena associated with spraying of the fuel and therefore the combusting timing, already disturbed by the low cetane number of these oils (about 30 to 40), well below the 51 limit imposed by Diesel standard EN 590 [25,26,27,28].

Vegetable oils contain significant amounts of oxygen. Its ignition characteristics are such as poor cold engine start-up, misfire, and ignition delay, and latter includes incomplete combustion, e.g. deposit formation, carbonization of injector tip, ring sticking, lubricating oil dilution and degradation, polymerization during storage [29].

Carbon deposits around the nozzle orifice, upper piston ring grooves and on piston rings are the main problems during the use of vegetable oil as fuel [30]. They are also biodegradable, non-toxic, and have a potential to significantly reduce pollution. Vegetable oils and their derivatives in diesel engines helps to reduce the emissions of sulfur oxides, carbon monoxide (CO), poly aromatic hydrocarbons (PAH), smoke, particulate matter (PM) and noise [31].

In addition, some of the difficulties mentioned above will be further amplified with improvements in diesel engine technologies (smaller injector nozzles, more injectors resulting in higher risk of clogging). Direct use of vegetable oils with technologies currently being developed will become increasingly critical [32].

3.3. Impact on emissions

Due to the need to adapt the combustion time, use of vegetable oils in diesel engines generally leads to higher CO, HC and PM. In contrast, due to their slower combustion and lower temperatures in the combustion chamber, vegetable oils reduce NO_x emissions . The emissions vary depending on the condition of the vehicle. The differences may increase with the mileage, the age of the engine technology and the degree of engine clogging [1].

Experiments have also been conducted on use of vegetable oils in mixtures. These tests were performed with 25/75 mixtures of sunflower or safflower oil in diesel. Performance with the fuel formulated using sunflower oil rapidly deteriorated due to deposits on injectors and piston add to gumming of the piston rings. Mixtures based on safflower oil did not generate any special problems [33,34,35].

Other isolated and endurance tests have been conducted [13] with various fuel formulations based on cotton oil and diesel, containing between 30% and 65% vegetable oil and with a 50/50 mixture of cotton oil and cotton oil ester. Although beneficial effects may be observed in the short term, serious problems of deposits, ash, wear and gumming appeared during endurance tests, in the longer term.

In the experiment [4], the tests have been carried out to evaluate the performance and gaseous emission characteristics of a diesel engine when fuelled with vegetable oil and its blends of 25%, 50%, and 75% of vegetable oil with ordinary diesel fuel separately. A Lister Petter T series diesel engine is selected for the study and is mounted on a test-bed. The engine is type TS2, 9.5 kW capacity, fixed speed (1500 rpm) with air-cooled and direct injection.

Figure 5 shows the comparison of the CO emissions of different fuels at different engine load. Within the experimental range, the CO emission from the vegetable oil and vegetable oil/diesel blends are nearly all higher than that from pure diesel fuel. Only on the point of engine full load, the CO emission of vegetable oil and vegetable oil/diesel fuel blends were all lower than that of diesel fuel. This is possibly due to two factors: (1) at the engine full load, the temperature in the cylinder of engine is higher, which makes the vegetable oil and it blends easier to atomize, a better air/fuel mixture and then a better combustion can be achieved; (2) the oxygen contents in the vegetable oil makes it easier to be burnt at higher temperature in the cylinder [4].

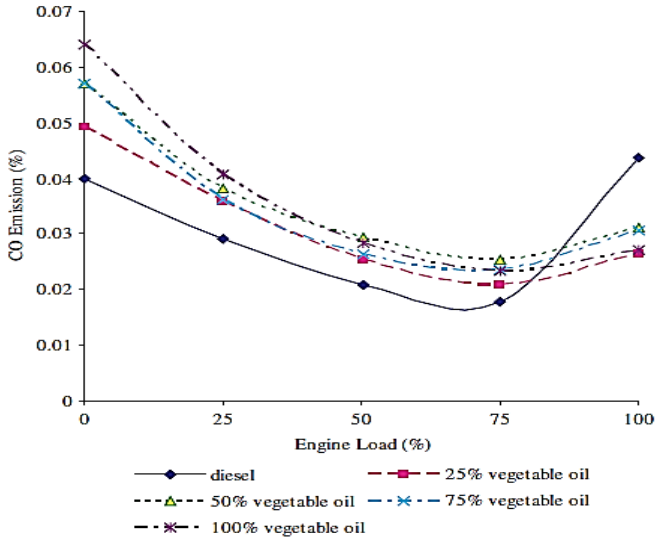


Fig. 5 *Comparison of CO emission versus engine power output for different fuels/oil blends [4].*

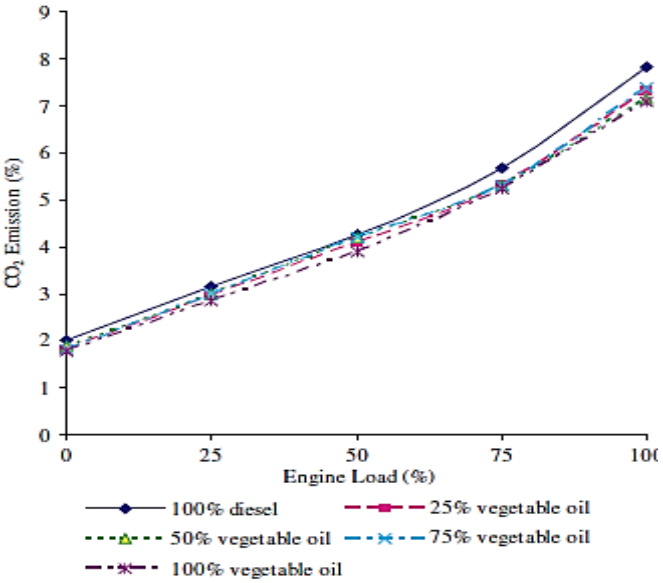


Fig. 6 *Comparison of CO_2 emission versus engine power output for different fuels/oil blends [4].*

In the range of whole engine load, the CO_2 emissions of diesel fuel are all higher than that of the other fuels (figure 7). This is because vegetable oil contains oxygen element; the carbon content is relatively lower in the same volume of fuel consumed at the same engine load, consequently the CO_2 emissions from the vegetable oil and its blends are lower [4].

Rakopoulos et al. [36] have evaluated the use of sunflower, cottonseed, corn and olive straight vegetable oils of Greek origin, in blends with diesel fuel at proportions of 10 vol.% and 20 vol.%, in a six-cylinder, turbocharged and after-cooled, heavy duty, direct injection diesel engine.

For the speed of 1500 rpm, for the neat diesel fuel, and the 10% and 20% blends of the four vegetable oils with diesel fuel, at the three loads, it can be observed that the NO_x emitted by all vegetable oil blends (Fig. 7) are equal or slightly higher than the ones for the corresponding diesel fuel case, with this increase being higher the higher the percentage of the vegetable oil in the blend [36].

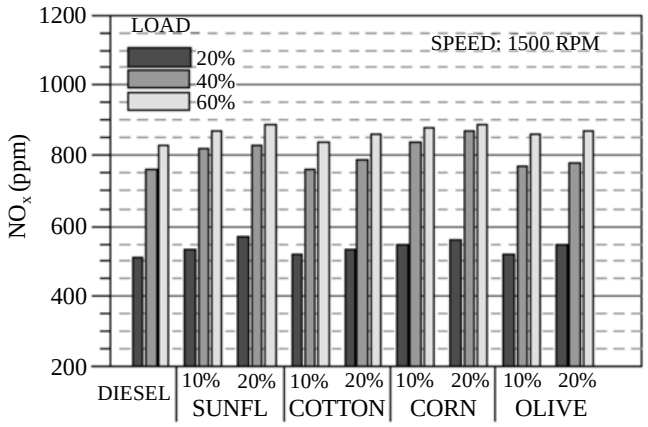


Fig. 7 *Emissions of nitrogen oxides (NO_x) for neat diesel fuel, and the 10% and 20% blends of the four vegetable oil with diesel fuel [36].*

In [4], the HC emissions of all fuels are lower at partial engine load, but increased at higher engine load (Fig. 8). This is due to relatively less oxygen available for the reaction when more fuel is injected into the engine cylinder at higher engine load. The HC emissions of vegetable oil and vegetable/diesel fuel blends are lower than that of diesel fuel, except that 50% of the vegetable oil with 50% diesel fuel blend is a little higher than that of diesel fuel [4].

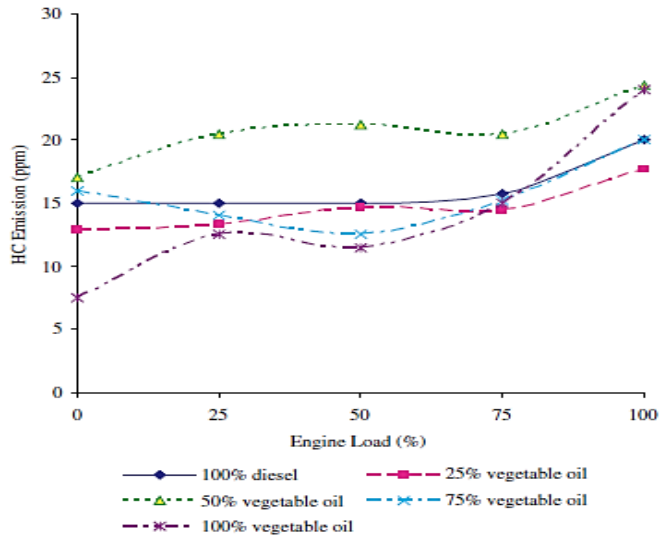


Fig. 8 *Comparison of HC emission versus engine power output for different fuels/oil blends [4].*

Cottonseed and sunflower oils need to be at least degummed for fuel use, as shown in short-term performance tests with an engine having a pre combustion chamber, but even at the state of refinement, they are unsuitable for runs of more than 40 hours when used as the straight, unblended fuel. Although vegetable oils apparently can be tolerated in direct-injection engines only as dilute blends in diesel oil, there is accumulating evidence worldwide that the simple esters can function as a diesel fuel by themselves because of improved viscosity and volatility properties compared to triglyceride [37].

The results from the experiments prove that vegetable oil and its blends are potentially good substitute fuels for diesel engine in the near future when petroleum deposits become scarcer [4].

4. Conclusion

First generation biofuels for diesel engines are produced from vegetable oils. After more or less deep purification, they can be used directly as fuel in diesel engine and are still currently used in some limited applications.

A number of investigations have been made, and the test results have proved that vegetable oils are feasible substitutes for diesel fuel.

The usage of vegetable oils as diesel fuel depends on world market prices for mineral products and is therefore of special interest at present only for countries with a large excess of vegetable oil production

Vegetable oils are available everywhere in the world and are renewable as the vegetables which produce oil seeds can be planted year after year. Also, they are “greener” to the environment, as they seldom contain sulphur element in them.

The main problem of using vegetable oils in diesel engines is the high viscosities of such fuels.

Due to the need to adapt the combustion time, use of vegetable oils in diesel engines generally leads to higher CO, HC and PM. In contrast, due to their slower combustion and lower temperatures in the combustion chamber, vegetable oils reduce NO_x emissions.

While vegetable oils represent an alternative fuel, they will continue to present risks related to their intrinsic characteristics, which neither car nor agricultural tractor and machinery manufactures are willing to assume.

The results from some experiments prove that vegetable oil and its blends are potentially good substitute fuels for diesel engines in the near future when petroleum deposits become scarcer.

Acknowledgements

The authors would like to acknowledge to the “Dunărea de Jos” University of Galați Romania for supporting this research and paper publishing.

References

[1] Ballerini, D. Biofuels. Meeting the Energy and Environmental Challenges of the Transportation Sector. Editions Technip, Paris, 2012.

[2] McDonnell, K.P., et al. Results of engine and vehicle testing of semi-refined rapeseed oil. 10th International Rapessed Congress, Proceedings, Camberra, Australia, 1999.

[3] Nigam, P.S., Singh, A. Production of liquid biofuels from renewable resources-review. Prog Energy Combust 2011 (37:52–68).

[4] Wang, Y.D., et al. An experimental investigation of the performance and gaseous exhaust emissions of a diesel engine using blends of a vegetable oil. Applied Thermal Engineering 26 (2006) 1684–1691.

[5] Sidibe, S.S., et al. Use of crude filtered vegetable oil as a fuel in diesel engines state of the art: literature review. Renew Sustain Energy Rev 2010 (14:2748–59).

[6] Yilmaz, N. Temperature-dependent viscosity correlations of vegetable oils and biofuel–diesel mixtures. Biomass Bioenergy 2011 (35:2936–8).

[7] Hazar, H., Aydin, H. Performance and emission evaluation of a CI engine fueled with preheated raw rapeseed oil (RRO)–diesel blends. Applied Energy 2010 (87:786–90).

[8] Daho, T., et al. Influence of engine load and fuel droplet size on performance of a CI engine fueled with cottonseed oil and its blends with diesel fuel. Appl Energy 2013 (111:1046–53).

[9] Agarwal, A.K. Biofuels (alcohols and biodiesel) applications as fuels for internal combustion engines. Prog Energy Combust 2007 (33:233–71).

[10] Yilmaz, N., Morton, B. Effects of preheating vegetable oils on performance and emission characteristics of two diesel engines. Biomass Bioenergy 2011 (35(5):2028–33).
[11] Karaosmanoglu, F. Vegetable oil fuels: a review. Energy Sources 21 (3) (1999).
[12] Ramadhas, A.S. Use of vegetable oils as I.C. engine fuels—a review. Renewable Energy 29 (5) (2004) 727–742.
[13] Soo-Young No. Application of hydrotreated vegetable oil from triglyceride based biomass to CI engines – A review. Fuel 115 (2014) 88–96.
[14] Demirbas, A. Biodiesel Fuels from Vegetable Oils via Catalytic and Non-catalytic Super-critical Alcool Transesterification and Other Methods: a Survey, Energy and Management 44 (2003) 2093-2109.
[15] Mittelbach, M. Diesel fuel derived from vegetable oils, III. Graz Austria, 2012.
[16] Blin, J., et al., Characteristics of vegetable oils for use as fuel in stationary diesel engines—Towards specifications for a standard in West Africa, Renewable and Sustainable Energy Reviews 22 (2013) 580–597
[17] Srivastava, A., Prasad, R. Triglycerides-based diesel fuels. Renewable and Sustainable Energy Reviews 2000; 4:111–33.
[18] Misra, R.D., Murthy M.S. Straight vegetable oils usage in a compression ignition engine: a review. Renewable and Sustainable Energy Reviews 2010; 14:3005–13.
[19] Russo, D., et al. State of the art of biofuels from pure plant oil. Renewable and Sustainable Energy Reviews 2012; 16:4056–70.
[20] Daho, T., et al. Study of droplet vaporisation of various vegetable oils and blends of domestic fuel oil: cottonseed oil under different ambient temperature conditions. Biomass and Bioenergy 2012; 46:653–63.
[21] Knothe, G. Analyzing biodiesel: standards and other methods. Journal of the American Oil Chemists' Society 2006; 83:823–33.
[22] U.S. Department of Energy. Vehicle technologies program. Energy efficiency and renewable energy. DOE/GO-102010-2989, May 2010.
[23] Sidibe, S.S., et al. Use of crude filtered vegetable oil as a fuel in diesel engines state of the art: Literature review. Renewable and Sustainable Energy Reviews 2010; 14:2748–59.
[24] Espadafor, F.J., et al. The viability of pure vegetable oil as an alternative fuel for large ships. Transportation Research Part D2009.
[25] Clevenger, M.D., et al. Developing an Accelerated Test of Coking Tendencies of Alternative Fuels. ASAE 31, 4, 1054-1058, 1988.
[26] Hawkins, C.S. Engine Durability Tests with Sunflower Oil in an Indirect Injection Diesel Engine. SAE 831357.
[27] Vellugh, G. Performance of Vegetable Oils and their Monoesters as Fuels for Diesel Engines. SAE 831358.
[28] Suda, K.J. Vegetable Oil Or Diesel Fuel – A Flexible Option. SAE 840004.
[29] De, B., Panua, R.S. An experimental study on performance and emission characteristics of vegetable oil blends with diesel in a direct injection variable compression ignition engine. Procedia Engineering 90 (2014) 431 – 438.
[30] Thomas, R.W., Maurin, B.O. Identification of chemical change occurring during the transient injection of selected vegetable oils. SAE-paper. 1993, pp. 201- 210.
[31] Bona, S., Mosca, G., Vamerli, T. Oil crops for biodiesel production in Italy. Renewable Energy 16 (1999), pp. 1053–1056.
[32] Murayama, T., et al. Low Carbon Flower Buildup, Low Smoke and Efficient Diesel Operation with Vegetable Oils by Conversion to Mono-Esters and Blending with Diesel Oil or Alcohols. SAE 841161.
[33] Ziejewski, M., Kaufman, K.R. Endurance Test of a Sunflower Oil/Diesel Fuel Blend, 1982, SAE 820257.
[34] Ziejewski, M. Vegetable Oils as a Potential Alternate Fuel in Direct Injection Diesel Engines, 1983, SAE 831359.
[35] Ziejewski, M., Goettler, H. Influence of Vegetable Oil Based Alternate Fuels on Residue Deposits and Components Wear in a Diesel Engine, 1986, SAE 860302.
[36] Rakopoulos, C. D. et al. Comparative environmental behavior of bus engine operating on blends of diesel fuel with four straight vegetable oils of Greek origin: Sunflower, cottonseed, corn and olive, Fuel 90 (2011) 3439–3446.
[37] Pryde, E.H. Vegetable oils as diesel fuels: overview. 73rd AOCS Annual Meeting held in Torornto, Canada, May 2-6, 1982.

DETERMINING THE EFFECTS OF CANOLA BIODIESEL ON ENGINE PERFORMANCE AND TORQUE RISE

Prof. Dr. SESSİZ A[1], Assoc. Dr. BAYHAN Y.[2], Assoc.Dr. SÜMER S. K. [3], Phd. Student EROL O.[4]

Dıcle University, Faculty of Agriculture, Department of Agricultural Machinery and Technologies Engineering, Diyarbakır, Turkey[1]

Namık Kemal University, Faculty of Agriculture, Biosystem Engineering Department, Tekirdağ, Turkey[2], Onsekız Mart University, Faculty of Agriculture, Department of Agricultural Machinery and Technologies Engineering, Canakkale, Turkey[3],

Namık Kemal University, Vocational School, Automotive Technology Department, Çorlu, Turkey[4].

Email: asessiz@dicle.edu.tr, ybayhan@nku.edu.tr, sarpksumer@comu.edu.tr, oerol@nku.edu.tr.

Abstract

This study aims to determine the effects of canola biodiesel on engine performance characteristics and torque rise. In the experiments, canola biodiesel (B100) and diesel (B0) were used as fuel with mixtures by introducing canola biodiesel into diesel in proportions of 5% (B5), 10% (B10), 20% (B20), 50% (B50), and 80% (B80). These fuels were tested on an air-cooled direct injection four-cylinder diesel engine. Tests were run based methods indicated by the standard No. TS 1231. According to the results of the study, the engine's torque rise values for diesel (B0), B5, B10, B20, B50, B80 and biodiesel (B100) fuels were 27%, 26%, 25%, 24%, 23%, 22% and 21% respectively. It was found that the increasing ratio of biodiesel in the mixture reduced the torque rise values. It was observed that the difference between the torque rise values of B5 and B0 were insignificant.

KEYWORDS: *CANOLA, BIODIESEL, ENGINE PERFORMANCE, TORQUE RISE.*

1.Introductıon

Torque rise is determined by the amount of fuel feeding the cylinder. By injecting a higher amount of fuel into an engine at full load, the engine's torque at nominal revolutions can be achieved with higher torque. The difference between maximum torque and the engine's torque at nominal revolutions is called torque rise. This study determined the effects of fuels obtained by mixing canola biodiesel into diesel in different proportions on engine performance and torque rise. Additionally, engine characteristics determined in the study were investigated and the usability of diesel-biodiesel mixtures that may be alternative to diesel was evaluated.

2. Preconditions and Means For Resolving The Problem

In the experiments in the scope of this study, biodiesel produced with canola oil in the Energy and Agriculture Laboratory of the Karadeniz Institute of Agricultural Research and commercially sold diesel (B0) were used. The results of the analyses on the B100 fuel produced at Black Sea Agricultural Research Institute Research and kinematic viscosity, flash point, pour point values of the biodiesel – diesel mixtures were determined via analyses run at the Fuel Analysis Laboratory of TUBITAK Marmara Research Center, Energy Institute. Some properties of the fuels determined after measurements are provided in Table 1. Physical and chemical property information of the B0 fuel was taken from TUPRAS Turkish Petroleum Refineries Company.

Table 1. *Analysis Values of the B0, B5, B10, B20, B50, B80 and B100 fuel*

Fuels	B0	B5	B10	B20	B50	B80	B100
Density (g/cm^3, 15 °C)	0,83	0,84	0,84	0,84	0,86	0,86	0,88
Kinematic Viscosity (mm^2/s, 40°C)	2,0…4,5	2,83	2,91	3,12	3,88	4,69	4,90
Flash Point (°C)	>55	61,50	64,00	67,00	77,50	90,50	150,00
Pour Point (°C)	-35…-15	-24,00	-23,00	-21,00	-18,00	-9,00	-19,00
Net Combustion Heat (MJ/kg)	-	45,92	45,51	44,78	42,88	40,97	40,00

In the experiment, a Fiat 50 NC four-cylinder four-cycle, air-cooled diesel engine was used. General properties of the engine are provided in Table 2.

Torque rise; the percentage change between maximum torque

Table 2. Technical properties of the engine used in the experiment

Engine Type	Fiat 50 NC
Number of cylinders	4
Type	Direct Injection Diesel
Diameter × Stroke	104×115 mm
Volume (cm^3)	3908
Engine revolution at maximum power	3500 rpm
Engine revolution at maximum torque	1700 rpm
Fuel pump	Rotary type, automatic advance
Air filter	Oil bath, pre-cleaner

Engine tests were conducted based on the Turkish Standard No. TS 1231 (Anonymous 2010b). Experiments were done by using B0, B5, B10, B20, B50, B80 and B100 fuels. For every experiment (on each mixture), engine power, torque and engine revolution were measured. In the experiment, based on the standard No. TS 1231, ambient temperature was 23°C or higher. When the engine had been run in this ambient temperature and cooling water exit temperature reached 85°C, atmospheric pressure, air humidity ratio, air temperature, engine air entry temperature, engine oil temperature and fuel temperature were measured. Measurements in engine tests were run simultaneously. Experiments were repeated 3 times and the engine was stabilized before each experiment.

Effective power is the power obtained from the flywheel which is the exit point of the power taken from the engine. This power is the real engine power that takes into account factors that are ignored in terms of internal power such as friction losses, and power spent on supporting pieces in lubrication, ignition and valves (Alpgiray 2006). Equation (1) was utilized in determining the effective power of the engine.

$$Pe = \frac{(Md.n)}{9549} \qquad (1)$$

Here;

Pe : Effective power (kW),

Md : Torque of the engine (Nm),

n : Engine speed (rpm).

and the torque in nominal speed. In the experiment, the engine was stabilized by running in full throttle with no loads. Then the load was increased incrementally and measurements were made. In each experiment, nominal and maximum torque values were computed. Torque rise values were calculated. Torque rise value was computed using the equation (2) below (Bolat 2007).

$$Tr = \frac{(Tmax - Tmin)}{Tmax} .100 \qquad (2)$$

Here;

T_r *: Torque rise (%),*

T_{max} *: Maximum torque (Nm),*

T_{min} *: Torque at nominal engine speed (Nm).*

3. Solution Of The Examined Problem

In the experiments, as a results of the engine performance tests on diesel and biodiesel mixtures mixed in different proportions, power, torque and torque rise values were determined.

3.1. Comparison Of Biofuel and Diesel

The density of the B100 fuel in the experiment was higher than the B0 fuel. As the amount of canola biodiesel in the mixture increased, the density increased. The viscosity of the B100 fuel in the experiment was higher than the B0 fuel. As the amount of canola biodiesel in the mixture increased, the viscosity increased. The viscosity of the canola biodiesel fuel was found within the viscosity limits as indicated by biodiesel standards ASTM 6751 and EN 14214 (Anonymous 2010a). The density of the B100 fuel was found within the density limits as indicated by EN 14214 standards. The density of the B100 fuel was approximately 5% higher than that of the B0 fuel. Flash point of the B100 fuel was higher than the B0 fuel. Pour point of the B0 fuel, which was lower than that of B100 fuel, was between -35 and -15°C. The pour point of the B100 fuel reached up to -19°C.

3.2. Power Changes

For all fuels used in the experiment, the highest engine power values were obtained at 3500 rpm. At the maximum engine speed, the effective power value of the B0 fuel was 66 kW, while the effective power value was 61.4 kW for the B100 fuel. The maximum power of the B100 fuel was 6.97% lower than the B0 fuel. At the same engine speed, the effective power value decreased 1% in the B5 fuel when compared to the B0 fuel. At 1700 rpm, the effective power of the B0 fuel was 43.9 kW, while this value was 38 kW for the B100 fuel. The effective power of the B100 fuel was 12.45% lower than the B0 fuel at this speed. At the same engine speed, the effective power value decreased 1.9% in the B5 fuel when compared to the B0 fuel. The effective power change increased up to 3500 rpm, and then started to drop (Figure 1). Another reason for the decrease in engine power is that density and viscosity of the canola biodiesel is higher than those of the standard diesel. High viscosity and density prevents the desired level of atomized spraying of fuel from the injector. This increased the combustion latency, which affects combustion quality. In the study by Cengelci et al. (2011), it was found that engine speed decreased by usage of biodiesel by 6.27% compared to usage of B0, and the reasons given for the decrease were viscosity, density and heating value. In their study, Behcet and Cakmak (2014) indicated that engine power decreased by 4.2-5.7% in usage of fuels that are mixtures of fish oil and methyl ester instead of B0. In Elicin's (2011) study, it was reported that the differences in power values between petroleum-based diesel and canola biodiesel were at an acceptable level, and these differences come from differences in density, heating value and viscosity.

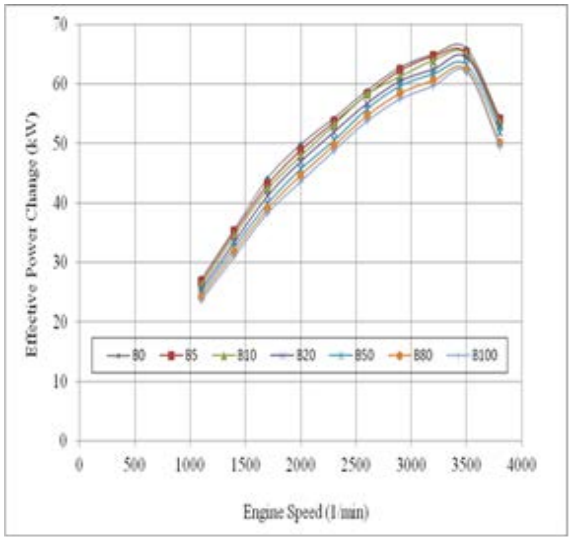


Figure 1. Effective power changes in diesel (B0) fuel and diesel-biodiesel mixtures based on engine speeds

3.3. Torque Rise Changes

The torque rise values of the B0, B5, B10, B20, B50, B80 and B100 fuels is the percentage change between maximum torque values and torque values in nominal speeds. The lowest torque values of differently-proportioned mixtures of diesel and biodiesel were obtained at 3500 rpm, where maximum power was reached. The maximum power change observed in the B0 fuel was not observed in the B5, B10, B20, B50, B80 and B100 mixtures. Maximum torque change was observed at 1700 rpm for all fuels. After the engine speed of 1700 rpm, torque values started to drop (Figure 2).

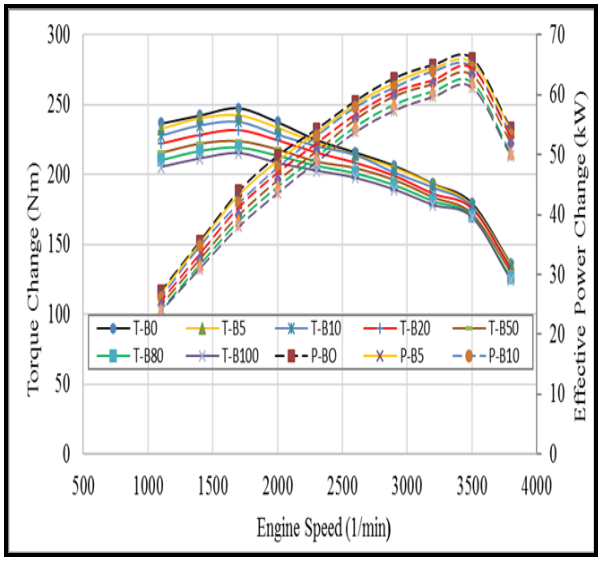


Figure 2. Changes in maximum torque and torque at the nominal speed

In usage of the fuels B100, B80, B50 and B20, torque rise values in comparison to the B0 fuel decreased by 22.2%, 18.51%, 14.81%, and 11.11% respectively. The torque rise value for the B10 fuel decreased by 7.4% when compared to the B0 fuel. This decrease was 3.7% for the B5 fuel. The torque rise value of the B0 fuel was closer to the B5 fuel (Table 3).

Table 3. Torque rise values of the B0 fuel, B100 fuel and diesel-biodiesel mixtures

Fuel Type	Torque at Nominal Speed (Nm)	Maximum Torque (Nm)	Torque Rise (%)
B0	246.76	180.01	0.27
B5	241.87	178.16	0.26
B10	235.17	176.20	0.25
B20	229.42	173.74	0.24
B50	224.12	172.41	0.23
B80	218.38	169.34	0.22
B100	213.29	167.32	0.21

As the proportion of biodiesel in the mixture increased, decrease was observed in torque rise. At the nominal engine speed, the decrease in torque rise is expressed by the regression equation, y = - 0.7821x+66.973 (R^2 = 0.9751) (Figure 3).

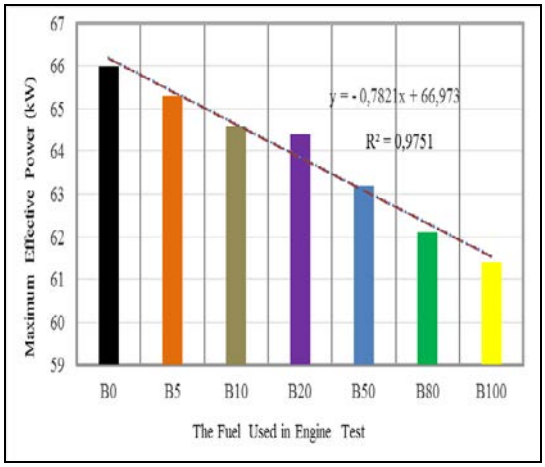


Figure 3. Torque change at the nominal speed of the engine based on the fuels used.

When the engine speed reached 3500 rpm, the decrease in maximum torque with the fuels were calculated with the regression equation y = – 2.1036x+182.3 (R^2 = 0.9951). The decrease continued in the regression equation y = – 0.01x+0.28 (R^2 = 1.00) which shows the percentage change in maximum torque. In engine's torque rise, this decrease in the regression equation y = - 0.012x + 0.288, continued through the B5, B10, B20, B50, B80 and B100 fuels after the B0 fuel. As the ratio of biodiesel in the mixture increased, the torque rise value of the engine decreased (Figure 4).

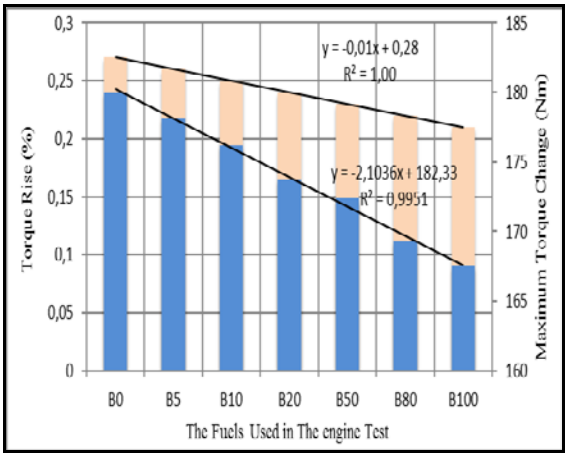


Figure 4. *Change in the torque rise and maximum torque curves based on the fuels used*

In this study where the effects of pump usage life span were ignored, the power levels of the B10, B20, B50, B80 and B100. As the change in maximum torque and nominal torque curves decreases, the torque rise changes also decrease. As the ratio of biodiesel in the mixture increased, torque rise, as well as torque at maximum speed, and change at maximum torque values decreased. In the study by Bolat (2007) taking the torque rise parameter into account, the effects of the 3% maximum torque difference among different fuels on work performance were more thoroughly explained. Accordingly, it was found that increasing proportion of the added biodiesel linearly decreased torque values at each expansion point. Similar results were achieved in a study by Fioresel et al. (2012), where they argued that the decrease in the maximum torque and maximum power shift values based on the introduction of biodiesel into the mixture, caused a decrease in the change of the engine's torque rise and this change in the regression equation y= □ 0.094249x+245.64 continued for the fuels B5, B20, B40, B60, B80 and B100 after the fuel B0.

4. Conclusion

As a result of the study, the increase in proportion of biodiesel in the mixture decreased the engine's power. In changing rates from B5 through B100, at all speeds of the engine, there was a decrease in the engine's effective power in comparison to the B0 fuel. There was a small decrease in the effective power values of the B5 fuel when compared to the B0 fuel in high speeds. In this study where the effects of pump usage life span were ignored, the power levels of the B10, B20, B50, B80 and B100 fuels decreased based on the decrease in combustion efficiency dependent on viscosity. In usage of the fuels B100, B80, B50 and B20, torque rise values in comparison to the B0 fuel decreased by 22.2%, 18.51%, 14.81%, and 11.11 respectively. The torque rise value for the B10 fuel decreased by 7.4% when compared to the B0 fuel. This decrease was 3.7% for the B5 fuel. The torque rise value of the B0 fuel was closer to the B5 fuel. As the proportion of biodiesel in the mixture increased, the torque rise value decreased. The reason for this is that based on the introduction of biodiesel into the mixture, fuel consumption increases, power production decreases and the fuel's combustion efficiency is reduced. In all experiments, the B100 fuel did not provide any advantages over the B0 fuel in terms of the engine's characteristic curves, and proved less likely to act as an alternative to standard diesel by its lower performance. According to the results of this study, the values obtained on experiments on the B5 fuel were relatively closer to those obtained on the B0 fuel. In today's circumstances, the B5 fuel may be suggested as an alternative to the B0 fuel.

5. RESOURCES

Alpgiray, B. (2006). Determination of the Effect of Rapeseed Oil Diesel Engine Performance and Emissions Characteristics. master's thesis. Ankara University, Graduate School of Natural and Applied Sciences, Ankara.

Anonymous (2010a). Sıvı Petrol Ürünleri - Yağ Asidi Metil Esterleri (YAME/Biyodizel) - Diesel Motorlarda ve Isıtma Uygulamalarında Kullanılan Özellikler ve Deney Yöntemleri https://intweb.tse.org.tr/standard/standard/Standard.aspx? Erişim Tarihi: 18.06.2014.

Anonymous (2010b). Türk Standardı. TS No: TS 1231. https://www.intweb.tse.org.tr. Erişim Tarihi: 02.03.2014.

Behcet, R, Cakmak, A. V (2014). Bir Diesel Motorda Yakıt Olarak Kullanılan Balık Yağı Metil Esteri Karışımlarının Motor Performans ve Emisyonlarına Etkisi, Bitlis Eren Üniversitesi Fen Bilimleri Dergisi, 3(1): 15–23.

Bolat, A. (2007). The Effect of Biodiesel On Engine Performance of An Mıd - Hp Agricultural Tractor and Sıgnıficance Of Bıodiesel For Turkey. Master Thesis, Trakya University Graduate School of Natural and Applied Sciences, Edirne.

Cengelci, E, Bayrakceken, H, Aksoy, F (2011). Bir Diesel Motorunda Hayvansal Yağ Metil Esterinin Kullanımının Motor Performansı ve Emisyonlarına Etkisi. Electronic Journal of Vehicle Technologies, 41-53.

Elicin, A, K. (2011) Investigation of the Effect of Air Intake Pressure on the Performance and Emmissions Characteristics in A Small Diesel Engine Using Biodiesel.. PhD Thesis, Ankara University, Institute of Science and Technology, Ankara.

Fioresel, D, A, Dallmeyer, A, U, Romano, L, N. Schlosser, J, F, MachadoI,, P, R, M. (2012). Performance of an agricultural tractor engine in dynamometer with chicken oil biodiesel and binary mixtures with diesel oil, 42: 660–666.

Sabancı, A., Atal, M., Yasar, A. (2006). Türkiye' de Biyodizel Kullanım ve Olanakları. Tarım Makinaları Bilim Dergisi, 2 (1) : 33-39.

DEVLOPMENT AND STUDY OF A MATHEMATICAL MODEL USED IN THE AUTOMATIC CONTROL SYSTEMS OF SMALL-SIZE UAVS

M.Sc. Kambushev M. PhD.[1], M.Sc. Biliderov S. PhD.[1]
Faculty of Aviation, Dolna Mitropolia – National Military University, Veliko Turnovo, Bulgaria [1]

m_kambushev@yahoo.com, biliderow_ss@yahoo.com

Abstract: *This paper presents the process of developing and studying of a complete mathematical model of the spatial movement of drones. The model synthesized is used in their automatic control systems.*

Keywords*: mathematical model, small-size uavs, automatic control systems*

РАЗРАБОТВАНЕ И ИЗСЛЕДВАНЕ НА МАТЕМАТИЧЕН МОДЕЛ, ИЗПОЛЗВАН В СИСТЕМИТЕ ЗА АВТОМАТИЧНО УПРАВЛЕНИЕ НА МАЛОГАБАРИТНИ БЕЗПИЛОТНИЛЕТАТЕЛНИ АПАРАТИ

маг. инж. Камбушев М., д-р, маг. инж. Билидеров С., д-р [1]
Факултет “Авиационен”, Долна Митрополия – Национален Военен Университет, Велико Търново, България [1]

m_kambushev@yahoo.com, biliderow_ss@yahoo.com

Abstract: *В настоящият доклад е разработен и изследван пълен математичен модел на пространственото движение на безпилотни летателни апарати. Синтезираният модел се използва в системата му за автоматично управление.*

Keywords: *математичен модел, малогабаритни безпилотни летателни, системи за автоматично управление*

1. Introduction

Small-sized UAVs are increasingly used in human activity. This application extends from hobby activities to the performance of professional duties. To enable these aircraft to perform successfully the tasks for which they are intended it is necessary to manage their attitude in space and relative to the ground. This management is carried out thanks to information-managing complex placed aboard a the flying machine.

Management effectiveness of this type of drones is directly connected with both mathematical model that relies on algorithms ruling board computers and sensors necessary to provide this mathematical model with information about the flight.

In popular literature, which describes the dynamics of flight, equations of motion are displayed in the global coordinate system without considering the movement of small-sized unmanned aircraft to a local coordinate system related to the earth's surface. On the other hand, in the literature that describes the different navigation algorithms are reported mostly kinematic relationships without knowing the forces and moments that cause changes of speeds and accelerations of the aircraft. In fact these accelerations are measured on board the aircraft.

This leads to the idea of developing a full mathematical model of spatial movement of aircraft in terms of information tools that are placed on board. Hence the task of the study because it is necessary to examine the applicability of this model in the compact drones.

Depending on the design scheme (airplane or helicopter), which will be used to solve a specific task it is necessary for the equations in the model to undergo certain changes, namely to meet the requirements of each particular scheme. All this is directly related to the algorithm based on the laws for managing small-scale aircraft and copters.

These laws of control are implemented in the automatic control systems of small-sized aircraft, which are responsible for the spatial movement and trajectory of uavs.

2. Synthesizing mathematical model of the flight

In order to derive the equations of the mathematical model of spatial movement of small-sized aircraft some simplifications are made. These simplifications are related to the shape of the Earth, obtaining of the vertical over the location of the aircraft, the fuselage structure, etc.

In the first approximation the shape of the Earth is assumed to be a sphere with radius $\vec{r}$ (Fig. 1), to which the geocentric coordinate system and its vertical are connected. This acceptance simplifies many calculations because it renders it unnecessary to calculate both the radiuses of the curvature of the ellipsoid. Moreover, the global satellite navigation systems such as GPS and inertial navigation systems measure travel speeds and coordinates of the location of the aircraft in the global coordinate system.

In terms of construction, small-sized UAVs are considered rigid bodies with six degrees of freedom.

The equations for spatial movement of miniature unmanned aircraft are displayed with the adoption of the above assumptions, the movement itself is split into movement of the center of mass and movement around the center of mass.

The movement of the center of mass of miniature unmanned aircraft in inertial coordinate system is described by the vector equation of Newton's second law:

$$m.\vec{a} = \sum \vec{F} \qquad (1)$$

As the accelerations $\vec{a}$ act in inertial coordinate system, where the amount forces $\sum \vec{F}$ are deployed along the axes of the body-

fixed , wind and local frames all of them have to be brought into the body-fixed frame.

Information on the accelerations measured on board the small-sized aircraft is taken from the platform $\vec{\xi}\vec{\eta}\vec{\zeta}$ (Fig. 1), which accommodates the accelerometers and gyros of the inertial navigation system. When on board the aircraft is put a strapdown inertial navigation system then that is a computing platform.

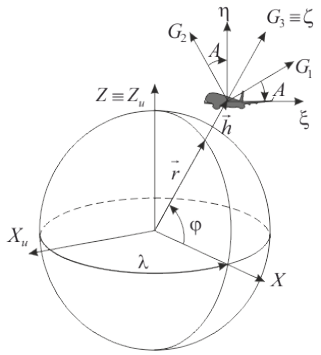


Fig. 1 *Coordinate systems used to navigation purpouse.*

Thus, orienting the axes of the platform in the cardinal directions and the local vertical (Fig.1) on board small-sized drones information is received about the course and the horizon. Accelerations measured by the accelerometers designed are projected onto the axes of the platform.

The accelerometers placed on the platform measure acceleration equal to the difference between the absolute and the relative ground projected onto the axes of the platform $\vec{g}_{\xi\eta\zeta}$:

$$\vec{a}_{\xi\eta\zeta} = \vec{a}^{a}_{X_u Y_u Z_u} - \vec{g}_{\xi\eta\zeta} \tag{2}$$

Bearing on board the readings of the accelerometers located along the axes of the platform of the inertial system and adding these indications to the projections of the relative acceleration of gravity on the axes of the platform to give we obtain the value of the absolute acceleration of the center of the platform. For obtaining a solution of an equation (1) this acceleration (2) must be designed along the axes of an UAV's body-fixed frame.

Vector equation of the absolute acceleration of the center of mass of small-sized aircraft designed on the axles of the body-fixed frame has the form:

$$\frac{d\vec{V}}{dt} = \frac{\tilde{d}\vec{V}}{dt} + \vec{\omega} \times \vec{V} \tag{3}$$

where with $\frac{\tilde{d}\vec{V}}{dt}$ is marked the acceleration measured in the body-fixed frame and the member $\vec{\omega} \times \vec{V}$ describes the angular velocity of rotation of the body-fixed frame related to inertial frame.

The absolute acceleration (3) is proportional to the sum of the external forces acting along the axes of the body-fixed frame. For different types of small-size aircraft that amount has a different kind.

In the event that a small-sized aircraft is performed constructed in a plane scheme, then the resultant of external forces acting on the axes of the body-fixed frame on the aircraft is described by the expression:

$$\sum \vec{F} = \vec{R} + \vec{P} + \vec{G} \tag{4}$$

where the sum forces $\vec{F}$ is:

- $\vec{P}$ - thrust engine.
- $\vec{G}$ - force on the weight.
- $\vec{R}(\vec{X}, \vec{Y}, \vec{Z})$ - aerodynamic forces.

It is assumed that the motor axis coincides with the axis (*Mx1*) of the body-fixed frame. In this case, this force will be a projection only along the longitudinal axis of the airplane.

Gravity is always directed along local vertical in the case of geocentric coordinate system to the center of the Earth. And projections on the axes of the aircraft are set by the following vector:

$$\begin{pmatrix} G_x \\ G_y \\ G_z \end{pmatrix} = \mathbf{C}^T \begin{pmatrix} 0 \\ 0 \\ -G \end{pmatrix} = \begin{pmatrix} -G\sin\vartheta \\ -G\cos\gamma\cos\vartheta \\ G\sin\gamma\cos\vartheta \end{pmatrix} \tag{5}$$

The aerodynamic forces acting on the aircraft developed on airplane scheme in the most general case are: $\vec{X}_a$ - drag force; $\vec{Y}_a$ - lift force and $\vec{Z}_a$ - side force.

They are created by the air flow and are located in the wind frame. Projections in the body-fixed frame are obtained by means of the rotation matrix $\mathbf{Q}_{(\alpha,\beta)}$:

$$\begin{pmatrix} R_x \\ R_y \\ R_z \end{pmatrix} = \mathbf{Q}_{(\alpha,\beta)} \begin{pmatrix} -X_a \\ Y_a \\ Z_a \end{pmatrix} \tag{6}$$

The case for airplane scheme has been developed in great detail in most of the textbooks on dynamics of flight [1,7,11].

For copter schemes and in particular for tricopter, external forces are projected along axes *Mx1y1z1*- of the body-fixed frame and obtain the equations that define the forward movement of the machine:

$$\sum \vec{F} = \begin{bmatrix} \sum \vec{F}_x \\ \sum \vec{F}_y \\ \sum \vec{F}_z \end{bmatrix} = \begin{bmatrix} -G.\sin(\vartheta) \\ F_A + F_B + F_C.\cos(\alpha) - G.\cos(\gamma).\cos(\vartheta) \\ F_C.\sin(\alpha) + G.\sin(\gamma).\cos(\vartheta) \end{bmatrix} \tag{7}$$

where: F_A, F_B, F_C is the thrust of the engine-propeller system for each of the tricopter's arms; ϑ, γ, ψ are the angles of roll, pitch and yaw; α is the angle of deflection of the tail rotor.

The spatial movement of a tricopter is described in [9] [10].

When considering the movement of quadrocopter (Fig. 2), for the forces acting in flight in its forward movement is obtained the expression:

$$\sum \vec{F} = \begin{bmatrix} \sum \vec{F}_x \\ \sum \vec{F}_y \\ \sum \vec{F}_z \end{bmatrix} = \begin{bmatrix} -G.\sin(\vartheta) \\ F_A + F_B + F_C + F_D - G.\cos(\gamma).\cos(\vartheta) \\ G.\sin(\gamma).\cos(\vartheta) \end{bmatrix} \tag{8}$$

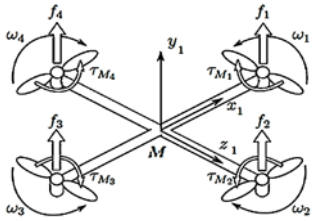


Fig.2 *The forces and the moments in quadrocopter flight.*

So with the help of equation (4) is described the movement of the center of mass of small-sized unmanned aircraft.

The description of the movement around the center of mass of this type of aircraft is carried out by integrating the derivative of the kinetic moment:

$$\frac{d\vec{K}}{dt} = \sum \vec{M} \tag{9}$$

where $\vec{K} = \sum\left(\vec{r}_k \times m_k \vec{V}_k\right)$ is the kinetic moment of the aircraft.

When switching to the axes of the body-fixed frame with the solution of equation (9) are obtained the projections of the absolute angular velocities of a small-sized unmanned aircraft from (3) on these axes.

Using the so obtained angular velocities is calculated the spatial angular position of the aircraft relative to the natural horizon and the vertical [6]. Actually, the measure angular speeds of the aircraft along the axes of the body-fixed frame on the platform are measured $\vec{\xi}\vec{\eta}\vec{\zeta}$ with the help of , angular speed sensors (gyroscopes).

If the platform is deflected at an angle of azimuth A of the coordinate system $OG_1G_2G_3$ looming cardinal directions (Fig. 3), then the relative angular speeds of the platform is available through the angle of azimuth and angular velocities of the basis relative to the spherical surface of the Earth:

$$\begin{aligned} \omega_\xi &= \omega_{G_1}.\cos(A) - \omega_{G_2}.\sin(A) \\ \omega_\eta &= \omega_{G_1}.\sin(A) + \omega_{G_2}.\cos(A) \\ \omega_\zeta &= \omega_{G_3} \end{aligned} \tag{10}$$

Unlike mounted platform accelerometers, which measure the absolute acceleration, gyroscops measure the sum of the angular velocity of the platform and the small-size unmanned aircraft.

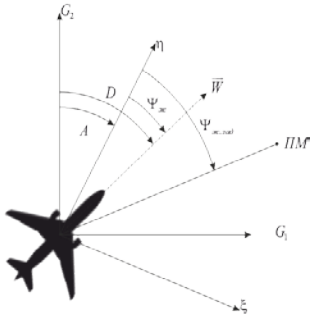


Fig. 3 *Determination of the angular position of the platform* $O\xi\eta\zeta$.

For an airplane scheme, the amount of moments (9) is :

$$\begin{aligned} \dot{\omega}_x &= \frac{1}{I_x}\left[M_x - \left(I_z - I_y\right)\omega_y\omega_z\right], \\ \dot{\omega}_y &= \frac{1}{I_y}\left[M_y - \left(I_x - I_z\right)\omega_x\omega_z\right], \\ \dot{\omega}_z &= \frac{1}{I_z}\left[M_z - \left(I_y - I_x\right)\omega_x\omega_y\right]. \end{aligned} \tag{11}$$

In case of tricopters for to the equations of the moments along the axes *Mx1y1z1*- of the trikopter's body-fixed frame are obtained ratios ratios:

$$\begin{aligned} &\sum M_x = \left(F_A - F_B\right).\sin\left(\beta/2\right).d; \\ &\sum M_y = F_C.\sin(\alpha).d - \left(M_{A_{yp}} f(F_A) + M_{B_{yp}} f(F_B) + M_{C_{yp}} f(F_C, \cos(\alpha))\right); \\ &\sum M_z = \left(F_A + F_B\right).d.\cos\left(\beta/2\right) - F_C.\cos(\alpha).d + M_{C_{zp}} f(F_C.\sin(\alpha)). \end{aligned} \tag{12}$$

where: $M_{A_{yp}}, M_{B_{yp}}, M_{C_{yp}}, M_{C_{zp}}$ are reactive moments created by the propellers and projected along the arms of the body-fixed frame; β is the angle between the arms of tricopter; *d* is the length of the arm of tricopter.

In the case of quadrocopter projections of the moments on the body-fixed frame are:

$$\tau_B = \begin{bmatrix} M_x \\ M_y \\ M_z \end{bmatrix} = \begin{bmatrix} lk(-\omega_2^2 + \omega_4^2) \\ \sum_{i=1}^{4} \tau_{M_i} \\ lk(-\omega_1^2 + \omega_3^2) \end{bmatrix} \tag{13}$$

where: k is the proportionality coefficient between engine speed and the thrust created by the motor, *l* is the distance between the rotor and the center of mass of quadcopter, *ωi* is the angular speed of the rotor *i*, *τMi* is reactive moment around the axis of the rotor.

Finding the coordinates of the center of mass of the aircraft is done with inertial navigation system or with GPS. The route points of unmanned aircraft are set on the map with geographic coordinates. When measuring coordinates to GPS, are obtained the coordinates in global geocentric coordinate system. To transfer to a local Cartesian system which is suitable for measuring the location of small-size UAVs is necessary: to know the starting point of the flight (B_0, L_0, h_0), and then to perform the transition (B_0, L_0, h_0)→(x_0, y_0, z_0)→(φ_0, λ_0, R).

Via a matrix of directing cosines transfers the fixed-body frame to the basic $\left(x_1, y_1, z_1\right) \xrightarrow{C(\psi_M, \gamma, \vartheta)} \left(G_1, G_2, G_3\right)$, and then trought (14) are calculated the coordinates in the local system.

$$\begin{bmatrix} x \\ y \\ z \end{bmatrix} = \begin{bmatrix} -\sin(\varphi).\cos(\lambda) & \sin(\lambda) & \cos(\varphi).\cos(\lambda) \\ -\sin(\varphi).\sin(\lambda) & \cos(\lambda) & \cos(\varphi).\sin(\lambda) \\ \cos(\varphi) & 0 & \sin(\varphi) \end{bmatrix}.\begin{bmatrix} G_1 \\ G_2 \\ G_3 \end{bmatrix} \tag{14}$$

Returning in the geographic system is carried out with the transition described in [2]. When the coordinates are measured by the inertial navigation system it has to perform a double integration of the absolute acceleration, and the transitions between the coordinate systems are the same as those described above.

3. Simulation of synthesising model

After finding the mathematical expression for the spatial movement of small-sized unmanned aircraft it is solved inverse problem – What will the instrumental systems installed on board show?

In simulation are used equations for quadrocopter because other are addressed to a airplane diagram [7] and [11], and for tricopter in [9] and [10].

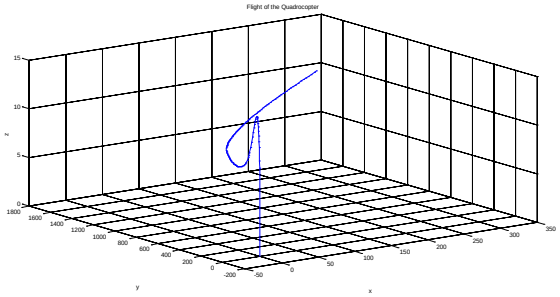


Fig.3 *The flight of the quadrocopter.*

Quadcopter climbs to 10 meters and carry out a straight flight for up to 55 sec., when it receives a signal for change of the heading (Fig. 3).

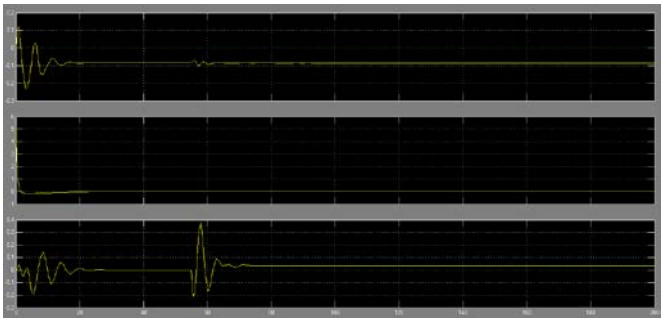


Fig.4 *The measurements of the accelerometers .*
Fig.4 *The measurements of the accelerometers .*

The readings of accelerometers on board without noise in the measurement are shown in Fig.4.

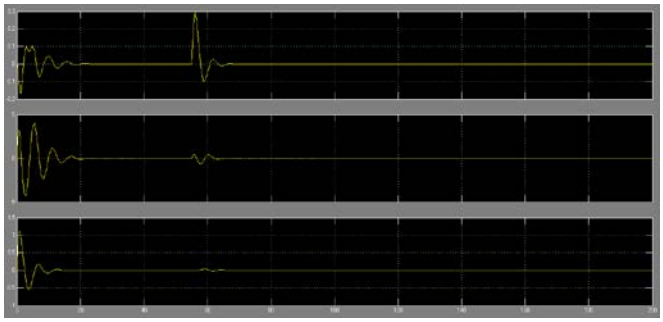


Fig.5 *The measurements of the gyros.*

On Fig.5 and Fig.6 are shown gyroscopic readings and calculated angles of yaw, roll and pitch.

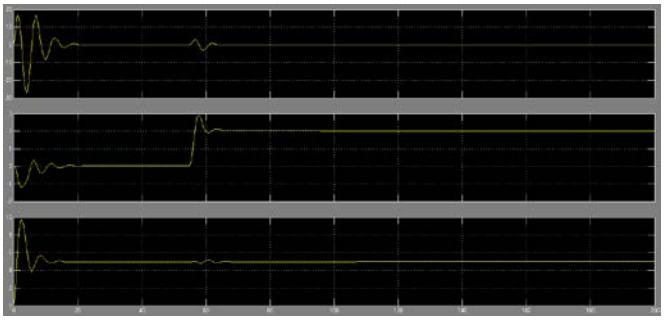


Fig.6 *The Euler's angles.*

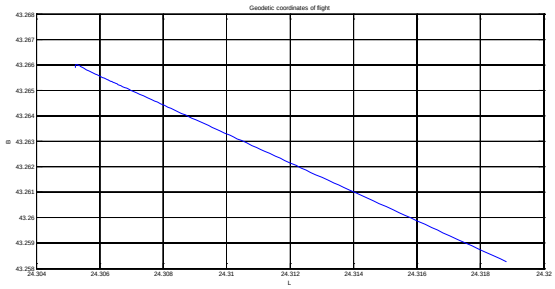


Fig.7 *The geographical coordinates of flight.*

4. Conclusions and results

1. Different models of small-size UAVs are examined in terms of the measurement information;
2. A fix of information from the global navigation systems to local coordinate system is made;
3. The proposed algorithms are used for navigation and management of small-size UAVs;

5. Bibliography

[1] Алаян О., В. Ромасевич, В. Совгиренко. Аэродинамика и динамика полета вертолета. София, 1975г.

[2] Бабич О., Обработка информации в навигационных комплексах. Москва 1991г.

[3] Билидеров С.С., М. М. Камбушев. Оценка на експериментално получени характеристики на системата двигател-витло за мини-безпилотни летателни апарати. ЮНС 2013, гр. Долна Митрополия, 2013г.

[4] Велева Е., Караколева С. Практикум по „Числени методи“ с Matlab. РУ“Ангел Кънчев“, Русе 2004г.

[5] Йончев А., Константинов М., Петков П. Линеини матрични неравенства в теория на управлението. София, 2005, 311с.

[6] Квакернак Х., Сиван Р. Линейные оптимальные системы управлениял. Москва ”Мир”, 1977, 653с.

[7] Лысенко Н. М. Динамика полета. София, 1977, 638с

[8] Маджаров Н. Е. Линейни системи за управление. София, 1998,208с.

[9] Kambushev M., Biliderov S. Defining the control law for yaw mechanism control of a tricopter. Trans&motAuto 2015.

[10] Kambushev M., Biliderov S., Varbanov Y. Synthesis and study of the mathematical model of a tricopter. AFASES 2016.

[11] Stevens B.L., Lewis F. L. Aircraft control and simulation. John Wiley&Sons,2003.

[12] Vinod KR Singh Patel, A. K. Pandey Modeling and Performance Analys of PID Controlled BLDC Motor and Different Schemes of PWM controlled BLDC Motor. International Journal of Scientific and Research Publications, Volume 3, Issue 4, April 2013.

1D SIMULATION AS AN ELEMENT OF AN EFFICIENT METHODOLOGY FOR ENGINE CONCEPT DEVELOPMENT

Dr. Dimitrov D.[1], Dr. Pirker G.[1], Dr. Schnessl E. [1], Prof. Dr. Wimmer A.[1,2]
LEC GmbH (Large Engines Competence Center), Graz, Austria [1]
Graz University of Technology, Graz, Austria [2]

Dimitar.Dimitrov@lec.tugraz.at

Abstract: *The development of highly efficient combustion concepts for internal combustion engines requires a suitable development methodology. In recent years, the LEC has created LDM (LEC Development Methodology), which is based on the intensive interaction between simulation and experimental investigations on single cylinder research engines. As new engine concepts are developed, many operating parameters are first defined and optimized with a 1D multicylinder engine model. This model illustrates the full complexity of the engine with its geometry, turbocharging and combustion parameters. The design of experiments (DoE) method is used in connection with 1D simulation to find the optimal engine configuration as well as parameters related to the combustion process, i.e. valve timing, compression ratio, ignition timing, excess air ratio. The maximum engine efficiency is found by taking into account the boundary conditions (brake mean effective pressure, turbocharger efficiency), where NOx level and knock limit are constraints.*

Keywords: INTERNAL COMBUSTION ENGINES, DEVELOPMENT METHODOLOGY, 1D SIMULATION

1. Introduction

The trend toward higher efficiencies and increasingly stringent emission legislation are greatly pushing forward engine development. A variety of degrees of freedom emerge in the optimization of engines because of the various possible ways to reach the targets as well as the interaction between individual operating parameters. A global optimum for these operating parameters should be found so the engine can be operated with the best possible efficiency and the required power output without the occurrence of knock and while complying with emission legislation [12].

Simulation is a central component of a development and optimization methodology for new engines. While commercially available software (AVL Boost, GT-Power) is relied upon to simulate the engine cycle, most of the required 0D submodels are developed or expanded at the Large Engines Competence Center (LEC).

This paper explains the basic characteristics of the development methodology and the important role that 1D simulation plays in the development of new engines. The required models and boundary conditions are discussed and several applications are provided as examples of successful use of the methodology.

2. LEC Development Methodology

LDM (**L**EC **D**evelopment **M**ethodology) is used to develop and optimize combustion concepts for engines at the LEC. LDM is based on the intensive interaction between simulation and experimental investigations on single cylinder research engines (SCE) and multicylinder engines (MCE), see Figure 1.

This methodology makes use of 3D CFD simulation and 0D/1D engine cycle simulation. While 3D CFD simulation is employed above all to optimize the details of relevant processes (e.g., mixture formation and combustion in the prechamber and main combustion chamber, determination of the location of knock), 0D/1D engine cycle simulation is applied to pre-optimize significant engine parameters (e.g., compression ratio, valve timing). In order that this methodology can be applied, it must be guaranteed that the results from single cylinder tests can be transferred to the multicylinder engine. To this end, it is necessary to achieve boundary conditions comparable to those of the multicylinder engine. Not only the thermal boundary conditions but also the conditions at the beginning of the intake stroke (temperature, pressure, and working gas composition) are required. These conditions are determined in an iterative process based on 1D engine cycle simulation of the multicylinder engine and the single cylinder setup. [2]

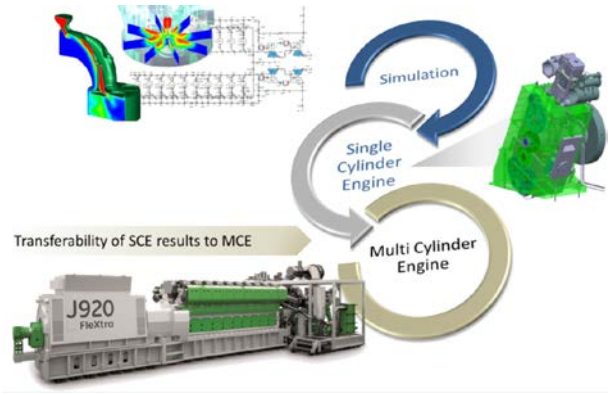


Fig. 1 *LDM: LEC Development Methodology.*

3. Submodels required for 1D simulation

1D simulation requires not only the standard boundary conditions but also the rate of heat release in the cylinder. Measurement data from comparable operating points on similar engines can also be used to determine the actual rate of heat release history using engine cycle calculation. However, this has the disadvantage that the rate of heat release history does not fit exactly to the actual boundary conditions. Ideally, the rate of heat release history is calculated with a 0D rate of heat release model implemented in the cylinder of the engine cycle calculation software based on the conditions at intake valve closing calculated in 1D simulation. 0D models for calculating NOx formation and knock models can also be implemented in this manner.

The rate of heat release models discussed below are particularly suitable for use in this development methodology as they contain few empirical assumptions due to their physical basis and thus only a few model parameters must be calibrated. In addition, they have very short calculation times.

3.1. Rate of heat release models for open chamber gas engines, prechamber engines, DI diesel engines and dual fuel engines

The basic principle of the 0D rate of heat release model for open chamber gas engines and prechamber gas engines rests on the propagation of a hemispherical flame of finite thickness that rushes through the pre-mixed charge in the combustion chamber [4]. The calculation of laminar flame speed, which is dependent on fuel type, temperature, pressure and mixture quality, and its increase due to effects of turbulent density and density differences between the unburned and the burned gas zones help to describe the reaction rate. The gas mass available in the flame front can either be converted into a rate of heat release according to the Magnussen model or by applying the well-known entrainment model [14].

To describe the ROHR in the prechamber engine, the effects of the gas jets issuing from the prechamber are modeled [7].

The main combustion chamber and the prechamber are treated as two combustion chambers connected by a restriction. After ignition occurs in the prechamber, the initially hemispherical surface of the flame front is restricted soon after combustion starts due to contact with the prechamber walls. The flame front moves away from the spark plug in the direction of the transfer ducts at the turbulent flame speed; the volume of the flame front is determined by the combustion chamber geometry. The burning gas jets issuing from the transfer ducts mingle with a part of the surrounding unburned charge and act as the starting point for the progression of a flame front in the main combustion chamber.

The LEC has also developed models for DI diesel engines that describe combustion as well as ignition delay and pre-mixed combustion, all of which are either based on the MCC approach (mixing controlled combustion) [5], [6], or on a package model [17]. The quality of the results improves when an injection rate curve is specified and a quasidimensional spray model is applied.

Taking these requirements into account, a 0D simulation approach that predicts the rate of heat release in dual fuel engines was developed [15],[16]. The characteristics of dual fuel combustion require a two-stage simulation approach that combines the first phase of combustion, which is dominated by diesel fuel combustion, with the second phase of combustion, which involves homogeneous combustion of a background mixture consisting of natural gas and air. A package model similar to models used to simulate diesel engines is applied to describe the first phase; the second phase is modeled using an entrainment model [14].

3.2. NOx model

The NOx concentration that arises during combustion is calculated from the well-known Pattas and Häfner model [8], which only accounts for the formation of thermal NO using an extended Zeldovich mechanism with a total of six chemical equations. The differential equation derived in this model was adopted unchanged. The required equilibrium concentrations of the individual species are calculated with a gas properties program based on the JANAF thermochemical tables. The temperature of the burned zone for simulating the post-flame reactions was calculated from the ROHR model with a two-zone model.

In the case of a prechamber engine, the prechamber and the main combustion chamber must be treated separately; nevertheless, their interaction has to be considered. The detailed approach for calculating NOx emissions from prechamber engines is described in [13].

3.3. Knock model

Simple 0D models were developed to describe and predict the phenomena associated with knocking combustion in gas engines [9], [10]. An Arrhenius equation that calculates the rise in the concentration of radicals in the unburned charge is used to determine the onset of knock. The reaction rate is determined between intake valve closing and knock onset from the cylinder pressure, the temperature of the unburned zone and the methane number and then the integral is taken. A simulated combustion cycle is described as knocking if the integral value between the start and end of combustion reaches a certain threshold. At the same time, a specific amount of unburned fuel mass must still be present in the cylinder at the calculated start of knock and the knock intensity of the simulated cycle (pressure amplitude of the high-frequency oscillations at the start of knock) must also exceed a given threshold value. All these thresholds must be calibrated from existing measurements or from empirical values before simulation.

3.4. Measurement data analysis as the basis for calibrating 0D models

Measurement data is required for development and calibration of 0D models as well as calculation of the rates of heat release for direct specification in 1D simulation. Developed at the LEC, the engine cycle calculation program LEC-CORA is used to analyze the operating points measured on the test bed. The software package CORA (Combustion, Optimization, Research and Analysis) was designed to analyze and simulate the high pressure cycle of the working process of combustion engines. It enables analysis of measured pressure histories as well as simulation of cylinder conditions during the high pressure cycle upon specification of rate of heat release histories or rate of heat release models. The software is used in combustion analysis mainly for pressure level adjustment, pressure history analysis (high pressure cycle) and loss analysis of direct injection diesel engines and spark ignition gas engines with external mixture formation.

The great demands on the measurements that form the basis of analysis also make it necessary to check the quality of measurements automatically whenever possible directly at the test bed to allow early detection of errors [1]. In this context, a methodology for automated error diagnosis on engine test beds was developed at the LEC. The algorithms it relies upon are provided in the “LEC-MCheck” (LEC Measurement Check System) software solution and are used directly on the test bed.

Intensive use of these tools guarantees the high quality of measurements and the resulting rate of heat release histories, which in turn is advantageous when calibrating simulation models and interpreting the results.

4. Application of 1D simulation as part of the development methodology

The following section provides examples of applications that show how 1D simulation is used in a variety of areas in the process of developing a new engine.

4.1. Design of a single cylinder test bed and determination of boundary conditions for testing

Single cylinder research engines were set up at the LEC in order to optimize the thermodynamics of large engines; one example of an engine setup can be seen in Figure 2.

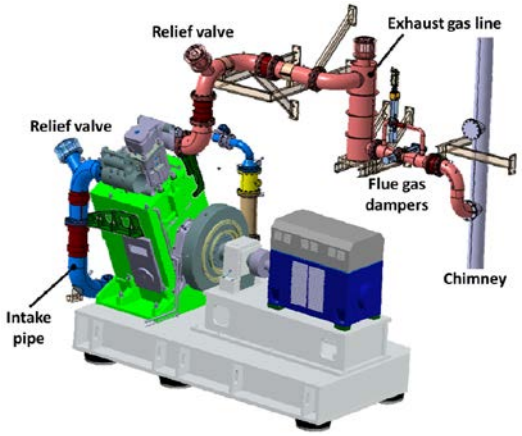


Fig. 2 *Single cylinder research engine (SCE).*

The main dimensions of the single cylinder research engine correspond to those of the multicylinder engine. When the single cylinder research engines are supplied with conditioned charge air (temperature, pressure and humidity), it is possible to adjust the conditions to those of the multicylinder engine and maintain them, thereby guaranteeing the transferability of the results of single cylinder tests to the multicylinder engine.

To ensure comparable operating conditions between the single cylinder research engine and the multicylinder engine in the broadest area possible, the intake and exhaust system is specially calibrated using comparative analysis with the multicylinder engine model based on 1D engine cycle analysis and adapted to the specific situation on the test bed. To evaluate the quality of the calibrated result, Figure 3 shows the simulated gas exchange pressure histories on the intake and exhaust sides of the MCE and the histories measured on the single cylinder research engine at the

same operating point. The following procedure is used to ensure the same conditions at the start of the high pressure cycle (temperature, pressure and composition of the working gas).

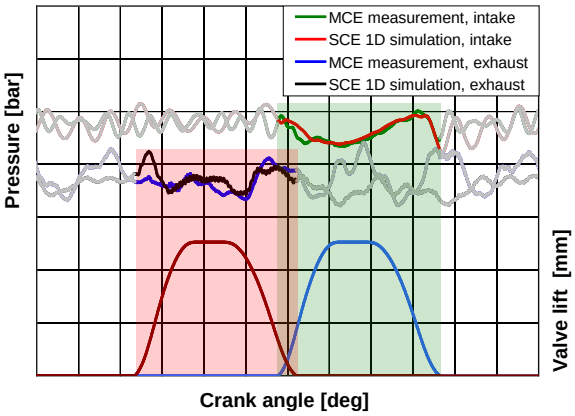


Fig. 3 *Calibration of gas dynamics in the intake and exhaust system of the single cylinder research engine.*

Based on 1D engine cycle simulation with the multicylinder engine model, the conditions in one representative cylinder at intake valve closing are determined using a simulated rate of heat release history as well as the parameters of the turbocharger and the specifications for load and excess air ratio. These results provide the basis for 1D engine cycle simulation with the model of the setup of the single cylinder research engine. Charge air and exhaust back pressure are varied until identical starting conditions appear at intake valve closing when the same conditions are set as with multicylinder engine simulation (rate of heat release history, load and excess air ratio). Measurements are conducted on the single cylinder research engine with the values thus determined for charge air pressure and exhaust back pressure. The rate of heat release history is then inserted into the calculation with the multicylinder engine model and run through a second time. Normally satisfactory agreement between the rate of heat release histories already appears after the second iteration loop and the procedure can be completed by determining the relevant values from multicylinder engine simulation. [3]

4.2. Detailed analysis of various processes within the engine

A great variety of processes within the engine can be analyzed using a 1D model. This section analyzes how NOx formation is determined in detail using the example of an engine with a prechamber and discusses the reasons for differences between the cylinders in multicylinder engines.

The prechamber concept is applied to large gas engines in particular. Figure 4 shows the modeling of both combustion chambers in the commercial GT-Power software.

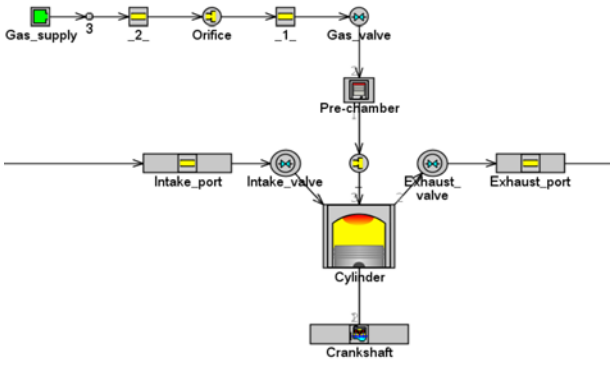


Fig.4 *Screenshot of the 1D model of a single cylinder research engine with a prechamber.*

The model is especially helpful for investigating knock behavior and NOx formation in both combustion chambers. Combustion is modeled using a thermodynamic two zone model because the determination of the temperature in the burned zone is required in order to simulate NOx accurately. The amount of NOx in the prechamber is determined separately from the amount in the cylinder using the NOx submodel described above. Results from measurements and from 3D CFD simulation are used to calibrate the NOx models. NOx concentrations in the prechamber and in the main combustion chamber are calculated with 1D simulation, results are shown in Figure 5. For low NOx concepts without exhaust gas aftertreatment, the engines are run with a leaner mixture (Lambda > 1.6) [11]. The enleanment of the cylinder produces several negative effects, for example a rise in HC emissions and subsequent loss in efficiency.

The goal of the investigation is to discover an optimal configuration that does not exceed the NOx limit and at the same time has the fewest losses. The following factors can be optimized:

- Charge composition in the prechamber at ignition timing. The excess air ratio in the prechamber can be controlled by the amount of gas that flows through the gas valve before the prechamber, see Figure 4.
- Prechamber size. Larger prechambers produce more NOx, but a certain amount is required for the momentum of the flame torches with which the mixture is ignited in the cylinder.
- Charge composition and combustion phasing in the cylinder.
- Prechamber geometry. It is depicted in the 1D model by the rate of heat release history. The rate of heat release histories used are obtained from the combustion analysis of measured operating points or from 3D CFD simulation.

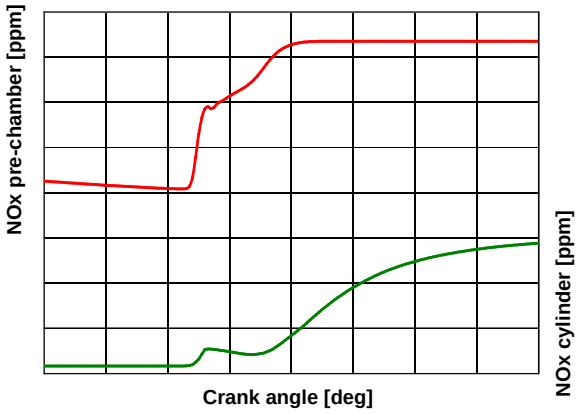


Fig. 5 *Simulated NOx concentrations with the NOx submodel in the prechamber and in the cylinder of a large gas engine.*

Another issue with the multicylinder engines that were investigated are the cylinder specific differences that are mainly detected as differences in peak firing pressure. They increase pollutant formation and knock tendency in spark ignition gas engines. Possible reasons for these differences are:

- Different cylinder masses due to gas dynamics in the intake system
- Different amounts of residual gas in each cylinder due to gas dynamics in the exhaust system and during valve overlap
- Different gas mixtures in the cylinders due to the characteristics of mixture formation (e.g., differences in air mass with gas engines with port fuel injection)
- Different combustion phasing in the cylinders due to the different charges and gas mixtures

With a calibrated 1D model, these effects can be modeled and measures can be taken that reduce these differences. Control strategies that can be applied to the multicylinder engine can also be elaborated.

3D CFD simulation is used to analyze the processes in the combustion chamber in detail. It can model spatial events such as

the location of knock or the mixture distribution. The required boundary conditions are prepared with a 1D model.

4.3. Preoptimization of the overall system using simulation

Based exclusively on simulation, virtual combustion process development places very great demands on the quality of the used simulation methodology. Preoptimization is crucial in the area of large engines in particular. First, stroke/bore ratio, compression ratio, excess air ratio, turbocharger configuration and valve timing are predesigned using engine cycle simulation based on ROHR, NOx formation and knock behavior models that have been calibrated on other research engines. 3D CFD methods are applied to preoptimize the fuel-mixture concept, the design of the prechamber, and combustion in detail. Preoptimization of the combustion results in a rate of heat release history that is used to calibrate 0D simulation models.

To apply the methodology, it is necessary to link together the 0D, 1D and 3D calculation models intensively so that the boundary conditions required for the calculations can be exchanged. This is largely carried out using standardized and automated processes.

The entire system is then optimized using 1D engine cycle simulation; Figure 6 provides an overview of the optimization process.

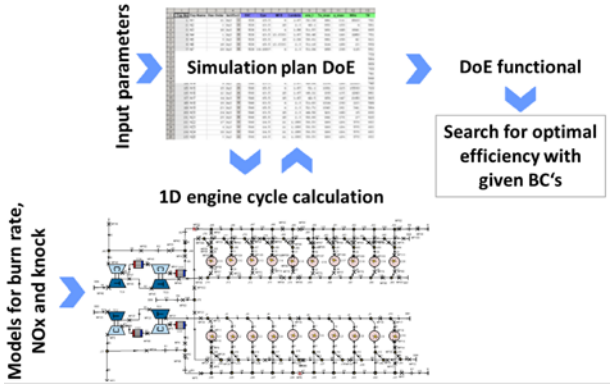


Fig. 6 *Procedure for applying DoE methods for 1D simulation.*

Due to the high complexity of the system and the large number of free parameters, the statistical method Design of Experiments (DoE) is heavily relied upon. The free parameters optimized on the basis of this approach are typically compression ratio, control of the combustion process, valve timing and turbocharger design. The goal of design is to achieve the greatest engine efficiency possible while staying within the boundary conditions of permissible NOx limits, maximum cylinder peak firing pressure and knock-free operation [2].

5. Summary and Conclusions

This paper presented the LEC development methodology, focusing in particular on the role 1D simulation plays in the methodology. The submodels as well as the required boundary conditions were presented and discussed. Selected examples of applications were used to show how the methodology can be put into practice.

In summary, the following conclusions can be drawn: LEC Development Methodology combines simulation with experimental investigations on single cylinder research engines in order to optimize fuel consumption and emissions. 1D simulation has become an important part of the process of developing highly efficient combustion concepts. The predictive quality of the simulation models also allows reliable thermodynamic predesign of a new engine on the basis of simulation alone. Using this approach, development time can be kept to a minimum and development costs can be significantly reduced.

6. References

[1] Wohlthan, M., Pirker, G., Krenn, M., Wimmer, A.: LEC-MCheck – Eine Methodik zur Fehlerdiagnose an Motorprüfständen. 15th Conference „The Working Process of the Internal Combustion Engine“, 2015

[2] Wimmer, A., Pirker, G., Schneßl, E., Trapp, C., Schaumberger, H., Klinkner, M.: Assessment of Simulation Models for the Development of Combustion Concepts for the New Generation of Large Gas Engines. Internationales Symposium für Verbrennungsdiagnostik, 2012

[3] Trapp, C., Laiminger, S., Chvatal, D., Wimmer, A., Schneßl, E., Pirker, G.: Die neue Jenbacher Gasmotorengeneration von GE – mit zweistufiger Aufladung zu höchsten Wirkungsgraden. 32. Internationales Wiener Motorensymposium, 2011

[4] Schlick, H., Pirker, G., Chmela, F., Wimmer, A.: Weiterentwicklung eines nulldimensionalen Brennratenmodells für direktgezündete Gasmotoren auf Basis der Computertomographie. Tagung „Motorische Verbrennung“, München, 2009

[5] Chmela, F., Engelmayer, M., Pirker, G., Wimmer, A.: Prediction of turbulence controlled combustion in diesel engines. Conference on thermo- and fluid dynamic processes in diesel engines (THIESEL), Valencia, 2004

[6] Pirker, G.; Chmela, F.; Wimmer, A.: ROHR Simulation for DI Diesel Engines Based on Sequential Combustion Mechanisms. SAE Paper 2006-01-0654, 2006

[7] Chmela, F., Dimitrov, D., Wimmer, A.: Simulation der Verbrennung bei Vorkammer-Großgasmotoren. 11. Tagung Der Arbeitsprozess des Verbrennungsmotors, Graz, 2007

[8] Pattas, K.; Häfner, G.: Stickoxidbildung bei der ottomotorischen Verbrennung, Motortechnische Zeitschrift, MTZ 34 (1973), 12

[9] Dimitrov, D., Chmela, F., Wimmer, A.: Eine Methode für die Vorausberechnung des Klopfverhaltens von Gasmotoren. 4. Dessauer Gasmotoren-Konferenz, 2005

[10] Dimitrov, D., Strasser, C., Chmela, F., Wimmer, A.: Vorhersage des Klopfverhaltens für Groß-Gasmotoren mit Direktzündung oder Vorkammer, 2. Tagung Klopfregelung für Ottomotoren - Trends für Serienentwickler, Berlin, 2006

[11] Tinschmann, G., Birgel, A., Trapp, C., Schnessl, E., Redtenbacher, C., Wimmer, A.: Large Gas Engines – 75 mg/Nm^3 @ 15%O_2 NOx `Engine-Internal Measures or Exhaust After-treatment?`. CIMAC Congress, Shanghai, 2013

[12] Krenn, M., Pirker, G., Mühlberger, M., Wimmer, A.: Einsatz der DoE-Methode zur simulationsbasierten Optimierung von Großgasmotoren. 14. Tagung Der Arbeitsprozess des Verbrennungsmotors, Graz, 2013

[13] Pirker, G.; Mayr, Ph.; Zelenka, J.; Krenn, M.; Redtenbacher, Ch.; Wimmer, A.: Method for Analyzing Prechamber NOx Emissions from Large Gas Engines. Paper No.130, 28th CIMAC World Congress, Helsinki, 2016.

[14] Tabaczynski, R et al.: A Turbulent Entrainment Model for Spark-Ignition Engine Combustion, SAE-Paper 770647, 1977.

[15] Krenn et al. : Methodology for Analysis and Simulation of Dual Fuel Combustion in Large Engines. THIESEL Conference on Thermo- and Fluid Dynamic Processes in Direct Injection Engines, Valencia, 2014

[16] Krenn, M.; Pirker, G.; Redtenbacher, C.; Wimmer, A.: A new approach for combustion modeling of large dual-fuel engines, in: Heavy-Duty, On- and Off-Highway Engines, 10th International MTZ Conference, Speyer, 2015

[17] Hiroyasu H et al.: Development and Use of a Spray Combustion Modeling to Predict Diesel Engine Efficiency and Pollutant Emissions. Bulletin of the JSME, No. 214, 1983.

THE INFLUENCE OF VEHICLE OPERATION ON THE BRAKE FLUID BOILING POINT

Ing. Skrucany T.[1], Ing. Semanova S.[1], dr hab. inz. Tomasz Figlus.[2] , Bc. Scurok O. [1],
Faculty of Operation and Economics of Transport and Communication – University of Zilina, the Slovak Republic [1]
Silesian University of Technology, Faculty of Transport, Department of Automotive Vehicle Construction, Poland [2]

tomas.skrucany@fpedas.uniza.sk

Abstract: *The possibility to brake is the most important thing in the road transport safety. The effectiveness of the vehicle braking is influenced by brake fluid state – exactly the water volume share in the fluid. The brake fluid boiling point describes water volume in the fluid. By measuring the boiling point, this paper examines how a boiling point decline is influenced by the vehicle operation.*

Keywords: BRAKE FLUID BOILING POINT, VEHICLE OPERATION, MEASUREMENT

1. Introduction

Brakes are an important safety feature of vehicles. The quality of brake fluid is important for the operation of a hydraulic braking system. Quality characteristics of the brake fluid affect significantly the functionality of operated brakes and thus the safety of vehicle occupants and other road users.

2. Physical and Chemical Properties of Brake Fluid

Many international, national and corporate standards and specifications exist to describe physical and chemical properties of brake fluid produced based on glycol. They are derived mainly from standard SAE J 1703, e.g. FMVSS CFR571.116, ISO 4925, NF 12-640, RS 1305-68, and etc. These standards include not only basic physical and chemical properties of brake fluid but also the exact procedure for an evaluation of brake fluid before placing in the market (e.g. colour, boiling point, viscosity, evaporation, and etc.).

The boiling point should be as high as possible in order to prevent from the formation of air (steam) bubbles at high temperature during braking in a brake system. The viscosity should be the lowest in the cold state and the highest during heat (a high viscosity index is required). Corrosion protection of metal parts of a braking system is important because it significantly affects lifetime of brake fluid. The lubricating properties are also important because of the protection of brake system components which move against to each other. The compressibility should be minimal and it should be independent on temperature and pressure if possible. The brake fluid should not evaporate under no conditions, any temperature or other impacts that occur in a brake system. It should remain as stable as possible and to be miscible with other brake fluid. Operating temperature of brake fluid in brake systems of vehicles range from -50 °C to +200 °C and more, particularly for sports cars.[1, 2]

Table 1: *Classification of brake fluid. [4]*

Standard	FMVSS 116			ISO 4925	SAE J1703
	DOT 3	DOT 4	DOT5.1		
Dry boiling point [°C]	≥ 205	≥ 230	≥ 260	≥ 205	≥ 205
Wet boiling point [°C]	≥ 140	≥ 155	≥ 180	≥ 140	≥ 140
Viscosity at -40 [mm^2/s]	< 1500	< 1800	< 900	< 1500	< 1800
Viscosity at +100 [mm^2/s]	> 1,5	> 1,5	> 1,5	> 1,5	> 1,5

Dry boiling point is the boiling point of brake fluid which does not contain water (0 % of water i.e. immediately after opening the original packaging).

Wet boiling point is the critical value of boiling temperature of brake fluid and it corresponds to water content of approximately 3,5 percent by weight i.e. it rep-resents a certain allowable amount of water set by the standard for each kind of brake fluid.[5]

While braking, the friction releases considerable heat. Therefore, brake fluid must be design for the highest possible boiling point in order to withstand these high temperatures. However, brake fluid is hygroscopic, meaning that it naturally absorbs water. In any hydraulic brake system during operation, brake fluid gradually absorbs humidity from the air mainly through a cap of the brake reservoir as well as rubber hoses and seals. This humidity lowers the boiling point of brake fluid.[6]

For example, the boiling point of brake fluid SYNTOL HD 265 with the value of at least +260 °C reduces during operation as follows:

- 0 % of water: ≥ +260°C
- 0,18 % of water: +259°C
- 1,15 % of water: +229°C
- 3,13% of water: +175°C
- 4,01% of water: +157°C

In operation, this means that the difference between 0 – 4 % of the water content in brake fluid causes a temperature decline of the boiling point by 102 °C thus to the threshold of functionality and usability of the brake fluid.[7]

In normal operation, brake fluid absorbs the water in the range of 1 – 2 % of its weight per one year. The actual amount of absorbed water, however, depends on the state of components of a brake system especially rubber hoses.[8]

3. Own Measurement

The boiling temperature of brake fluid is monitored on vehicles with hydraulic brakes by using the measuring instrument for boiling temperature of brake fluid. A manual for using this instrument is used in the process of measuring. A probe is inserted into the fluid reservoir or a sample of the fluid is taken from that reservoir. Inspection also verifies whether there are mechanical impurities and debris in the fluid. If construction design of vehicles does not allow accessing to fluid reservoir and thus inserting a probe or sampling, the boiling temperature of brake fluid is not assessed.



Fig. 1 *BOSCH BFT100 with accessories.*

The tester of brake fluid BOSCH BFT100 (Fig. 1) is an instrument for measuring the boiling point of brake fluid in vehicles with hydraulic brakes. The principle of measurement is based on heating of brake fluid by using a heating probe which is directly

inserted into the fluid reservoir. Subsequently, the temperature of brake fluid is measured.

Practical Measurement of Changes in Boiling Point of Brake Fluid during the Vehicle Operation

The measurement was carried out on seven different vehicle brands: Fiat, Alfa Romeo, Volkswagen, Audi, Citroen and Kia. The vehicles were divided according to their predominant operation as follows:

1. The operation of a vehicle type „City“ – Fiat Stilo 1.9JTD, Alfa Romeo GT, Volkswagen Passat 1.9TDI
2. The operation of a vehicle type „Outside City“ – Audi A6 3.0TDI, Citroen Berlingo
3. The operation of a vehicle type „Garaged“ – Kia Ceed 1.6, Citroen C6

The measurement was carried out in the localities of Bardejov, Zilina in the period from 10 November 2014 to 31 March 2015 at different time intervals. Based on the statistical data provided by Slovak Hydrometeorological Institute (SHMU), information about average air temperature and relative humidity were available for individual measurements carried out in mentioned localities.

No dependencies or calculations were further derived from the information provided by SHMÚ. The information was transferred into graphs to show development of temperature and humidity in mentioned localities during whole time period in which measurements were carried out. Each measurement of individual vehicles consisted of three consecutive measurements of the same collected or measured sample of brake fluid. The overall result was determined as the arithmetic average of the measured values. The role of the measurements was to also monitor the number of kilometers driven by the vehicle since the last carried measurement as well as the number of days since the last carried measurement. Two graphs were compiled for each vehicle:

- dependence of changes in boiling point of brake fluid on the number of days elapsed from the last carried measurement or refilling brake fluid,
- dependence of changes in boiling point of brake fluid on the number of driven kilometers together.

To determine long-term intensity of decline in boiling point of brake fluid as well as short-term intensity, we selected two vehicles (Fiat Stilo – operation “City” and Citroen Berlingo – operation “Outside City”). We bought new brake fluid DOT 3 and we refilled old brake fluid by this new one. Subsequently, we examined the intensity of increase and subsequent decline in boiling point of brake fluid during observed period.

4. Results and Discussion

Based on the results obtained from measurements, we were finally able to express decline in boiling point in relation to the number of days and kilometers driven in vehicle operation.

4.1 The Course of Average Daily Temperature and Relative Humidity

As previously mentioned, brake fluid is hygroscopic, meaning that it absorbs humidity from the air. Based on the information provided by SHMU, Fig. 2 depicts development of temperature and air humidity in localities Bardejov and Zilina.

We had to consider daily temperatures and especially air humidity in given localities during observed period because individual measurements were carried out during several months. This had to be taken into account so that we could conclude that decline in boiling point of brake fluid was caused by changes in temperature and air humidity in individual localities where the vehicles were operated.

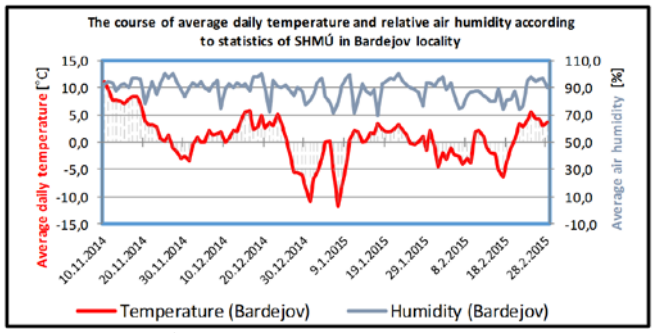


Fig. 2 *The course of average daily temperature and relative air humidity (Bardejov).*

4.2 The Course of Changes in Boiling Point of Brake Fluid during Vehicle Operation

The course of changes in boiling point is depicted in following graphs for each vehicle depending on kilometers driven and days of vehicle operation from the last measurement. The vehicles are divided according to type of operation.

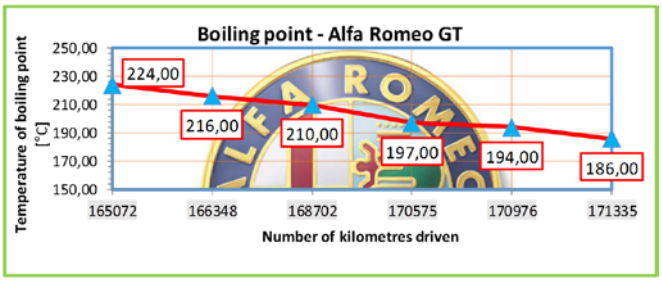


Fig. 3 *Decline in boiling point of brake fluid in terms of driving performance.*

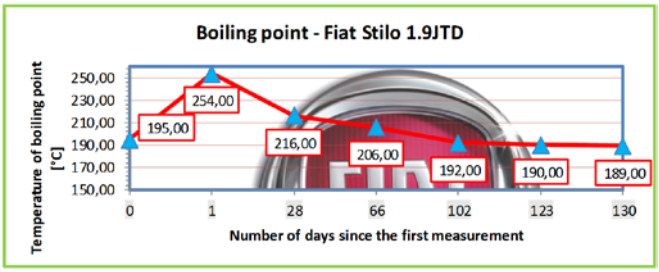


Fig. 4 *Decline in boiling point of brake fluid in terms of operation time (after refilling by new brake fluid).*

4.2 Comparison and Evaluation of the Average Rate of a Boiling Point Decline

Under calculating the average rate of a boiling point decline for each vehicle and each category, smaller differences of the decline can be observed in the recalculation for one day compared to the recalculation for 1000 kilometers. Therefore, it is necessary to exchange brake fluid with respect to the distance travelled and not in terms of time.

Tested vehicle - Fiat Stilo has a high value of the decline rate (marked in red in Tab. 2). This is due to the fact that the new brake fluid absorbs great percentage of humidity after refilling. However, an increasing proportion of water in brake fluid decreases the rate of further absorption. Therefore, if the test had lasted longer, the average rate of decline would have been lower (Fig. 4).

In the case of garaged vehicles with almost no operation (constant conditions), the decline was only minimal (almost none). This represented a reference sample.

Table 2: *The average rate of a boiling point decline of brake fluid. [4]*

Category	*Vehicle*	*Decline intensity of BPBF (°C/day)*	*Decline intensity of BPBF (cat.) (°C/day)*	*Decline intensity of BPBF (°C/1000km)*	*Decline intensity of BPBF (cat.) (°C/1000km)*
City	*Alfa Romeo GT*	*0,29*	*0,34*	*6,07*	*22,07*
	VW Passat	*0,24*		*20,46*	
	Fiat Stilo	*0,50*		*39,68*	
Outside City	*Audi A6*	*0,08*	*0,14*	*1,31*	*4,17*
	Citroën Berlingo	*0,19*		*7,03*	
Garage	*Citroën C6*	*0,03*	*0,03*	-	-
	Kia Ceed	*0,03*		-	

5. Conclusion

If we recalculated the average rate of a boiling point decline from one day to two years (i.e. recommended time interval for exchanging brake fluid) for the category of "City" and "Outside City" vehicle operation, the average decline of boiling point would be about 175 °C. This means the decline of boiling point to the threshold values brake fluid functionality. Therefore, it is recommended to exchange brake fluid at least once every two years. Besides the mentioned vehicle Fiat Stilo (see Tab. 2), it must be taken into account that the measurement was also influenced by the fact that it was carried out during the worst operating conditions – winter season of the middle continental climate zone. Lower absorption of fluid humidity in the summer operation (higher temperature and lower air humidity) would result in a lower decline rate of boiling point of brake fluid. Therefore, these results cannot be applied to year-round operation. Given the mentioned facts, long-term measurements should be carried out at least for one year.

References

[1] Caban J., Komsta H., Vrabel J. Charakterystyka pojazdów samochodowych przeznaczonych do transportu paliw gazowych. In: TTS Technika transportu szynowego: koleje - tramwaje – metro, 2013.

[2] Holes L., Sarkan B. Analysis of impact of selected group of factors of vehicle work conditions on the fuel consumption. In? Doprava a spoje, Zilina. University of Zilina, 2012.

[3] http://www.testek.sk/files/prez/BK-Tatry2007-text.pdf.

[4] Bratsky D., Janosik S., Stacho D. Tovaroznalectvo: Ucebne texty pre pracovnikov cerpacich stanic, Bratislava, 2000. 78 p.

[5] Hlavna V. et al., Dopravny prostriedok a jeho motor, Zilina, 2003.

[6] http://www.autotechna.sk/subory/noviny-2013-04-web.pdf.

[7] Stepina V., Vesely, V. Maziva a specialni oleje, Bratislava, Veda, vydavatelstvo SAV, 1980, 696 p.

[8] ISO 4925. Specification for non-petroleum based brake fluid for hydraulic systems. 15. 02. 1995.

DATABASE DESIGN AT SYNTHESIS OF ELECTROMECHANICAL MODULES

Assoc. Prof. Dahterova D., M. Eng. Nikolova I.

Technical University of Sofia, Faculty of Engineering and Education – Sliven, Sliven, Bulgaria

dimitrinka_sl@yahoo.com

Abstract: *In accordance with the global concepts for machine design based on the modular principle, the main modules, which are the same for the different types of working machines, are the electromechanical modules, also called geared-motor modules. Because of the multivariance of the task for their design, a database containing the technical parameters and characteristics of the main constructive units needs to be build.*

Key words: ELECTROMECHANICAL MODULES, DATABASE, GEARED-MOTOR, ELECTRIC MOTOR, GEAR REDUCER

1. Introduction

The electromechanical modules (EMM) represent the constructive unification of the electrical and the mechanical part of the drives of the different types of working machines. In the majority of cases, the combination is between an electrical motor and a gear reducer, known also in the literature and the practice under the name geared-motor, respectively geared-motor module. In some case, the connection between the electric motor and the gear reducer is realized by means of a clutch. Depending on the selection of electric motor, gear reducer and clutch, at the same values for the input data, the realization of multiple variants of EMM is possible [Genova, etc. 2011]. Their unification in a single database facilitates the process for selecting the suitable for a concrete application EMM, as well as gives an opportunity for creating a software for optimal selection.

2. Formulating the problem

In terms of the structure, the database (DB) must contain information about the main constructive units of the EMM – electric motors, gear reducers and clutches. At certain point, this can turn out to be large amount of data, for the unification of which in a single DB, the most simple and functional structure that is easy to update and maintain needs to be built. Furthermore, the interface of the database needs to be user-friendly and to ensure fast and easy access to the information. This can be achieved by designing a relational DB, which is the most commonly used type [Hernandez 2003]. This is due to the fact that in comparison with the other models – hierarchical, network and object-orientated, at the relational DB structuring and updating the information, as well as building the relations between the separate tables is performed very easy. The nature of a relational DB is the correct building of the relations between the different tables that compose it [Garcia-Molina et al., 2009].

Fig. 1 shows an exemplary block-scheme of the general view of the database structure. The rectangles indicate the main tables that built the database – electric motors, clutches, gear reducers and the possible combinations between them. These tables contain technical parameters of the components:

- table electric motors – type of motor (for AC or DC current, asynchronous, synchronous, etc.), nominal power, nominal and synchronous speed of the motor shaft, nominal and maximal torque, nominal current, efficiency, IE efficiency class, weight, manufacturer;
- table gear reducers – type of gear reducer (cylindrical, bevel, worm, etc.), number of stages, mounting (horizontal or vertical), ration, efficiency;
- table electromechanical modules – the possible combinations between electric motors and gear reducers and their respective technical and geometrical parameters.

The blue rhomb indicates between which tables a relationship needs to be built. The block-scheme given on fig. 1 is exemplar. The information, which is contained in the tables, could be supplemented or removed, as well as the tables themselves.

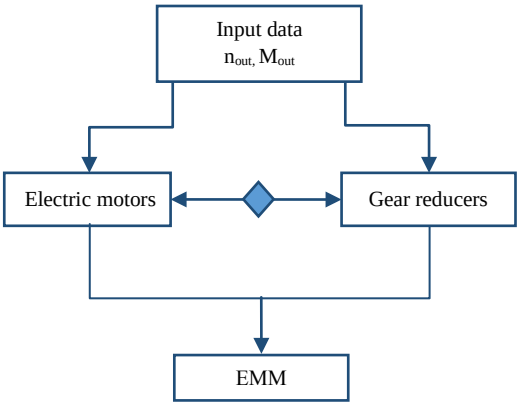


Fig. 1 Block-scheme of exemplary structure of the DB

3. Designing the database

In order to build a database, the so-called database management systems (DBMS) are used. These are the programs (software) by which a DB is designed and which ensures fast access to them and gives the opportunity for their updating and maintenance. One of the most commonly used DBMS are Oracle, MS Access, Paradox, FoxPro, Sybase, dBase, etc.

We have developed two versions of the database, using the software MS Access 2013. These versions differ from each other concerning their structure.

Version 1:

This version is the simplest one. It consists of only one table (shown in Table 1). The table contains information about all possible combinations of the structural units, obtained based on the input data. In order to simplify as much as possible the DB, the geometrical parameters of the obtained variants of EMM and some of the technical data about the electric motors and the gear reducers were exported in a separate file, for every concrete variant. The access to these files is done by clicking on the according hyperlink in the Gear_Mot_ID field.

For the convenience of the user, a search form has been created. Upon entering values for the input data and clicking on the functional button “Search”, the search results are outputted. This is done by the means of a so-called query, in which search criteria based on the entered values for the input data are assigned. Fig. 2 shows the general view of this query.

Version 2:

This version of the DB also consists of a table with the technical parameters of the possible combinations of EMM – identical in its

structure with the table in the first version, but in this case, there are also two more tables.

One of the tables contains data about electric motors of concrete companies and the other one contains data about the different types of gear reducers. In all three tables, there is one field, which indicates the identification number of every single record (row). This identifier is the so-called primary key and is unique for every record. The relations between the tables are built with the help of these primary keys. Another auxiliary table is built, which connects the three main tables, because it is not possible to create more than one relation from a single primary key.

This version of the DB also have a search form, which is identical with the form from the other version. The difference here is in the query, at which not only the search criteria are defined, but also the relations between the tables. Thereby, upon entering values for the input data in the search form and clicking on the functional button "Search", the results show preliminary defined fields from all tables. Fig. 3 shows the general view of the query for version 2 of the DB.

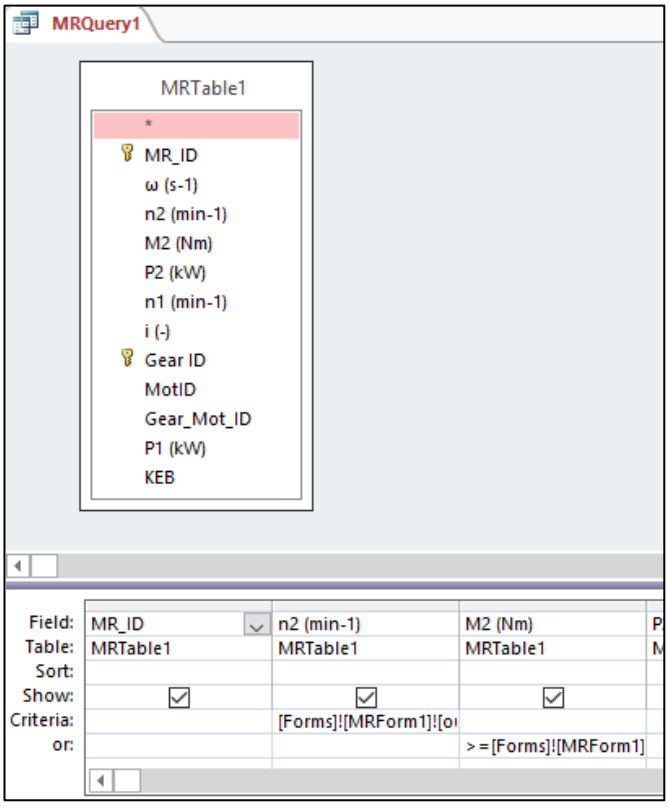


Fig. 2 Query - version 1

4. Numerical example

EMM design at the following input data: n_{out} = 65 min^{-1}; M_{out} = 95 Nm.

Depending on the type of the electric motor and the gear reducer, different variants of EMM are obtained. The database – electric motors contains asynchronous squirrel cage motors with different number of pole pair, i.e. different values for the speed of the input shaft n_{in}, namely: 2-pole electric motor (n_{in} = 3000 min^{-1}), 4-pole electric motor (n_{in} = 1500 min^{-1}), 6-pole electric motor (n_{in} = 1000 min^{-1}) and 8-pole electric motor (n_{in} = 750 min^{-1}).

The input power is calculated (P_{in} = 0,67 kW), based on the output power (P_{out} = 0,65 kW) and previously accepted indicative value for the efficiency. For the concrete case, an electric motor with nominal power $P_{nom.}$ = 0,75 kW has been selected that guarantees the realization of the input data. The ratios are calculated, based on which are defined the gear reducers by which these variants can be obtained – cylindrical, bevel, cylindrical-bevel, worm and worm-cylindrical. 51 different variants of EMM are obtained. Fig. 4 shows the results of the search in the search form of version 1 of the DB, and fig. 5 shows the results at version 3 of the DB.

5. Conclusion

Version 2 of the DB is more complex, but updating and maintaining such structure is easier. Also, the volume of the DB is smaller, because at his version there are no external files.

At version 1, for every EMM that is added in the DB, a new file with technical parameters of the electric motor and gear unit, that comprise it, needs to be created, which additionally compounds the DB. On the other hand, at version 1 the information is better illustrated in the search form, because the user can open only the file with technical data of this variant of EMM that satisfies its requirements.

Acknowledgments: this development is financed by the NATIONAL FUND for "Scientific research" under contract No. 152ПД 0060-06/ 2015.

6. Literature

Genova P., Dahterova D., Tsoneva M., Theory of machine design. Sofia, 2011.

Hernandez M. Database Design for Mere Mortals™: A Hands-On Guide to Relational Database Design, Second Edition. USA, 2003.

Hector Garcia-Molina H., Ullman J., Widom J. DATABASE SYSTEMS The Complete Book, Second Edition. USA, 2009.

Table 1: General view of the table in the first version of the DB

MR_ID	ω	n_{out}	M_{out}	P_{out}	P_{in}	n_{in}	i	Gear_Mot_ID
MRi i=1, 2, .. n	const calc	const	const	const calc	const calc	var	var calc	var hyperlink

Description: const-constant values; var-variable value; calc-calculated values; hyperlink-link to external file; MR_ID – identification number of all of the obtained variants; ω – input angular speed, it is calculated, [s^{-1}]; n_{out} – output speed, [min-1]; M_{out} – output torque, [Nm]; P_{out} – output power, it is calculated, [kW]; P_{in} – input power, it is calculated, [kW]; n_{in} – input speed, [min-1]; i – ratio, it is calculated, [-]; Gear_Mot_ID – hyperlink type of field

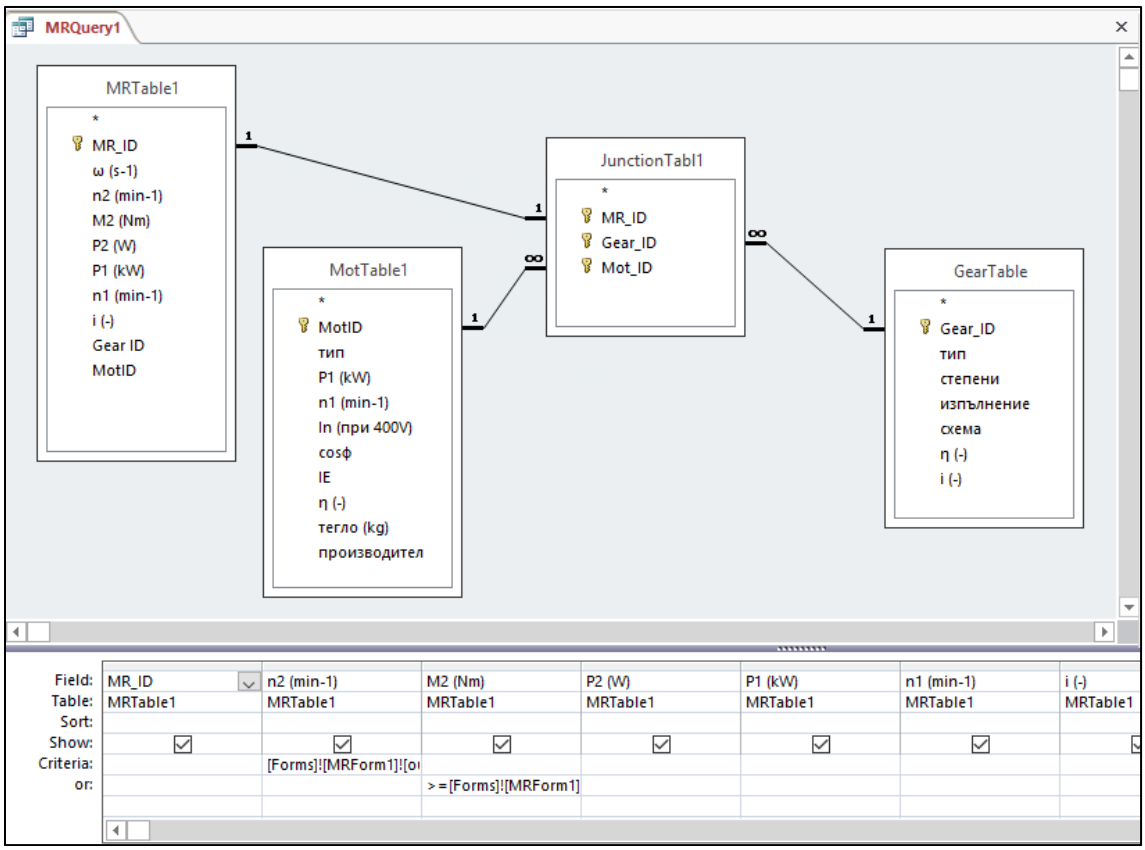


Fig. 3 Query – version 2

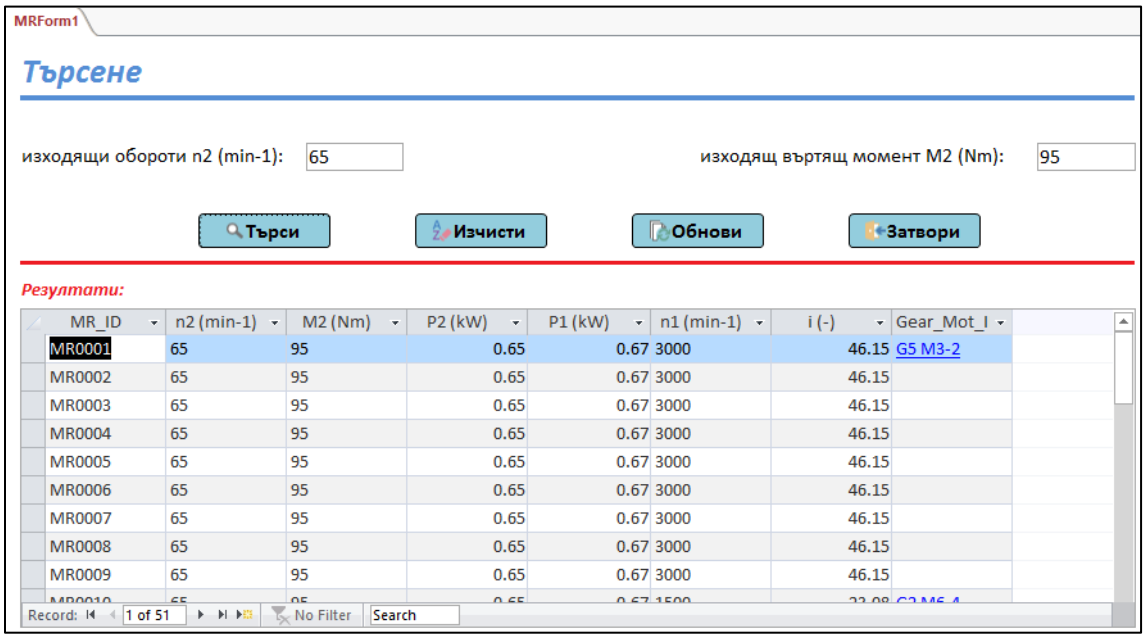


Fig. 4 Results from the search (version 1 of the DB)

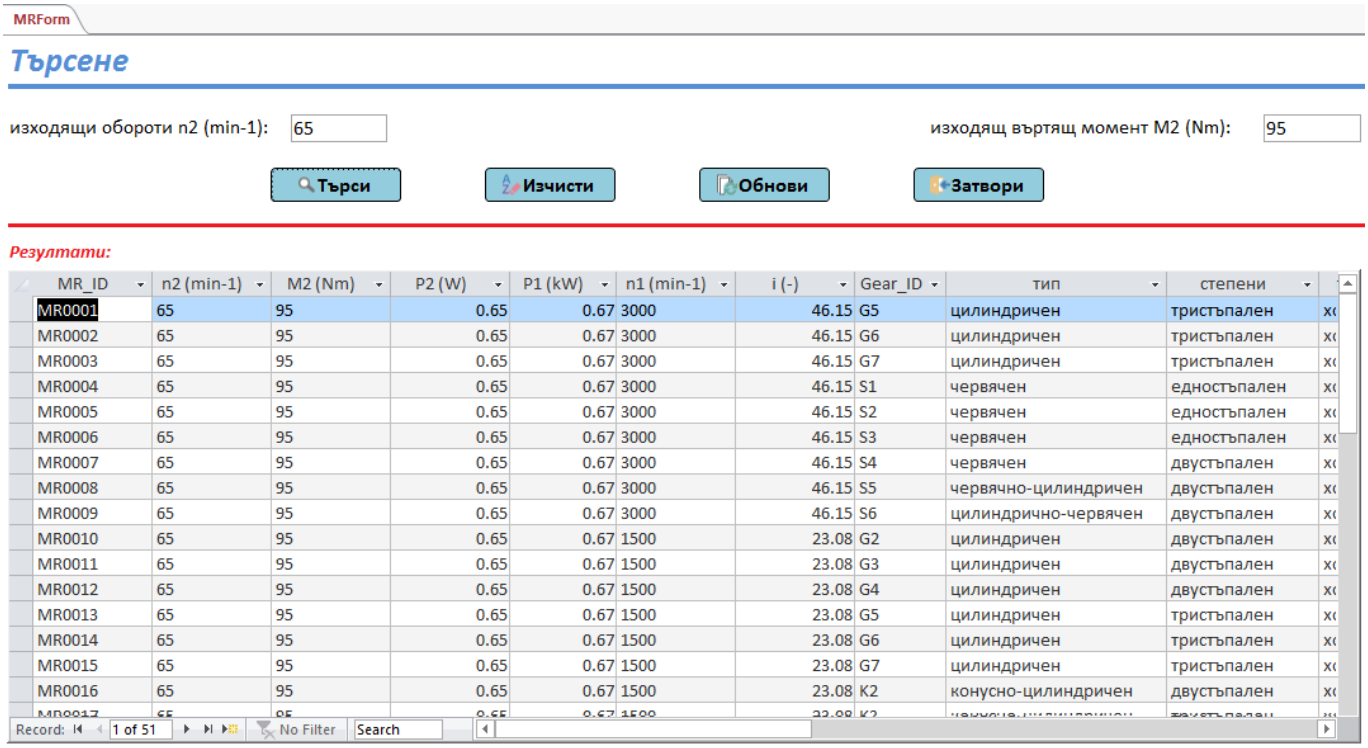


Fig. 5 Results from the search (version 2 of the DB)